EXPLORING BIOMIMETIC CATALYSTS FOR ALCOHOL GENERATION

by

JOSHUA KELLY

A thesis submitted to the Department of Pure and Applied Chemistry, University of Strathclyde, in part fulfilment of the regulations for the degree of Master of Philosophy in Chemistry.

Declaration

This thesis is the result of the author's original research. It has been composed by the author and has not been previously submitted for examination which has led to the award of a degree.

The copyright of this thesis belongs to the author under the terms of the United Kingdom Copyright Acts as qualified by University of Strathclyde Regulation 3.50. Due acknowledgement must always be made of the use of any material contained in, or derived from, this thesis.

Signed: L. Kelly   Date: 15/6/2017

Abstract

The direct, selective and efficient functionalization of unactivated C-H bonds, such as those in naturally abundant hydrocarbons, remains one of the most difficult challenges in modern chemistry. However, in the last fifteen years much effort has been expended in developing various biomimetic catalysts that can perform the same functionalizations as those enzymes observed in nature.

This review discusses homogeneous monoiron and diiron catalysts, supported by various types of ligands and gives an up to date comparison on their hydroxylation reactivities with hydrocarbon substrates. The key intermediates involved in the reaction mechanisms are highlighted and those crucial steps such as hydrogen atom abstraction and OH rebound are investigated in order to rationalise how a catalyst's design influences its reactivity and also its stability.

Acknowledgements

Contents

1 Abbreviations

BDE	Bond dissociation energy
Bpin	4,4,5,5-tetramethyl-1,3,2-dioxaborolane
bpym	2,2′-bipyrimidinyl
Cp*	pentamethylcyclopentadienyl
Cys	Cysteine
DFT	Density functional theory
DHA	9,10-Dihydroanthracene
dpaq	2-[bis(pyridin-2-ylmethyl)]amino-N-quinolin-8-yl-acetamidate
e^-	Electron
E_{ox}	Oxidation potential
E_{red}	Reduction potential
EPR	Electron paramagnetic resonance
EXAFS	Extended X-ray absorption fine structure
FAD	Flavin adenine dinucleotide
Fc	Ferrocene
FG	Functional group
FMO	Frontier molecular orbital
Glu	Glutamic acid
HAA	Hydrogen atom abstraction

|	
His	Histidine
HOMO	Highest occupied molecular orbital
6-hpa	1,2-bis{2-[bis(2-pyridylmethyl)-aminomethyl]pyridin-6-yl}ethane
KIE	Kinetic isotope effect
L	Ligand
LUMO	Lowest unoccupied molecular orbital
M	Metal
MCET	Metal-coupled electron transfer
*m*CPBA	*meta*-Chloroperoxybenzoic acid
MeCN	Acetonitrile
Me$_3$NTB	tris((*N*-methylbenzimidazol-2-yl)methyl)amine
MMO	Methane monooxygenase
N$_4$Py	*N,N*-bis(2-pyridylmethyl)-*N*-bis(2-pyridyl)methylamine
NADH	Nicotinamide adenine dinucleotide (reduced)
NMR	Nuclear magnetic resonance
OAT	Oxygen atom transfer
PaPy$_3$	*N,N*-bis(2-pyridylmethyl)amine-*N*-ethyl-2-pyridine-2-carboxamidate
Pc^{t}Bu$_4$	tetra-*tert*-butylphthalocyanine
PCET	Proton-coupled electron transfer
PCP	1,3-bis(dialkylphosphinomethyl)-phenyl
Ph	Phenyl group
Piv	Pivalate

R	Alkyl group
RDS	Rate-determining step
r.t.	Room temperature
Sol	Solvent
TAML	Tetra amido macrocyclic ligand
TMC	1,4,8,11-Tetramethyl-1,4,8,11-tetraazacyclotetradecane
TMG$_3$tren	1,1,1-Tris{2-[N^2-(1,1,3,3-tetramethylguanidino)]ethyl}amine
TMP	*meso*-Tetramesitylporphyrin
4-TMPyP	5,10,15,20-Tetrakis(N-methyl-4'-pyridyl)porphinato
TON	Turnover number
TPA	tris(2-Pyridylmethyl)amine
TPP	Tetraphenylporphyrin

2 Introduction

2.1 Overview

The earth is abundant in hydrocarbon feedstocks such as crude oil and natural gas which can be used as starting materials in the synthesis of many useful organic molecules.[1] However, alkanes themselves are of very low synthetic utility as they consist of relatively inert C-H bonds and are therefore mainly burned for energy or used as non-polar solvents. As a result, C-H bond activation is a very important area of research because it greatly increases the synthetic utility of these molecules by introducing a functional group which can then act as a starting point in a series of organic transformations.[2] However, functionalizing unactivated C-H bonds is a very difficult challenge as carbon and hydrogen have similar electronegativities and also do not have any suitable lone pairs for a metal complex to coordinate to. With bond dissociation energies (BDEs) ranging from 97 to 105 kcal mol^{-1} (**Figure 1**), these are among the hardest bonds to cleave in organic chemistry.[3]
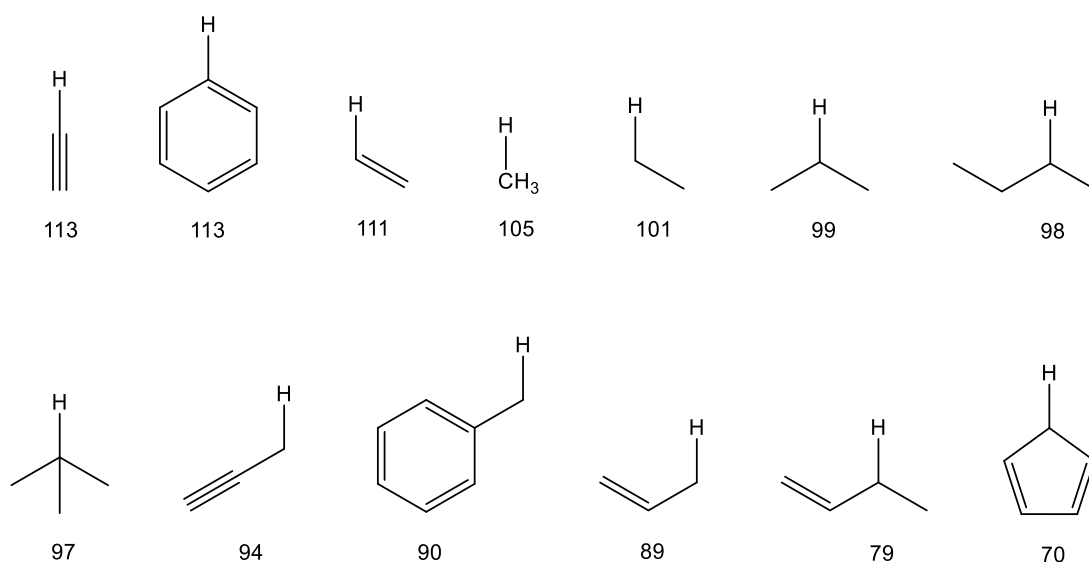
Figure 1. BDEs of various C-H bonds (kcal mol^{-1}).[3]

C-H bond activation generally proceeds through three main types of reaction mechanism:

(i) **Hydrogen atom abstraction**

In this case a metal oxo complex (**1**) abstracts a hydrogen atom and then the alkyl radical recombines with the hydroxyl complex (**2**) to yield the hydroxylated product (**3**) (**Scheme 1**).[4] This mechanism will be the focus of this review.
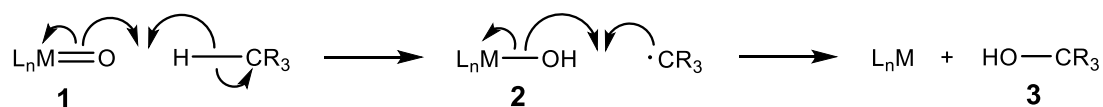
Scheme 1. Hydrogen atom abstraction mechanism.[4]
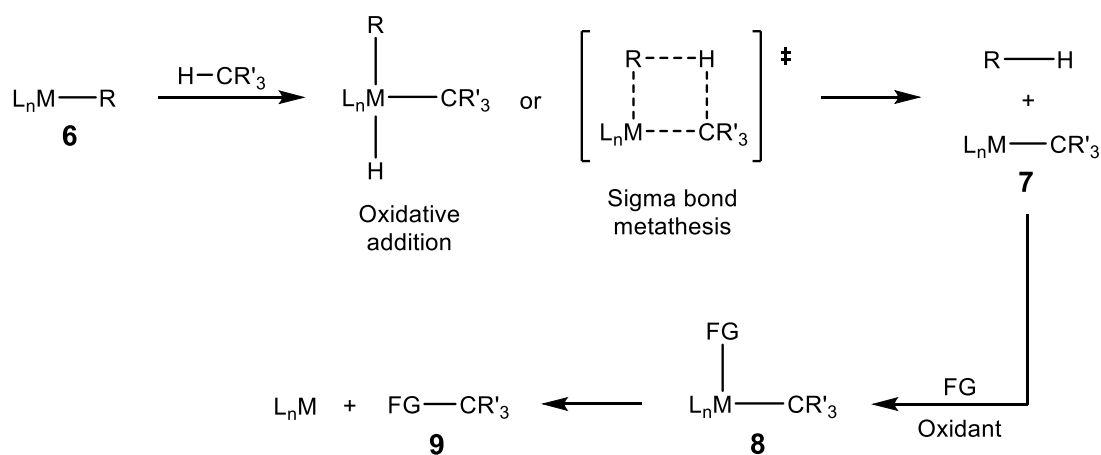
(ii) **Direct insertion**

In this case the heteroatom in the unsaturated complex (**4**) directly inserts itself into a C-H bond and the functionalized product (**5**) is obtained in a concerted fashion (**Scheme 2**). Metal carbenes and nitrenes can be used in this mechanism.[5,6]
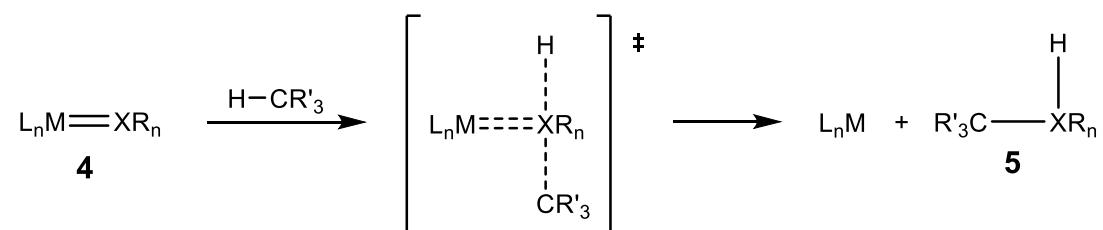
Scheme 2. Direct insertion mechanism.[5,6]

(iii) *Via* **an organometallic intermediate**

In this case an organometallic intermediate (**7**) is initially formed by oxidative addition, sigma bond metathesis, or by other reaction mechanisms with the starting complex (**6**) (**Scheme 3**). The functional group is then added to **7** by the use of an oxidant and the alkyl complex (**8**) undergoes reductive elimination to yield the functionalized product (**9**).[7,8]

L$_n$M—R →(H—CR'$_3$) L$_n$M(R)(H)—CR'$_3$ **or** [R----H / L$_n$M----CR'$_3$]‡ → R—H + L$_n$M—CR'$_3$

6

Oxidative addition

Sigma bond metathesis

7

L$_n$M + FG—CR'$_3$ ← L$_n$M(FG)—CR'$_3$ ←(FG Oxidant)

9

8

Scheme 3. Organometallic intermediate mechanism.[7,8]

Transition metals such as palladium, platinum, iridium, ruthenium and rhodium are traditionally used in C-H bond activation as they have dominated research in this area for decades.[1,2] However, these are very expensive (**Table 1**) and highly toxic metals.[9] Therefore, the development of synthetic iron oxidation catalysts is very important because iron has a number of practical advantages over these heavy metals.

- It is very inexpensive as it is the most abundant element on earth.[10]
- It is one of the least toxic metals, which is excellent for pharmaceutical synthesis.[11]
- It is also more environmentally friendly than other metals.

| Metal	Price (£/g)
Gold	32.17
Platinum	24.99
Palladium	17.46
Iridium	16.42
Ruthenium	1.06
Rhodium	17.30

Table 1. Prices of various metals (£/g) as of October 2016.[9]

Synthetic iron oxidation catalysts have enormous potential in C-H bond activation because their enzyme counterparts, cytochrome P450 and methane monooxygenase have been well known to hydroxylate unactivated C-H bonds very efficiently and under ambient conditions in nature.[12,13] Unfortunately, their capability has been relatively unexplored until recent years and deserves much more attention.[1]

This review investigates a wide variety of synthetic iron oxidation catalysts, including both monoiron and diiron systems. It discusses the various factors that influence their reactivity and also their stability.

2.2 C-H Bond Activation

Now we will discuss some literature examples of C-H bond activation of alkane substrates using various transition metal complexes. This includes both stoichiometric reagents and true catalysts.[1,2]
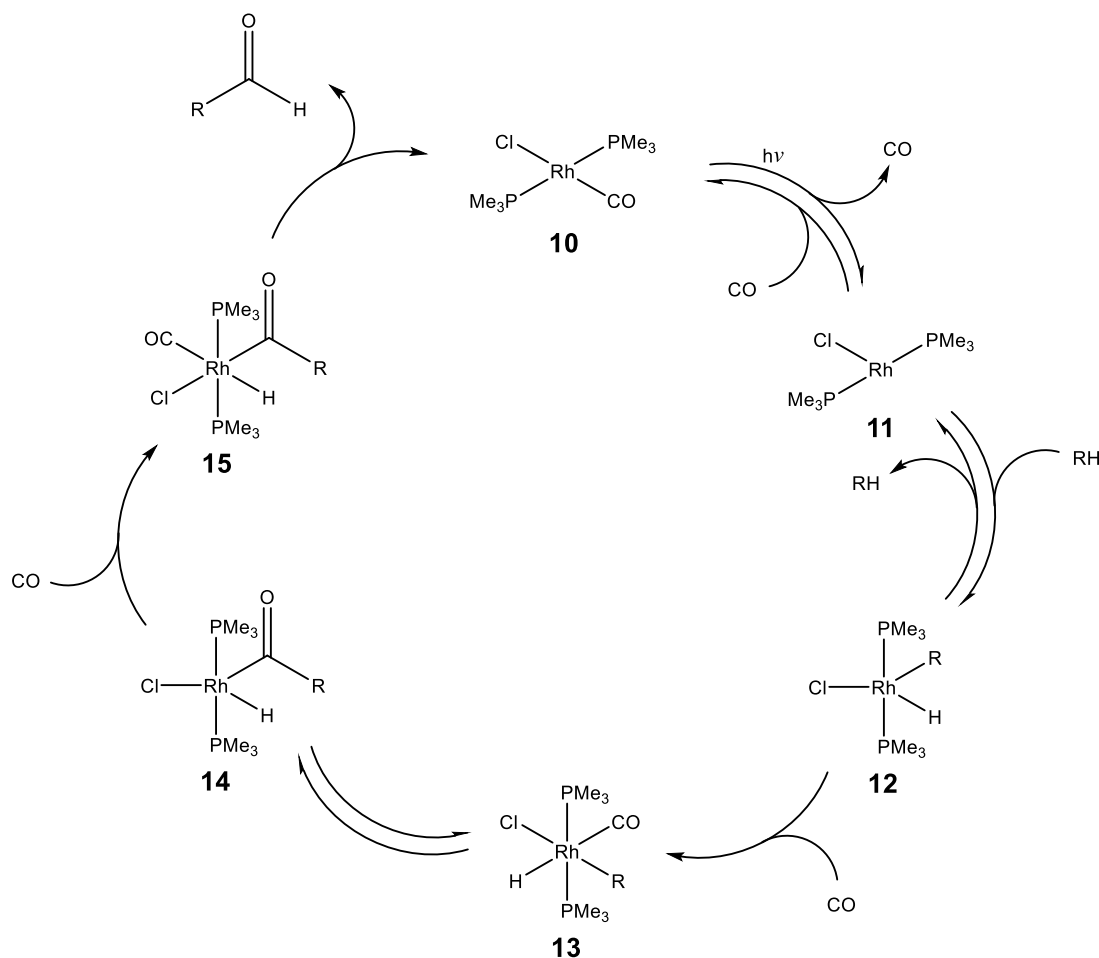
Scheme 4. Proposed catalytic cycle for the carbonylation of pentane by [RhCl(CO)(PMe3)2] (**10**).[14]

In 1990 Sakakura *et al.* reported a reactive carbonylation catalyst [RhCl(CO)(PMe3)2] (**10**) capable of carbonylating pentane to hexanal at room

temperature.[14] It is believed that upon UV irradiation a CO ligand dissociates from **10** to give the 14 electron complex (**11**), which then undergoes oxidative addition with pentane to produce the alkylhydride complex (**12**) and CO coordination gives the coordinatively saturated complex (**13**) which undergoes CO insertion to produce the acyl complex (**14**) (**Scheme 4**). Further CO coordination then produces a coordinatively saturated acyl complex (**15**) and this undergoes reductive elimination to yield hexanal and regenerate **10**. This selectively carbonylates the terminal C-H bonds as they are more accessible. However, approximately 80% of the hexanal product then undergoes a secondary Norrish Type II reaction to yield but-1-ene and ethanol.[14]
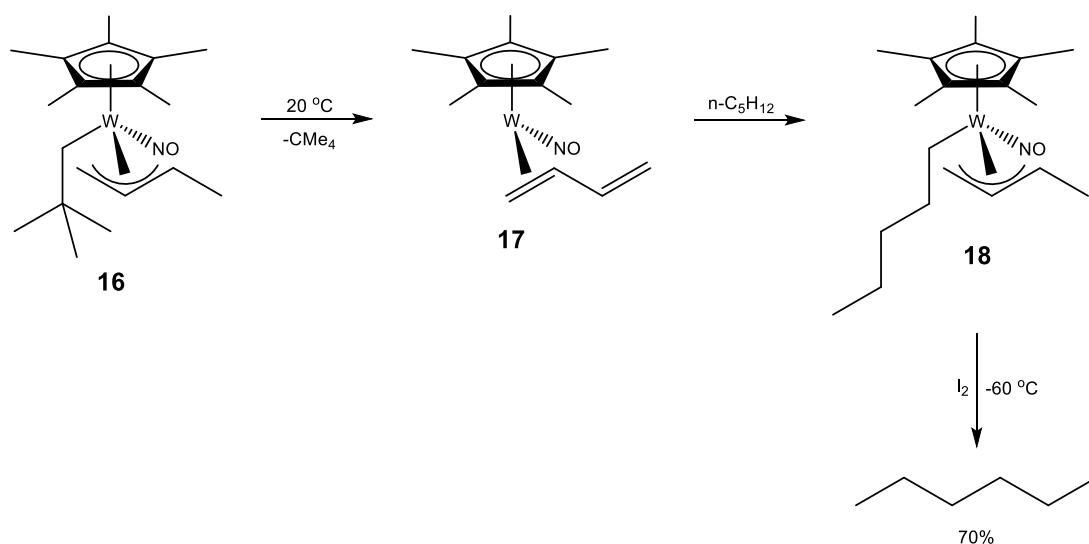

Scheme 5. Halogenation of pentane by [WCp*(NO)(η^3-CH$_2$CHCHCH$_3$)(CH$_2$CMe$_3$)] (**16**).[15]

In 2007 Tsang *et al.* reported a reactive tungsten complex [WCp*(NO)(η^3-CH$_2$CHCHCH$_3$)(CH$_2$CMe$_3$)] (**16**) capable of halogenating pentane to 1-iodopentane under mild conditions.[15] It was found that, when dissolved in pentane, **16** undergoes β-hydride elimination and reductive elimination which releases neopentane and produces a highly reactive 16 electron intermediate

(**17**). The reverse process then takes place between **17** and pentane which produces a stable alkyl complex (**18**) and then treatment with I$_2$ releases 1-iodopentane in 70% yield (**Scheme 5**). This selectively halogenates the terminal C-H bonds as they are more accessible.[15]
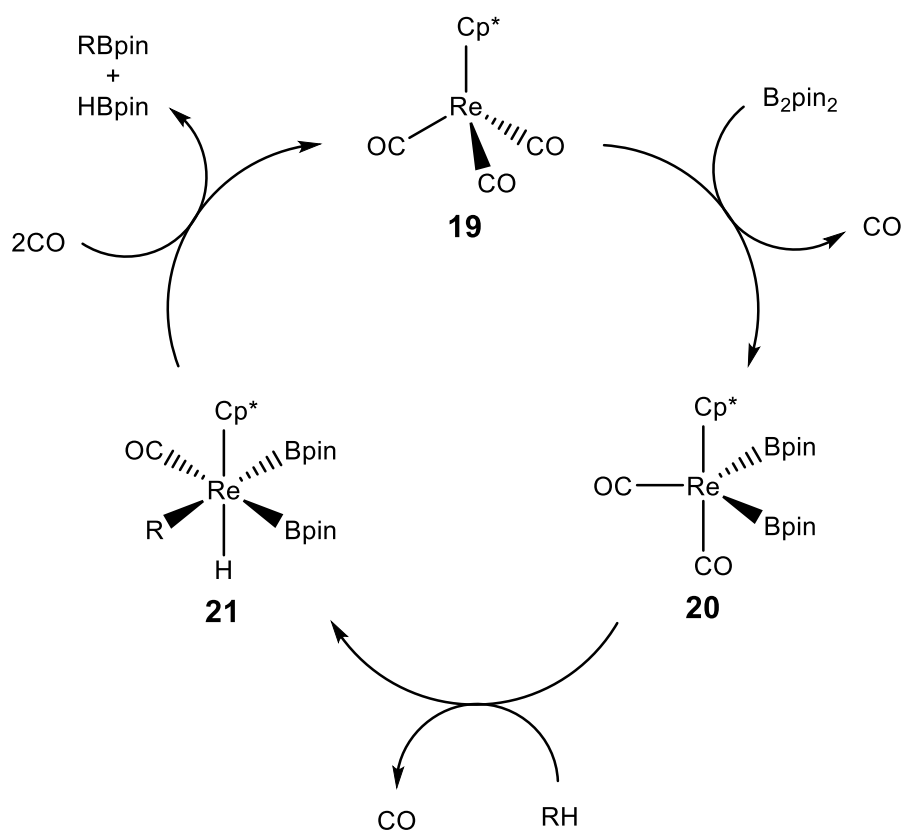
Scheme 6. Proposed catalytic cycle for the borylation of pentane by [ReCp*(CO)$_3$] (**19**).[16]

In 1999 Hartwig *et al.* reported a reactive borylation catalyst [ReCp*(CO)$_3$] (**19**) capable of borylating pentane to 1-pentylBpin at 25 °C.[16] It is believed that upon UV irradiation **19** undergoes CO dissociation and then oxidative addition with B$_2$pin$_2$ to produce the bis-boryl complex (**20**) which can exist as both the *cis* and *trans* isomers (**Scheme 6**). Complex **20** then undergoes a further CO dissociation and then oxidative addition with pentane to produce

the alkyl rhenium bis-boryl complex (**21**). Finally, **21** then undergoes reductive elimination to yield 1-pentylBpin and HBpin, and CO association regenerates **19**. Remarkably, 1-pentylBpin can be obtained in 95% yield with only 2.4% catalyst loading.[16] Further work revealed that the HBpin by-product can also be consumed in the catalytic cycle *via* oxidative addition.[17]
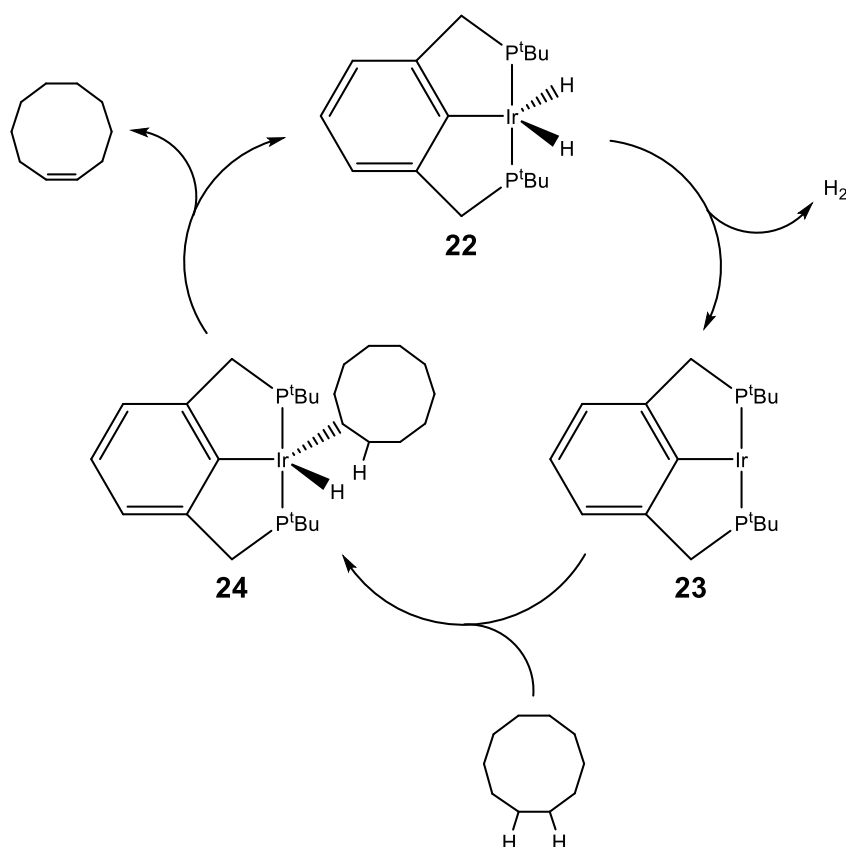
Scheme 7. Proposed catalytic cycle for the dehydrogenation of cyclodecane by [Ir(PCP)H$_2$] (**22**).[19]

In 1997 Goldman *et al.* reported a reactive dehydrogenation catalyst [Ir(PCP)H$_2$] (**22**) capable of dehydrogenating cyclodecane to cyclodecene at 201 °C without the use of a sacrificial hydrogen acceptor.[18] It is believed that upon heating **22** undergoes reductive elimination which releases H$_2$ and produces the 14 electron complex (**23**) (**Scheme 7**). Complex **23** then

undergoes oxidative addition with cyclodecane to produce the alkylhydride complex (**24**). Finally, **24** then undergoes β-hydride elimination to yield cyclodecene and regenerate **22**.[19] This demonstrates excellent thermal stability, which is essential for this reaction as high temperatures are required to overcome the large positive enthalpy of dehydrogenation without the use of a sacrificial hydrogen acceptor.[18]
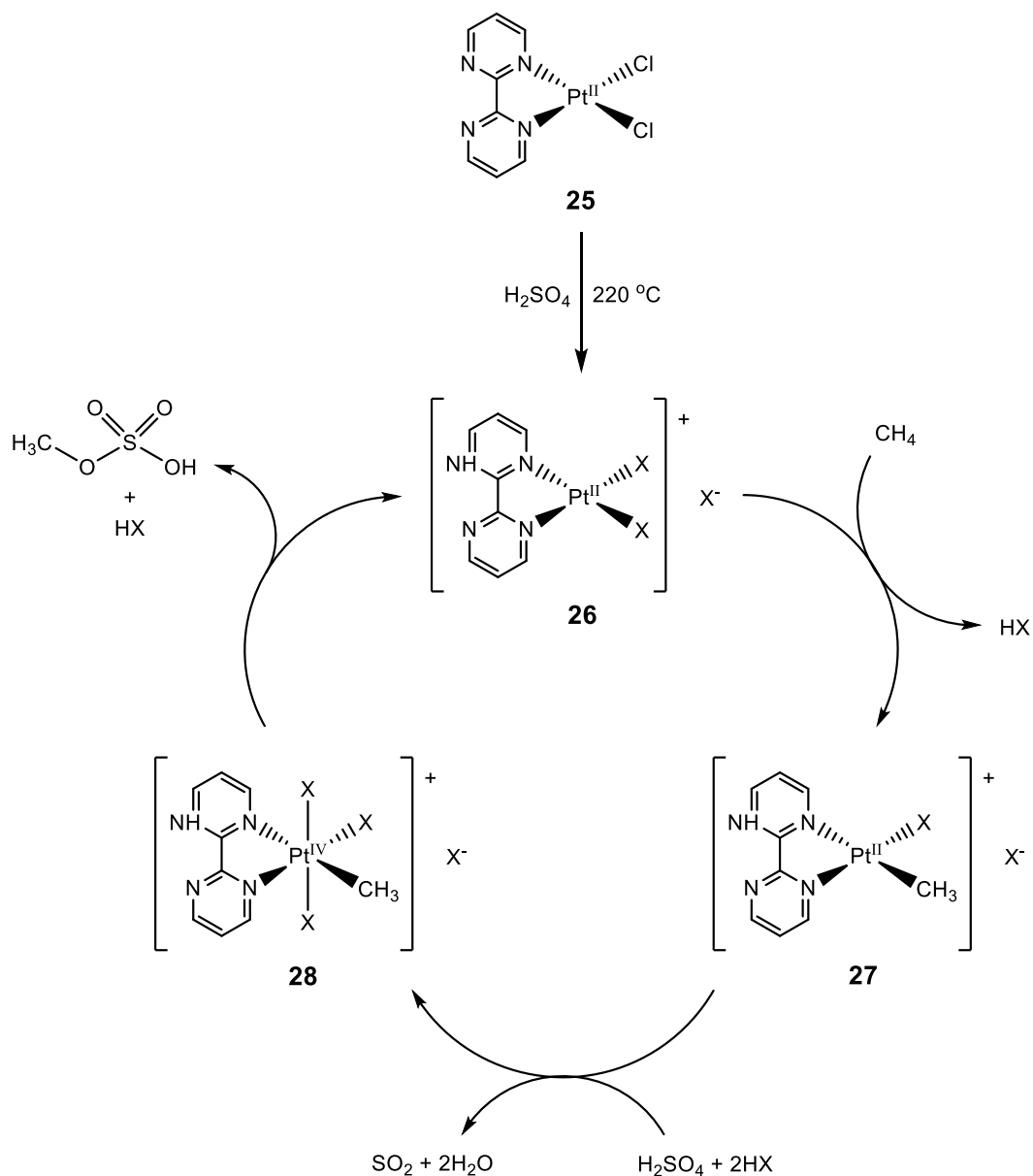

Scheme 8. Proposed catalytic cycle for the sulfation of methane by [Pt(bpym)Cl₂] (**25**).[20] (X = Cl or HSO₄)

In 1998 Periana *et al.* reported a reactive sulfation catalyst [Pt(bpym)Cl$_2$] (**25**) capable of sulfating methane to methylbisulfate in fuming sulfuric acid at 220 °C.[20] It is believed that when dissolved, **25** is protonated to its reactive form (**26**) which then reacts with methane to produce the alkyl complex (**27**) (**Scheme 8**). This is then oxidized to the Pt^{IV} complex (**28**) and this undergoes reductive elimination to yield methylbisulfate and regenerate **26**.[21] The product is protected from over-oxidation due to the electron-withdrawing nature of the bisulfate group and also the excess of methane used. It can then be simply deprotected by hydrolysis to yield methanol, which is a very useful molecule for further organic synthesis. Complex **26** is incredibly stable under these harsh conditions, such that the system is still active after 500 turnovers (TON).[20]

3 Iron-Based C-H Activation Catalysts

3.1 Monoiron Systems

### 3.1.1 Natural Enzyme Background

29
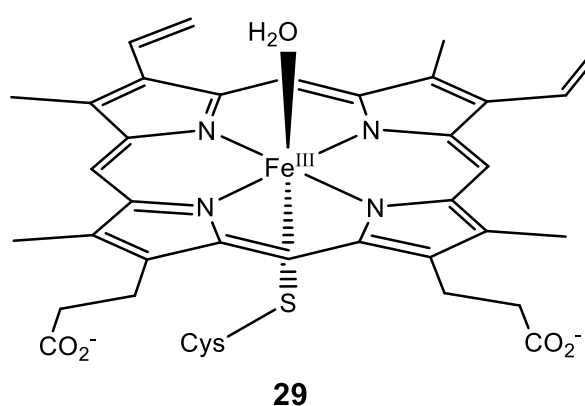
Figure 2. Cytochrome P450 enzyme active site prosthetic group (resting state).[22]

Cytochrome P450 (CYP) (**29**) is a superfamily of structurally diverse and functionally versatile enzymes that consist of a heme coenzyme with a cysteine thiolate ligand which is tethered to a protein (**Figure 2**).[23] The cytochrome P450 proteins have extremely diverse primary sequences and are grouped into families depending on their amino acid sequence identity: proteins with 40% identity or more are classed in the same family (CYP1, CYP2, CYP3 etc.), and members with 55% identity or more are classed in the same subfamily (CYP1A1, CYP1A2, CYP1A3 etc.).[24] The term P450 is derived from the characteristic absorption at 450 nm which is observed when the enzyme prosthetic group (**30**) is in its reduced state (**31**) and complexed with CO (**32**) (**Scheme 9**).[25]
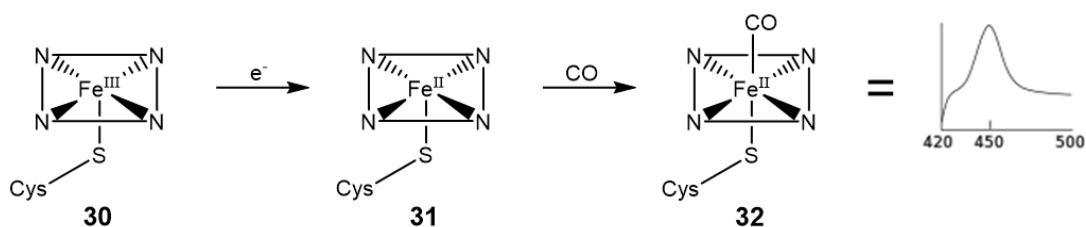
Scheme 9. 450 nm absorption of cytochrome P450 (**32**).[25]

CYPs are responsible for the phase 1 metabolism of approximately 75% of all known pharmaceuticals and they perform this and other important biological functions through the controlled activation of inert C-H bonds.[26] Most of the reactions catalysed by CYPs are mixed-function oxidations with the following general stoichiometry, in which R-H is the substrate.[27]

$$NADPH + H^+ + O_2 + R\text{-}H \longrightarrow NADP^+ + H_2O + R\text{-}OH$$
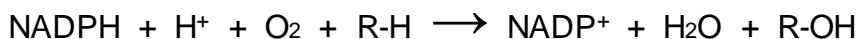
The mechanism of C-H bond hydroxylation by cytochrome P450 is shown in **Scheme 10** and is explained as follows.[28] The first step involves the binding of the substrate to the resting low spin Fe^{III} coenzyme (**29**). This binding induces structural changes in the protein which often, but not always, manifest themselves in the dissociation of the distally coordinated H_2O and the conversion of the heme from low spin to high spin (**30**). These substrate-induced structural changes facilitate reduction of the Fe^{III} species, allowing delivery of the first electron to generate the Fe^{II} substrate-bound form of the enzyme (**31**). O_2 then binds to the Fe^{II} heme, forming a species that is best described as an Fe^{III} superoxide complex (**33**). The subsequent reduction of this species forms an Fe^{III} peroxo species (**34**), which is protonated at the distal oxygen to generate an Fe^{III} hydroperoxo complex (**35**). The delivery of an additional proton to the distal oxygen cleaves the O-O bond, yielding an Fe^{IV} oxo radical cation complex known as "compound 1" (**36**) and a H_2O molecule. Compound 1 then abstracts a hydrogen atom from the substrate to yield an Fe^{IV} hydroxide complex known as "compound 2" (**37**) and an alkyl radical, which rapidly recombine to yield the hydroxylated product and Fe^{III} enzyme (**30**). This mechanism is described in **Scheme 1**.[4] The hydroxylated

16

product then dissociates from the enzyme cage and H_2O coordinates to the heme to regenerate the resting Fe^{III} enzyme (**29**).[28]
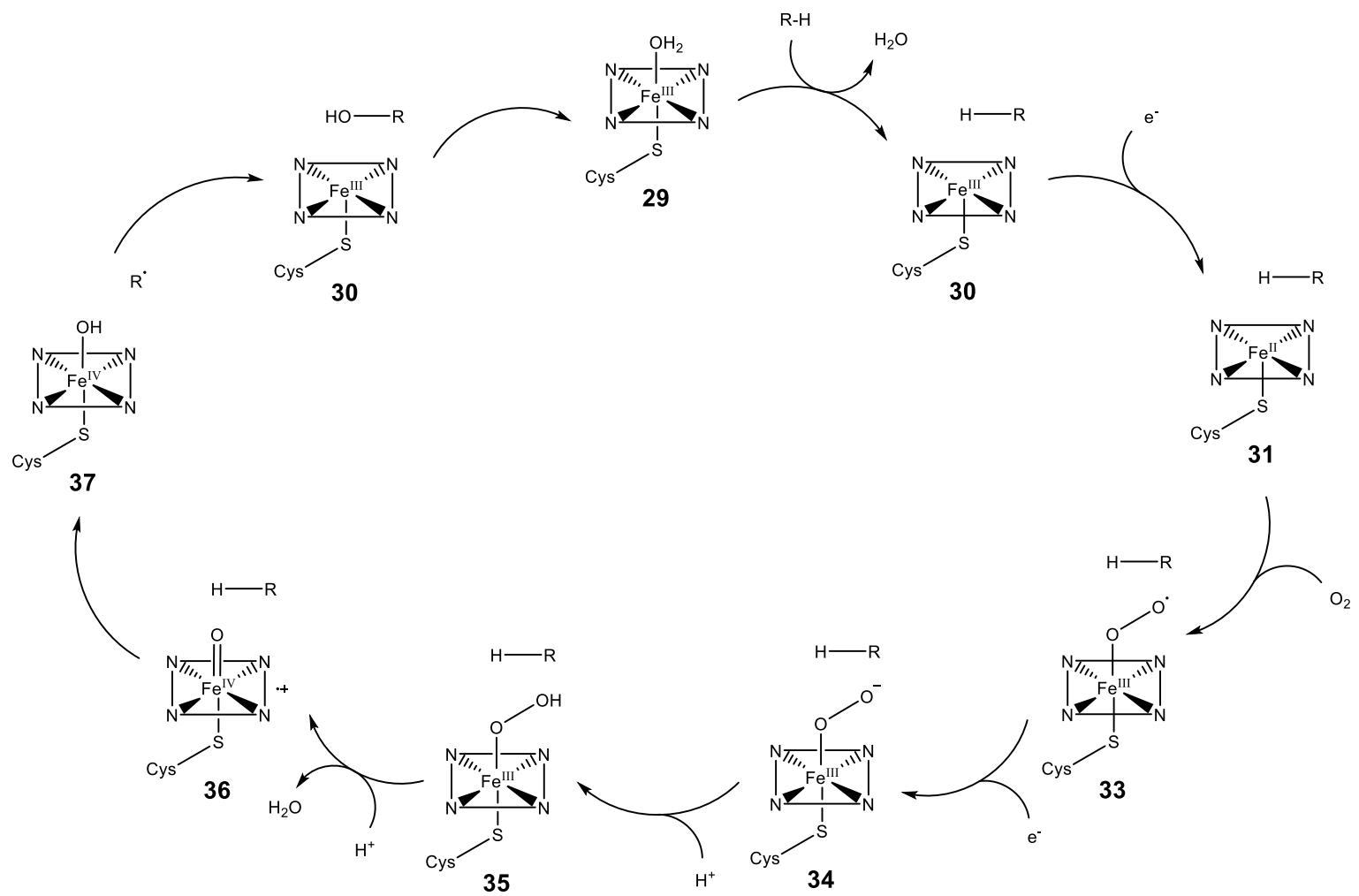
**Scheme 10.** Cytochrome P450 catalytic cycle.[28]

Cytochrome P450 compound 1 was previously believed to exist as an Fe^V oxo porphyrin, but it was just recently characterised as an Fe^{IV} oxo porphyrin radical cation (**36**) in 2010 by Rittle and Green.[26] Spectroscopic and kinetic characterisation was achieved by using a combination of Mössbauer, EPR and UV/vis spectroscopy.[26]

The best characterised enzyme of this class is P450cam, which catalyses the stereospecific hydroxylation of camphor. This reaction has been shown by deuterium labelling to proceed with retention of configuration at the position of hydroxylation (**Scheme 11**). Retention of configuration is generally found in other P450 enzymes.[22] It remains unclear why exactly this outcome is observed in a radical mechanism, however stereospecific hydrocarbon hydroxylations by cytochrome P450 can be attributed to the rigid and stereospecific binding of the substrates to the particular enzyme active sites.[29]
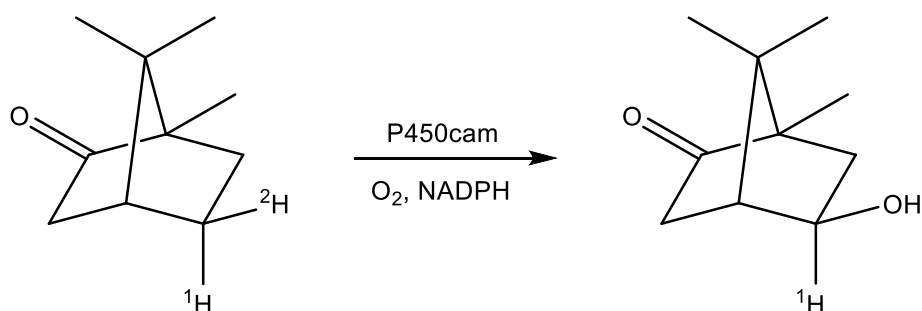

Scheme 11. Stereochemistry of P450cam.[22]

3.1.2 Iron^{IV} oxo Complexes

3.1.2.1 Spin State Effects

One factor that affects the reactivity of both heme and non-heme Fe^{IV} oxo complexes is their ability to change their spin state.[30] In 2009 Bell and Groves reported a highly reactive model compound of cytochrome P450 compound 1 [Fe^{IV}(O)-4-TMPyP]$^+$ (**38**) which demonstrated an extraordinary rate constant (k_2) of C-H bond hydroxylation (2.8 x 10^6 M^{-1} s^{-1}) of xanthene (**39**) at 14.5 °C, using *m*CPBA (**Scheme 12**).[31] This yielded 90% 9-xanthydrol (**40**) with a small amount of xanthone. It was suggested that the high kinetic reactivity observed for **38** could be both the result of a low lying a$_{2u}$ porphyrin HOMO and a facilitated low to high spin state crossing phenomenon during the reaction.
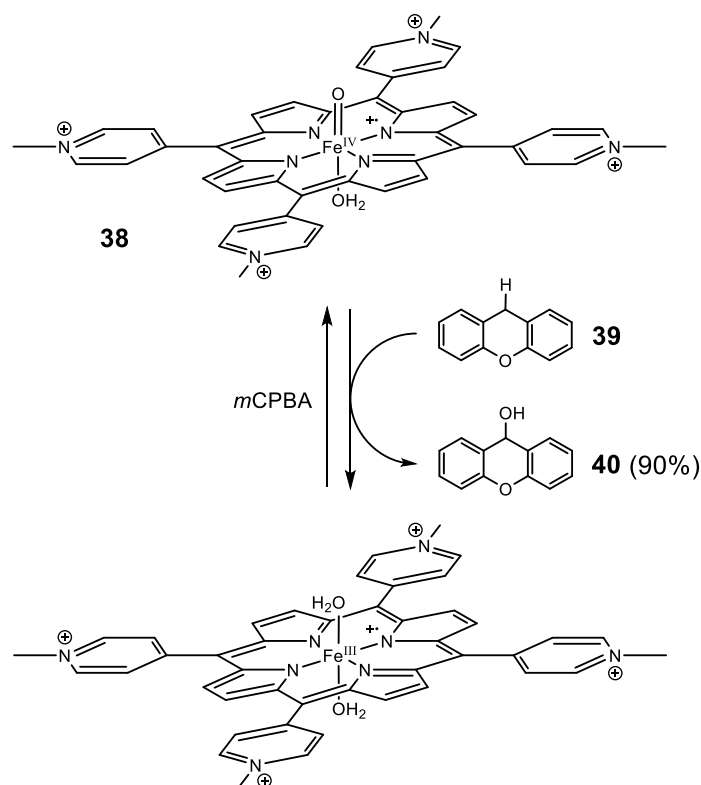
Scheme 12. Hydroxylation of xanthene by [Fe^{IV}(O)-4-TMPyP]$^+$ (**38**).[31]

In 2011 Seo and Kim reported another reactive Fe^{IV} oxo complex, $[Fe^{IV}(O)(Me_3NTB)(MeCN)]^{2+}$ (**41**) which demonstrated very high rate constants of C-H bond hydroxylation over a much broader range of substrates (**Figure 3**).[32] This also demonstrated exceptionally high rate constants of OAT, measuring 2.1×10^4 M^{-1} s^{-1} when tested on PhSMe, however the oxidation of PPh_3 was far too fast to be measured spectroscopically under the same conditions.
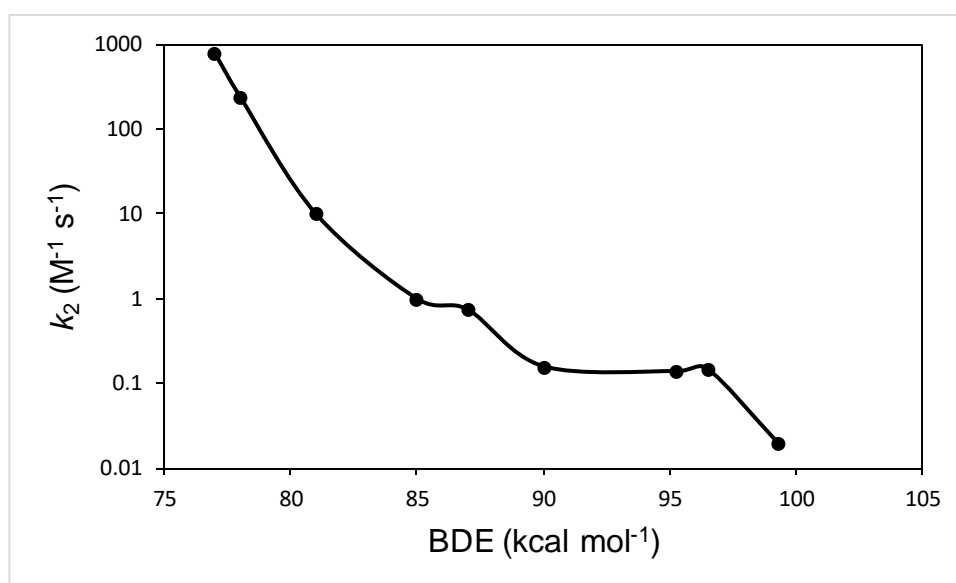
Figure 3. Second order rate constants (k_2) for the oxidation (HAA) of various substrates by $[Fe^{IV}(O)(Me_3NTB)(MeCN)]^{2+}$ (**41**) in MeCN at -40 °C.[32]

DFT calculations have shown the high spin state ($S = 2$) of the complex in its trigonal bipyramidal geometry to be significantly lower in energy than the low spin state ($S = 1$) due to enhancement of charge stabilisation, despite the fact that Mössbauer studies have shown it to be in a low spin state. This is very common as most synthetic non-heme Fe^{IV} oxo complexes are low spin and there are very few examples that high spin in the literature.[33] DFT calculations have also shown the high and low spin states of the complex in its octahedral geometry to be degenerate at room temperature. Therefore,

21

the ligation of a solvent molecule facilitates a very low energy spin crossover from the low spin state (**42**) to the high spin state (**41**) which makes it much more reactive (**Scheme 13**).
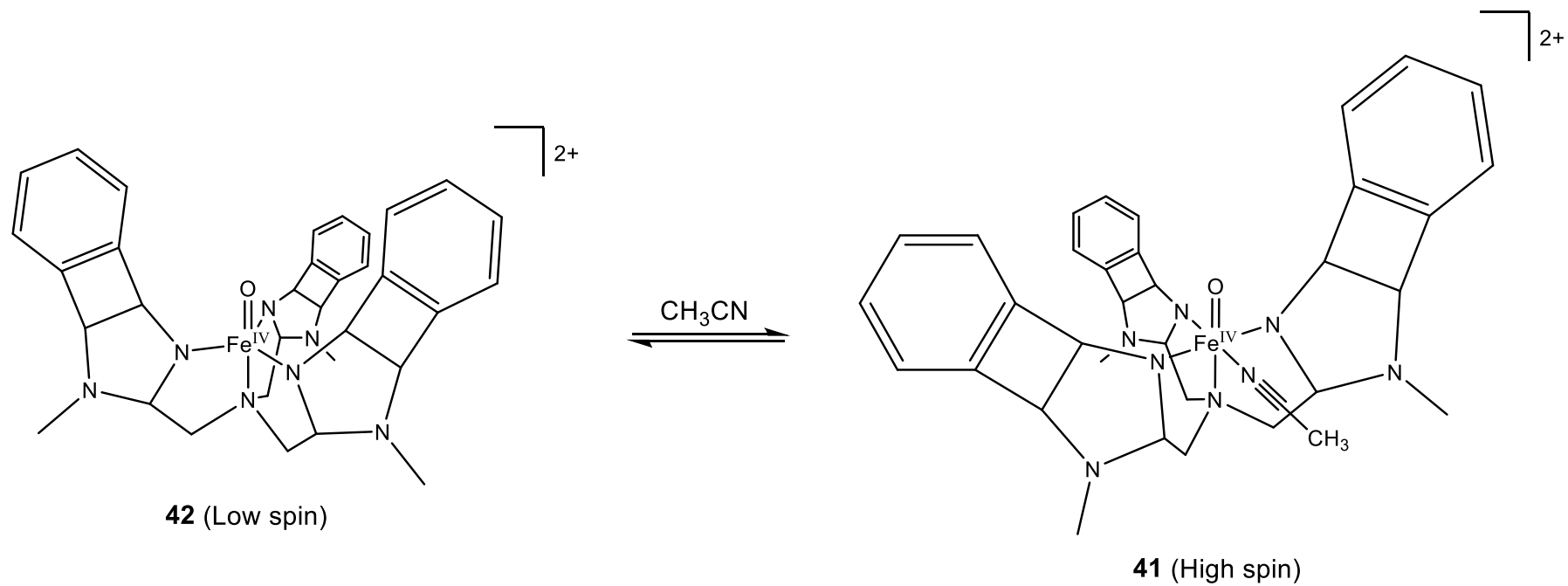
Scheme 13. Geometry equilibrium of $[Fe^{IV}(O)(Me_3NTB)(MeCN)]^{2+}$ **(41)**.[32]

In 2011 Que *et al.* reported another high spin Fe^{IV} oxo complex $[Fe^{IV}(O)(TMG_2dien)(CH_3CN)]^{2+}$ (**43**).[34] Despite being considerably less reactive than the complexes mentioned previously, it was found to be an improvement on its high spin predecessor $[Fe^{IV}(O)(TMG_3tren)]^{2+}$ (**44**) which just undergoes intramolecular ligand hydroxylation (decay) upon Fe oxidation.[35] Complex **43** performs HAA on 9,10-Dihydroanthracene (DHA) 630 times faster than **44** and also performs oxygen atom transfer (OAT) on Ph_3P extremely quickly. The improved stability of **43** is attributed to its tridentate ligand as this provides greater access for substrates to react at the oxo group as opposed to the more sterically encumbered tetradentate ligand of **44** (**Figure 4**). Therefore, **43** will react with substrates faster than with itself.[34]
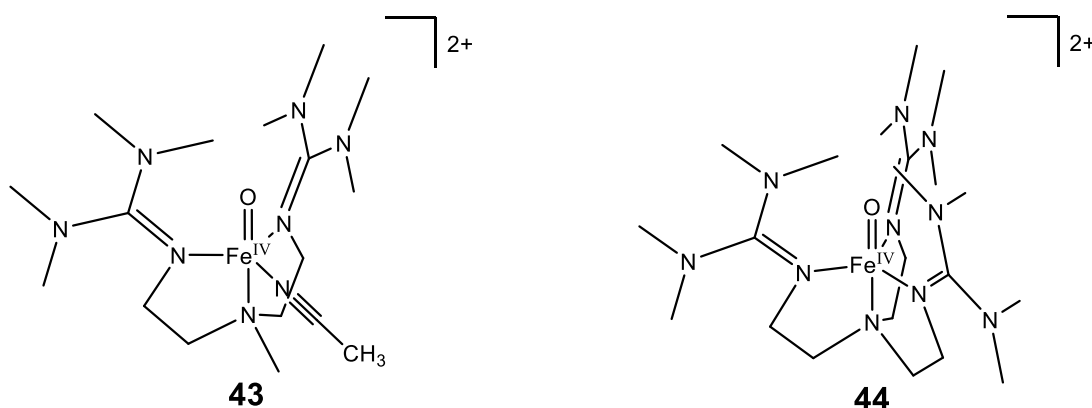

Figure 4. Steric comparison of $[Fe^{IV}(O)(TMG_2dien)(CH_3CN)]^{2+}$ (**43**) and $[Fe^{IV}(O)(TMG_3tren)]^{2+}$ (**44**) complexes.[34,35]

The greater HAA reactivity of high spin Fe^{IV} oxo complexes was rationalised by Que and Solomon.[36] It was found that both low spin ($S = 1$) and high spin ($S = 2$) Fe^{IV} oxo complexes are able to attack the C-H σ bond of a substrate with their unoccupied β-spin Fe-O π* orbitals (d_{xz}/d_{yz}), however the substrate is restricted to a horizontal approach (**Figure 5**). This mechanism is known as the π-FMO pathway. Whereas only high spin ($S = 2$) Fe^{IV} oxo complexes are

able to attack the C-H σ bond of a substrate with their unoccupied α-spin Fe-O σ* orbitals (d_z^2) and the substrate is open to a vertical approach. This mechanism is known as the σ-FMO pathway.

This additional reaction pathway is made possible due to spin-polarization because the unoccupied α-spin Fe-O σ* orbital (d_z^2) is stabilized to lower energies and has much more oxo character in the high spin state than in the low spin state. Therefore, Fe^{IV} oxo complexes are more reactive in their high spin state because they can engage in HAA *via* an additional σ-FMO pathway and this permits the substrate to approach the oxo group from an additional vertical trajectory.[36]
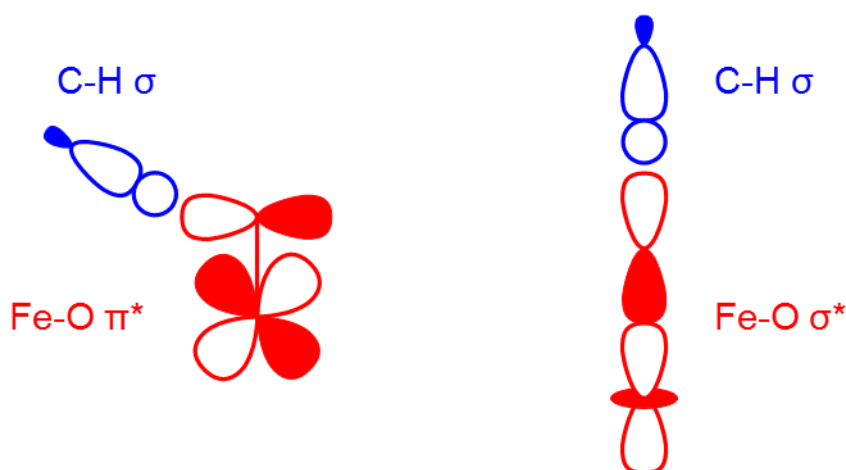
**Figure 5.** Hydrogen atom abstraction *via* the π-FMO pathway (left) and the σ-FMO pathway (right).[36]

3.1.2.2 Axial Ligand Effects

Another factor that affects the reactivity of non-heme Fe^{IV} oxo complexes is the presence of a ligand in the axial position, *trans* to the oxo group.[30] In 2007 Nam *et al.* reported that the various derivatives of $[Fe^{IV}(O)(TMC)(X)]^{n+}$ (**45a/b**) displayed varying rate constants of HAA and OAT towards substrates such as DHA and PPh$_3$, respectively (**Figure 6**).[37] Two different trends in reactivity were observed.

For HAA reactivity: SR > N_3^- > CF_3COO^- > CH_3CN.

For OAT reactivity: CH_3CN > CF_3COO^- > N_3^- > SR.


45a

45b
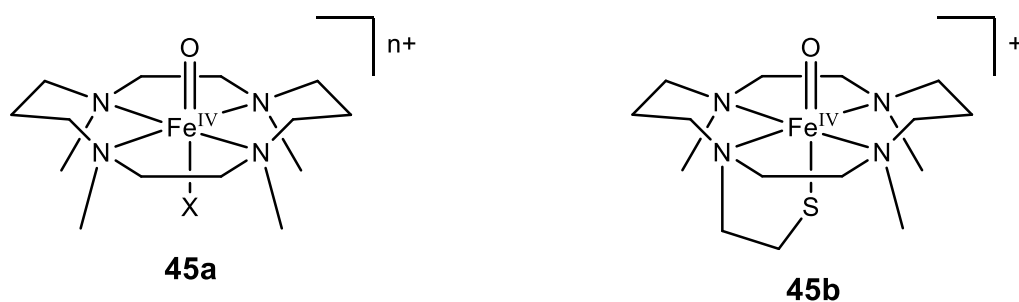
Figure 6. $[Fe^{IV}(O)(TMC)(X)]^{n+}$ (**45a**) and $[Fe^{IV}(O)(TMC)(SR)]^+$ (**45b**) complexes. X represents the different axial ligands: CH_3CN, CF_3COO^-, N_3^-, and SR (R represents S tethered to one of the equatorial N donors by a CH_2CH_2 group).[38]

The OAT reactivity trend correlates with increasing reduction potential (E_{red}) in which the most electron-withdrawing ligand (π-acidic) gives the highest reaction rate constant (k_2), and this is intuitive as the oxidation reaction is driven by the electrophilicity of the Fe^{IV} complex. However, the HAA reactivity trend correlates with decreasing E_{red} in which the most electron-donating ligand (π-basic) gives the highest reaction rate constant, and this is counter-

intuitive as the oxidation reaction is not driven by the electrophilicity of the Fe^{IV} complex (**Figure 7**). DFT calculations show that more electron-donating ligands compete with the oxo group for the Fe d_π orbitals which weakens the Fe^{IV}=O bond, making the oxo group more basic (higher pK_a) and forming a stronger O-H bond.[38] However, the O-H BDE has been shown to be independent of the ligand donor ability.[37,39] A two-state reactivity was instead postulated, in which the more electron-donating axial ligands increase the contribution from the more reactive high spin state as Fe^{IV} oxo complexes were believed to consist of a blend of both of their low spin and high spin states.[39,40]
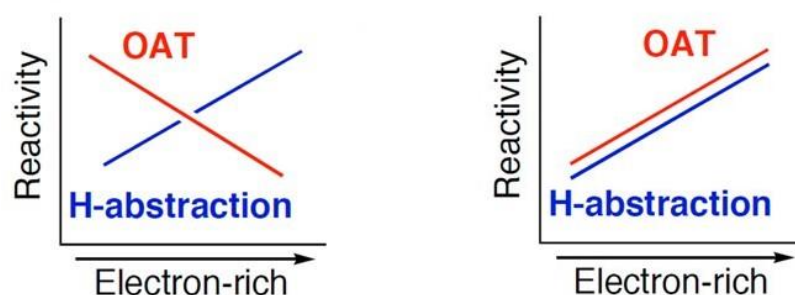

Figure 7. HAA and OAT reactivity trends of non-heme Fe^{IV} oxo complexes (left) and of heme Fe^{IV} oxo complexes (right).[39] Reproduced with permission of the publisher.

However, these reactivity trends are very different for heme Fe^{IV} oxo complexes. Nam later reported that the various derivatives of $[Fe^{IV}(O)(TMP^{\cdot+})(p\text{-}Y\text{-}PyO)]^+$ (**46**) displayed varying rate constants of HAA and OAT towards substrates such as xanthene and cyclohexene, respectively (**Figure 8**).[39] The same reactivity trend was observed for both HAA and OAT reactions: OCH_3 > CH_3 > H > Cl.

Both the HAA and OAT reactivity trends correlate with decreasing E_{red} in which the most electron-donating ligand gives the highest reaction rate

constant (**Figure 7**). This change in the OAT reactivity trend can be explained by the fact that heme Fe^{IV} oxo complexes (Fe^{IV} oxo porphyrins) are generally more electrophilic than non-heme Fe^{IV} oxo complexes. Therefore, more electron-donating ligands compete with the oxo group for the Fe d_{π} orbitals which weakens the $Fe^{IV}=O$ bond and encourages OAT when in the presence of the appropriate substrate. OAT could be viewed as the more favourable route as it is a 2 electron oxidation, whereas HAA is only a 1 electron oxidation.

46
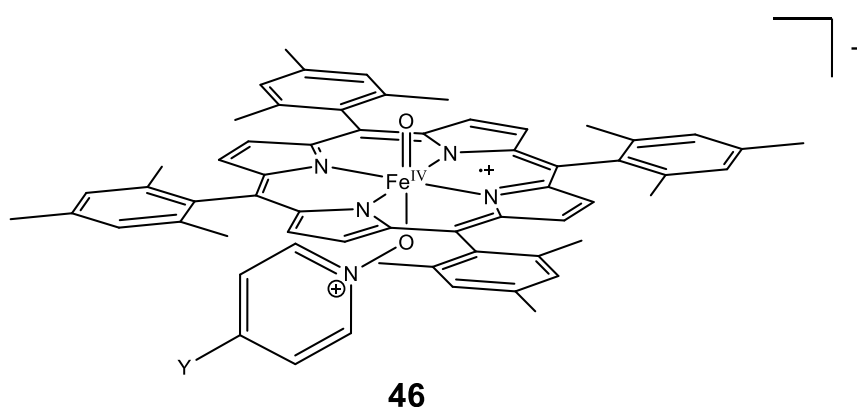
Figure 8. $[Fe^{IV}(O)(TMP^{\cdot+})(p\text{-}Y\text{-}PyO)]^+$ complex (**46**). Y represents the different *para* substituents on the axial pyridine *N*-oxide: OCH$_3$, CH$_3$, H and Cl.[39]

Interestingly, Chang *et al.* reported a thermally stable and water-soluble Fe^{IV} oxo complex $[Fe^{IV}(O)(Py_5Me_2\text{-}X)]^{2+}$ (**47**) which is capable of hydroxylating and epoxidizing the sodium salts of ethyl sulfonate and styrene sulfonate in H$_2$O at 25 °C (**Figure 9**).[41] The same reactivity trend was observed for both HAA and OAT reactions: CF$_3$ > H > CH$_3$. Unlike the complexes mentioned previously, both the HAA and OAT reactivity trends correlate with decreasing E$_{red}$ in which the most electron-withdrawing ligand gives the highest reaction rate constant. However, these reaction rate constants only vary by less than 10-fold, compared to **45a/b** and **46** which vary by orders of magnitude.[37,38,39]
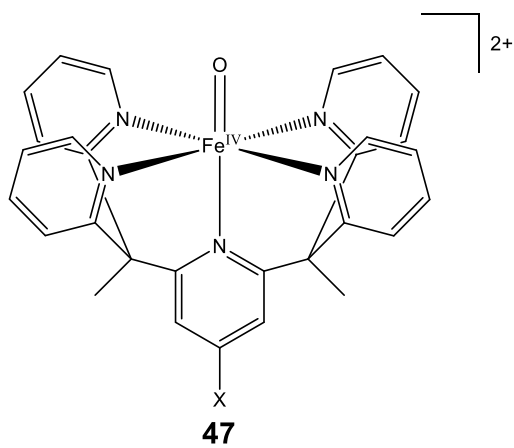
Figure 9. [Fe^{IV}(O)(Py$_5$Me$_2$-X)]$^{2+}$ complex (**47**). X represents the different *para* substituents on the axial pyridine: CF$_3$, H and CH$_3$.[41]

3.1.2.3 **Proton and Metal Coupled Electron Transfer**

Another factor that affects the reactivity of non-heme Fe^{IV} oxo complexes is the binding of redox-inactive metal ions and protons to the oxo group.[30] In 2014, Park *et al.* investigated the binding of $Sc^{III}(OTf)_3$ and also HOTf to $[Fe^{IV}(O)(N_4Py)]^{2+}$ (**48**) (**Figure 10**) and how this binding affects the HAA and OAT reaction rate constants of various toluene and thioanisole derivatives, respectively.[42]


48
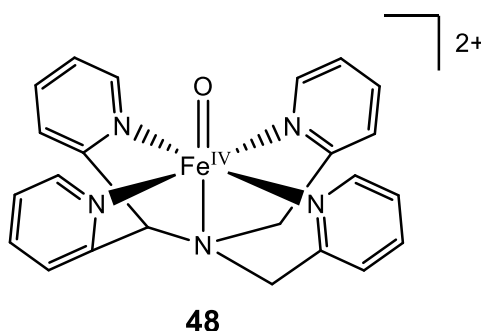
Figure 10. $[Fe^{IV}(O)(N_4Py)]^{2+}$ complex (**48**).[42]

It was found that the binding of protons and metal ions both give overall higher rate constants of HAA and OAT. However, protons give significantly higher oxidation rate constants than metal ions. However, no KIE was observed in the HAA reactions when toluene was compared with toluene-d_8 and this led to the discovery that instead of a single HAA step, the reaction actually proceeds *via* a stepwise electron transfer from the substrate to **48**, followed by a proton transfer. This is very unusual behaviour as a large KIE is a very common feature of Fe^{IV} oxo complexes, in which it is believed that HAA occurs *via* hydrogen tunnelling in the rate-determining step (RDS). This process is known as proton-coupled electron transfer (PCET) when protons

bind to the oxo group and metal-coupled electron transfer (MCET) when metal ions bind to the oxo group.[42,43,44]

It is widely believed that two protons bind to an oxo group in PCET and two metal ions bind to an oxo group in MCET. In both cases the binding of Lewis acids induces a lengthening of the metal-oxygen bond in the oxo group, but this occurs to a smaller extent in MCET and the fact that it is smaller here is probably due to the steric effect of two $Sc^{III}(OTf)_3$ molecules bound to the oxo group. However, the binding of two $Sc^{III}(OTf)_3$ molecules to an oxo group has only ever been inferred by kinetic studies, whereas the binding of just one $Sc^{III}(OTf)_3$ molecule to the oxo group in $[Fe^{IV}(TMC)(O)- Sc(OTf)_4]^{2+}$ (**49**) has actually been detected by X-ray crystallography to date (**Figure 11**).[45]
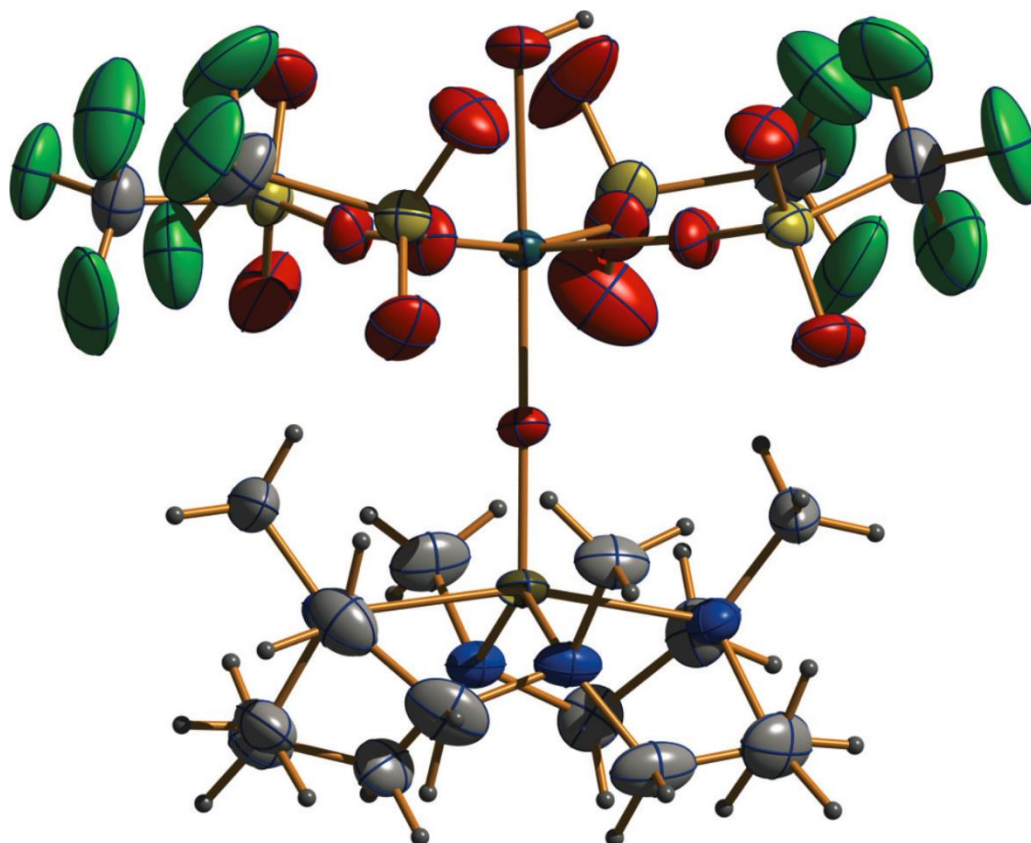
47

Figure 11. X-ray crystal structure of $[Fe^{IV}(TMC)(O)- Sc(OTf)_4]^{2+}$ (**49**).[45] Reproduced with permission of the publisher.

In previous work on MCET using **48** and 2,5-dimethoxybenzyl alcohol (**50**), oxidative coupling between benzyl alcohol radical cations (**51**) was observed by EPR spectroscopy, yielding 2,2',5,5'-tetramethoxybiphenyl-4,4'-dimethanol (**52**) as the major product (31%), 2,5-dimethoxybenzaldehyde (**53**) as the minor product (10%) and also 1% tetramethoxybiphenyl-4,4'-dicarbaldehyde (**54**) (**Scheme 14**).[44] The main inorganic products were $[Fe^{III}(OH)(N_4Py)]^{2+}$ and $[Fe^{III}(OCH_2C_6H_3(OMe)_2)(N_4Py)]^{2+}$ which indicates that **48** acts as a 1 electron oxidant rather than a 2 electron oxidant and therefore further confirms that the reaction proceeds by a MCET mechanism. This reaction then yielded 50% **53** when performed in the absence of Sc^{3+}, indicating that it proceeds by the traditional HAA mechanism.
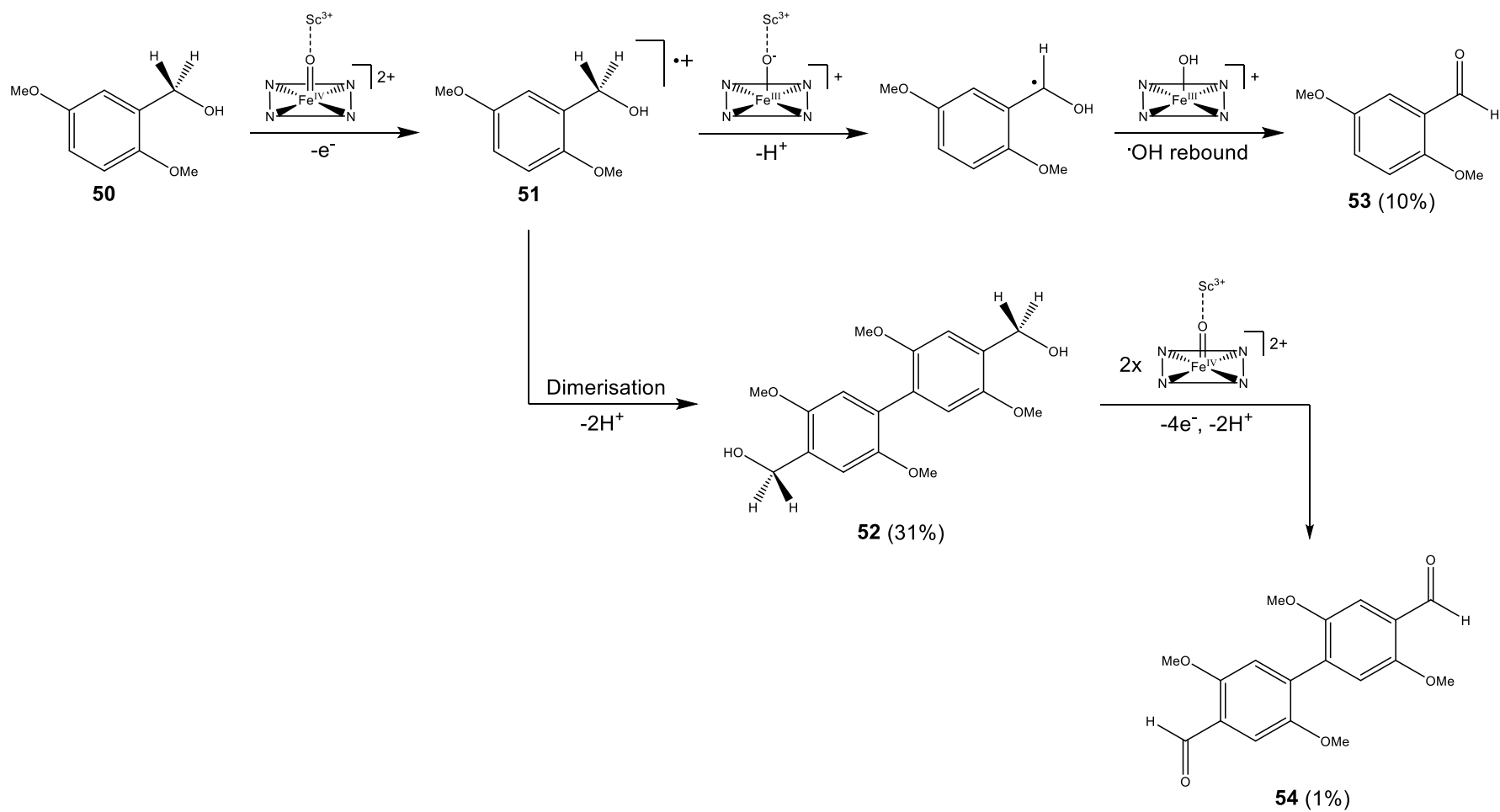
Scheme 14. Proposed reaction pathways for the oxidation of 2,5-(MeO)$_2$C$_6$H$_3$CH$_2$OH (**50**) by [Fe^{IV}(O)(N4Py)]$^{2+}$ (**48**) in the presence of Sc^{3+}.[44]

As a consequence of this reaction mechanism, PCET and MCET also differ from HAA in that the rate constant of oxidation depends on the driving force of electron transfer ($-\Delta G_{et}$) from the substrate to the Fe^{IV} oxo complex instead of the substrate's C-H BDE.[42,43,44] The rate of oxidation is measured experimentally as a pseudo-first-order rate constant (k_f) by measuring the decrease in absorbance of the Fe^{IV} oxo complex at 695 nm, in the presence of an excess of HOTf or $Sc^{III}(OTf)_3$ and at various concentrations of the substrate, at 298 K. The rate constant of electron transfer (k_{et}) is then determined as a second-order rate constant from the slope of the plot of k_f vs concentration of the substrate.

Alternatively, k_{et} can be represented by the Marcus equation of electron transfer:

$$k_{et} = Z\exp[-(\lambda/4)(1 + \Delta G_{et}/\lambda)^2/k_B T]$$

Z is the frequency factor, which is $(k_B T K)/h$. λ is the reorganisation energy of electron transfer, k_B is the Boltzman constant, T is the absolute temperature, h is Planck's constant and K is the formation constant of the precursor complex which forms when the substrate gets close to the Fe^{IV} oxo complex. Therefore, electron transfer is fast when K is large and this is the reason why PCET is faster than MCET as the steric bulk of $Sc^{III}(OTf)_3$ hinders the formation of a precursor complex. Also, $-\Delta G_{et}$ can be derived from the following equation:

$$-\Delta G_{et} = e(E_{red} - E_{ox})$$

E_{red} is the one electron reduction potential of the Fe^{IV} oxo complex in the presence of HOTf or $Sc^{III}(OTf)_3$. E_{ox} is the one electron oxidation potential of the substrate and e is the elementary charge, which is the electric charge of a single proton (1.602×10^{-19} C). E_{red} and E_{ox} are both measured experimentally *via* cyclic voltammetry.

k_{et} and E_{red} are also measured in the absence of HOTf and $Sc^{III}(OTf)_3$ and the resulting $\log k_{et}$ and $-\Delta G_{et}$ values are plotted and compared with those

measured in the presence of HOTf and $Sc^{III}(OTf)_3$. Interestingly, when $-\Delta G_{et}$ of PCET and MCET is more negative than -0.5 eV the reaction mechanism changes from PCET/MCET to HAA and OAT and this, therefore, results in a borderline between the different reaction mechanisms (**Figure 12**). It is believed that when $-\Delta G_{et}$ is more negative than -0.5 eV the HAA route is more energetically favourable than the highly endergonic PCET/MCET route.[42]
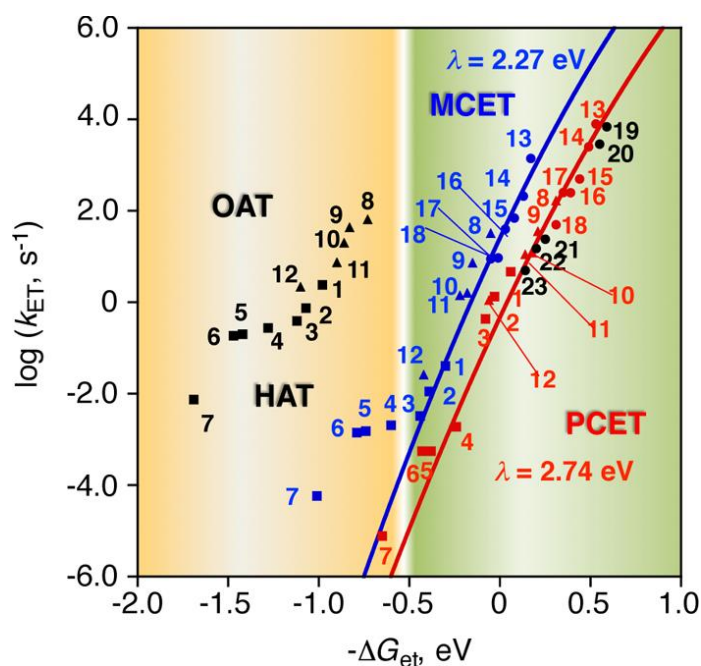
Figure 12. Plots of log k_{et} for C-H bond cleavage of toluene derivatives and sulfoxidation of thioanisole derivatives [hexamethylbenzene (1), 1,2,3,4,5-pentamethylbenzene (2), 1,2,4,5-tetramethylbenzene (3), 1,2,4-trimethylbenzene (4), 1,4-dimethylbenzene (5), 1,3,5-trimethylbenzene (6), toluene (7), *p*-Me-thioanisole (8), thioanisole (9), *p*-Cl-thioanisole (10), *p*-Br-thioanisole (11) and *p*-CN-thioanisole (12)] by **48** in the absence (black) and presence of acids (10 mM), HOTf (red) and Sc^{III}(OTf)$_3$ (blue), in MeCN at 298 K vs the driving force of electron transfer [-ΔG = e(E$_{red}$ − E$_{ox}$)] from toluene derivatives (squares) and thioanisole derivatives (triangles) to **48** in the presence of HOTf (red) and Sc^{III}(OTf)^3 (blue). The red and blue circles show the driving force dependence of the rate constants (log k_{et}) of electron transfer from electron donors [[Fe^{II}(Ph$_2$phen)$_3$]$^{2+}$ (13), [Fe^{II}(bpy)$_3$]$^{2+}$ (14), [Ru^{II}(4,4'-Me$_2$phen)$_3$]$^{2+}$ (15), [Ru^{II}(5,5'-Me$_2$phen)$_3$]$^{2+}$ (16), [Fe^{II}(Clphen)$_3$]$^{2+}$ (17) and [Ru^{II}(bpy)$_3$]$^{2+}$ (18)] to **48** in the presence of acids (10 mM), HOTf and Sc^{III}(OTf)$_3$, in MeCN at 298 K, respectively. The black circles show the driving force dependence of the rate constants (log k_{et}) of electron transfer from electron donors [decamethylferrocene (19), octamethylferrocene (20), 1,1'-dimethylferrocene (21), *n*-amylferrocene (22) and ferrocene (23)] to **48** in the absence of acids in MeCN at 298 K.[42] Reproduced with permission of the publisher.

As mentioned previously, it was found that the binding of protons and metal ions to the oxo group of **48** gives overall higher rate constants of oxidation of various thioanisole derivatives. It was proposed that the electron transfer step in PCET and MCET may be followed by a rapid $O^{\cdot-}$ transfer to produce the corresponding sulfoxide derivatives and $[Fe^{II}(N_4Py)]^{2+}$, which is also oxidized to $[Fe^{III}(N_4Py)]^{3+}$ by **48** in the presence of HOTf and $Sc^{III}(OTf)_3$. However, this reaction mechanism is yet to be clarified.[42]

3.1.3 Iron^V oxo Complexes

3.1.3.1 Tetra Amido Macrocyclic Ligands (TAML)

In contrast to Fe^{IV} oxo complexes, there are fewer examples of Fe^V oxo complexes that engage in C-H bond hydroxylation *via* HAA.[33]

In 2007 Collins and Que reported the first synthesis and characterisation of an Fe^V oxo complex [Fe^V(O)(TAML-CMe2)]$^-$ (**55**); this is also known as a first generation TAML activator.[46] **55** was generated from the starting complex [Fe^{III}(H2O)(TAML-CMe2)]$^-$ (**56**) using 1 equivalent of *m*CPBA in MeCN at -40 °C and demonstrated high HAA reactivity when tested on cumene, ethylbenzene and DHA (**Scheme 15**). The four amide groups in the TAML were found to be strongly electron-donating towards the Fe centre, supporting it in its fifth oxidation state. However, this was only relatively stable to decay at temperatures below -40 °C, above which electron transfer from the phenyl group to the Fe centre takes place and results in an Fe^{IV} complex that is unreactive to HAA. Decay is an extremely fast process! Also, **55** was observed in its low spin state which is different from all the previous examples of Fe^{IV} oxo complexes.
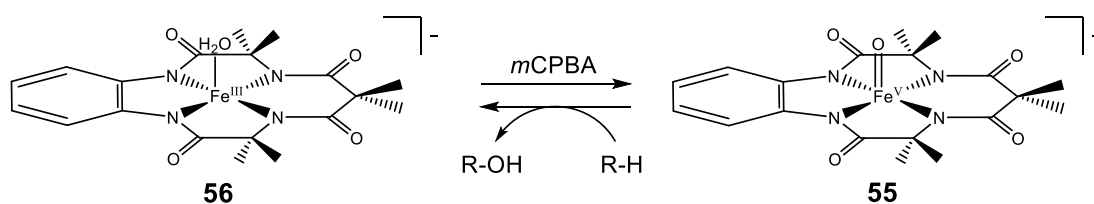
Scheme 15. [Fe^V(O)(TAML-CMe2)]$^-$ (**55**) hydroxylation cycle.[46]

Further work by Collins revealed that comproportionation is another rate-limiting factor, in which an electron is transferred from a reduced Fe^{III} complex to an unreacted Fe^V complex to produce a stable (Fe^{IV})2O dimer

complex (**57**) that is unreactive to HAA.[47] This process is fast and competes with hydroxylation. However, it is not as fast as decay. When derivatives of $[Fe^V(O)(TAML-CR_2)]^-$ were tested towards comproportionation in which R represents the different TAML tail group substituents: Me and Et, it was found that comproportionation between $[Fe^{III}(H_2O)(TAML-CEt_2)]^-$ (**58**) and $[Fe^V(O)(TAML-CEt_2)]^-$ (**59**) occurred 1000 times slower (**Scheme 16**). Therefore, this process is modulated by steric effects and can be decreased by the use of larger substituents on the TAML.
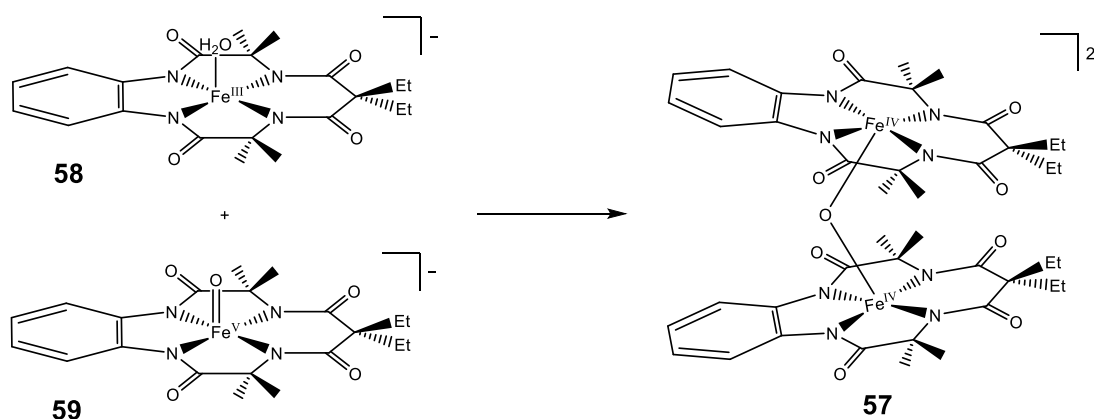

Scheme 16. Comproportionation.[47]

Complexes **55** and **59** both demonstrated extraordinary rate constants of sulfide oxidation when tested on various *para*-thioanisole derivatives (**Table 2**).[47] However, unlike the previous examples of Fe^{IV} oxo complexes which just react *via* conventional OAT, these extremely reactive Fe^V oxo complexes exhibit both OAT and ET in which an Fe^V oxo complex can undergo a 2 electron reduction to produce an Fe^{III} complex and PhS(O)Me and also a 1 electron reduction to produce an Fe^{IV} complex and $PhS^{+\cdot}Me$, which is believed to react with O_2 to form PhS(O)Me. Interestingly, it was found that the ET pathway is favoured for electron poor sulfides and the OAT pathway is favoured for electron rich sulfides. However, OAT dominates only slightly over ET and it is unknown how these reaction pathways compare (k^{OAT}/k^{ET})

for **55** as fast comproportionation also produces an Fe^{IV} complex. Also, it was found that the $(Fe^{IV})_2O$ dimer complex engages in OAT to produce two Fe^{III} complexes and one PhS(O)Me, but this occurs 10000 times slower than with **55** or **59**.[47]

X	R = Et (**59**)			R = Me (**55**)	
	K_1/M^{-1}	$k_{II}/M^{-1}\ s^{-1}$	k^{OAT}/k^{ET}	K_1/M^{-1}	$k_{II}/M^{-1}\ s^{-1}$
MeO	-	5000	-	-	9000
Me	800	600	1.9	-	3900
H	210	190	0.88	500	450
Cl	-	80	0.57	-	165
CN	-	4.4	0.2	23	13

**Table 2.** Rate (k_{II}) and equilibrium (K_1) constants for the oxidations of *p*-XC_6H_4SMe by $[Fe^V(O)(TAML-CMe_2)]^-$ (**55**) and relative contributions of the OAT and ET pathways (k^{OAT}/k^{ET}) for $[Fe^V(O)(TAML-CEt_2)]^-$ (**59**) in MeCN at -40 °C.[47]

In 2014 Collins *et al.* significantly improved the first generation **55** system by replacing the CMe_2 group in the six-membered macrocyclic subring with a NMe group to produce an Fe^V oxo complex $[Fe^V(O)(TAML-NMe)]^-$ (**60**) and this is also known as a fifth generation TAML activator (**Figure 13**).[48] This was generated from the starting complex $[Fe^{III}(Cl)(TAML-NMe)]^{2-}$ (**61**) using 1.2 equivalents of *m*CPBA in MeCN at 25 °C and demonstrated an unprecedented high thermal stability whilst also demonstrating the ability to hydroxylate a series of alkanes with C-H BDEs ranging from 84.5 kcal mol^{-1} to 99.3 kcal mol^{-1}.

60
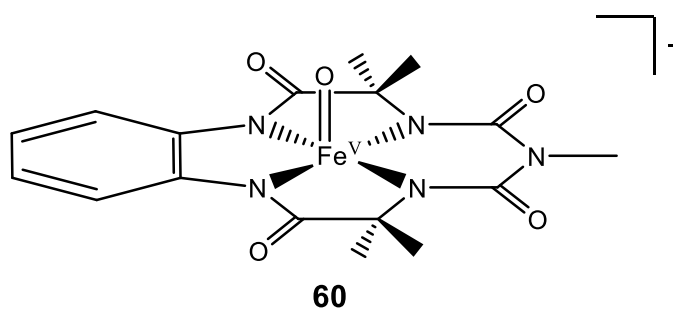
Figure 13. $[Fe^{V}(O)(TAML-NMe)]^{-}$ complex (**60**).[48]

The reaction of **60** with cyclohexane, with the exclusion of O_2 yielded 42% oxidized product, with a rate constant of 2.26×10^{-2} M^{-1} s^{-1} and an alcohol to ketone ratio of 9:1. It is believed that the six-membered macrocyclic subring allows electron donation from the NMe group and subsequent delocalisation of electron density throughout the ring, therefore supporting Fe in its fifth oxidation state; this was evident in electrochemical studies in which the E_{ox} of **61** was found to be 230 mV lower than its Fe^{III} first generation predecessor **58**.[49] However, the rate constant of comproportionation between **61** and **60** was found to be twice that between **56** and **55** due to the smaller steric effect of the NMe group. A significant KIE was observed when substrate toluene was compared with toluene-d_8 at 25 °C which supports the conclusion that the abstraction of a H atom from the substrate's C-H bond is the RDS (**Scheme 17**).[48]
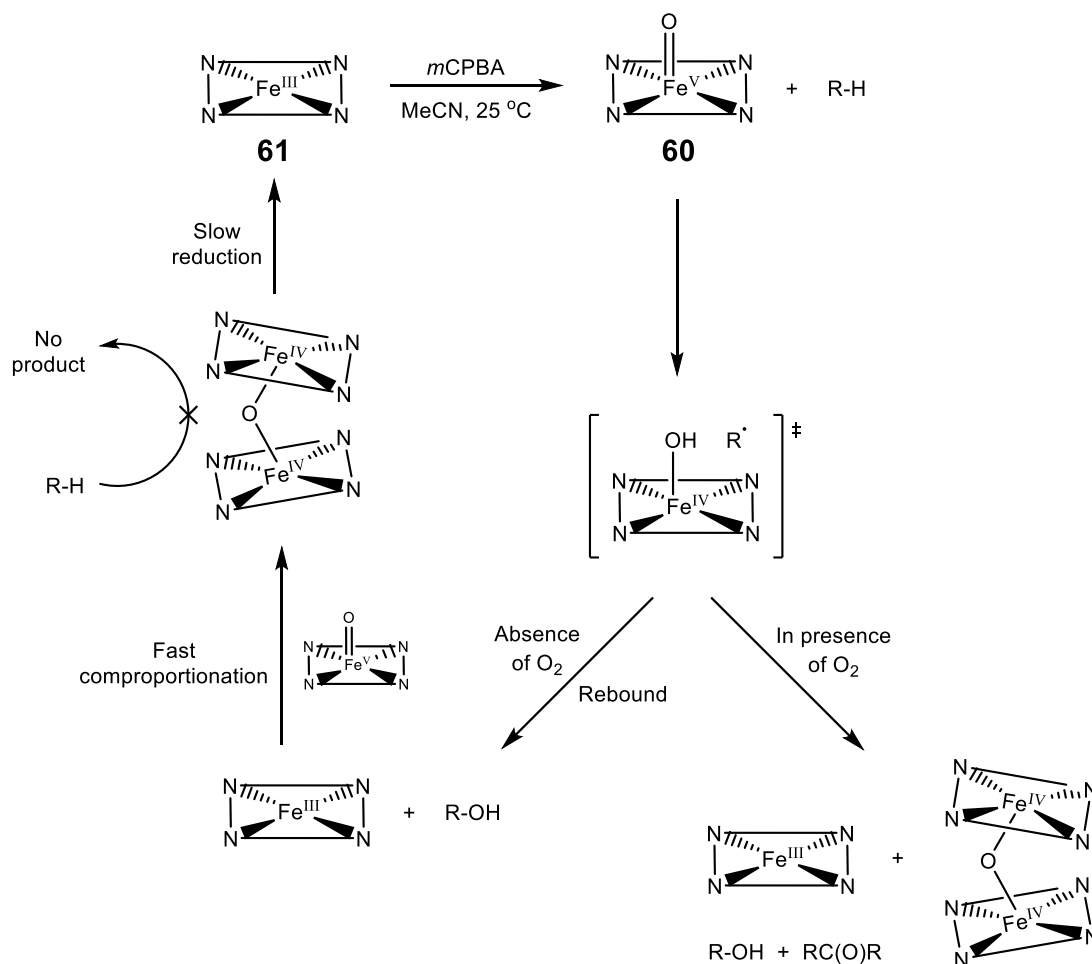
Scheme 17. Proposed reaction mechanism for the oxidation of cyclohexane by $[Fe^V(O)(TAML-NMe)]^-$ (**60**).[48]

As mentioned earlier, a large KIE is a very common feature of Fe^{IV} oxo complexes in which it is believed that HAA occurs *via* hydrogen tunnelling in the RDS.[50] Also, 35% of the cyclohexanol product was found to be enriched with O^{18} when 55% O^{18} labelled **60** was tested which supports the OH rebound mechanism.[48]

The OH rebound step is quite intuitive, however Nam disputed this mechanism in favour of an oxygen non-rebound mechanism in which a dissociation step takes place between the $Fe^{IV}(OH)$ complex and the alkyl radical, and this was supported by both experimental and DFT studies.[51] In

the experimental study cyclohexane was added to a MeCN solution of **55** and CCl3Br, under an Ar atmosphere and bromocyclohexane was found to be the sole product in the reaction, which demonstrates that the alkyl radical can react with molecules outside the Fe(OH)-substrate cage (**Scheme 18**). Also, the oxidation of ethylbenzene by **55** results in the formation of the monomeric species [Fe^{IV}(mCBA)(TAML-CMe2)]$^-$ which occurs 10 times faster than the natural decay of **55**.
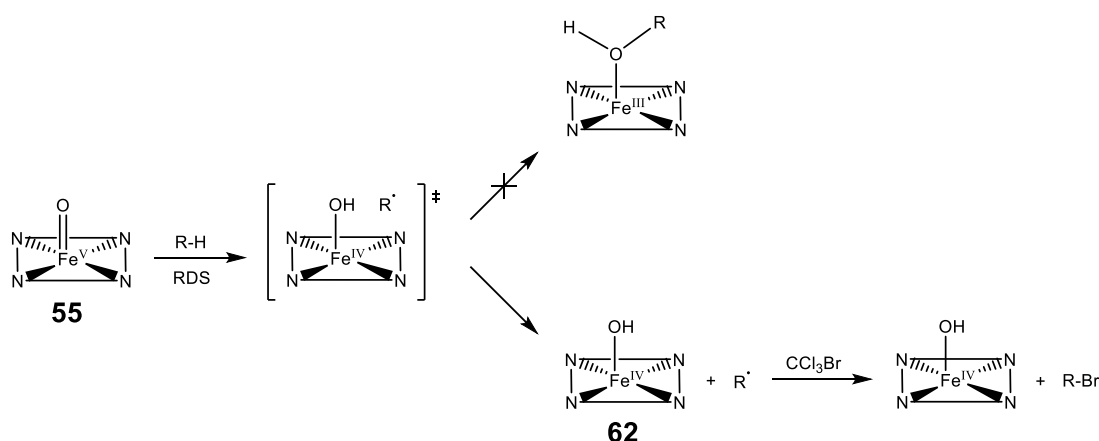
Scheme 18. Proposed dissociative mechanism.[51]

In the DFT study three possible reaction pathways were explored for the DFT optimised [Fe^{IV}(OH)(TAML-CMe2)]$^-$ complex (**62**) and the alkyl radical:

(1) OH rebound takes place to give the hydroxylated product.

(2) Another H atom is abstracted to give the desaturated product.

(3) The alkyl radical dissociates from **62**.

The dissociation pathway was found to be the most energetically favourable route as it only required a dissociation energy of 1.6 kcal mol^{-1} (**Figure 14**). Therefore, it is believed that dissociation of the alkyl radical from **62** is favoured over the OH rebound step and that the alkyl radical continues on to react with a second Fe^V oxo complex to produce the oxidized product.
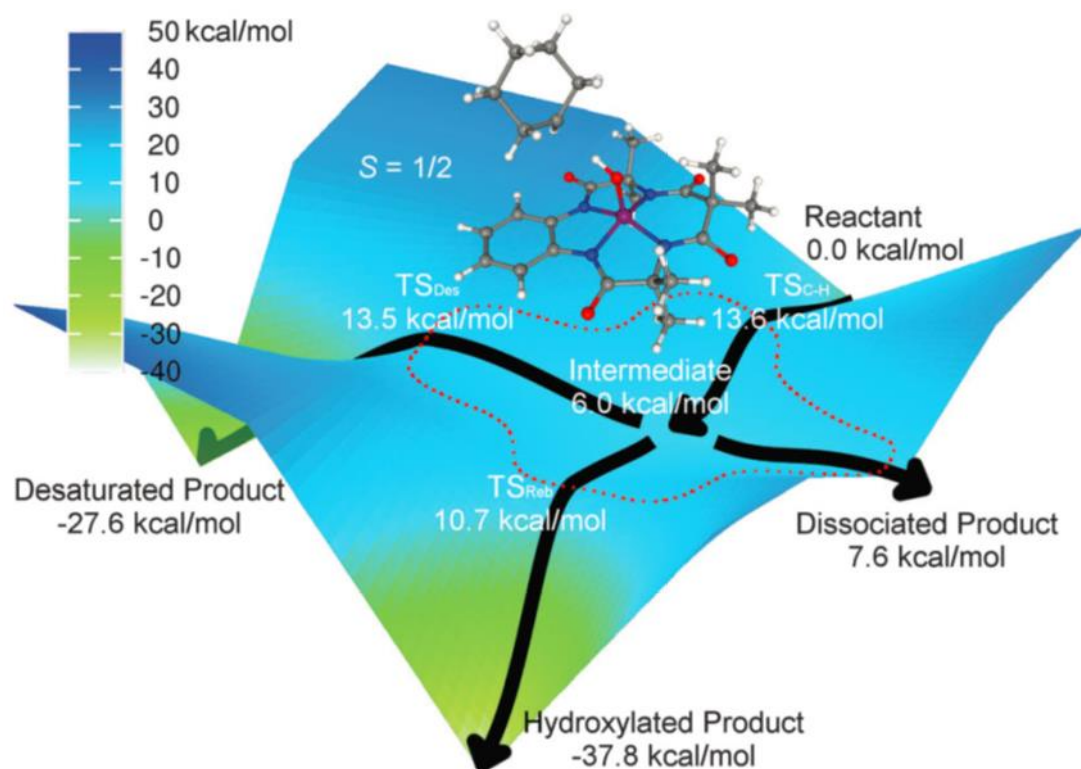
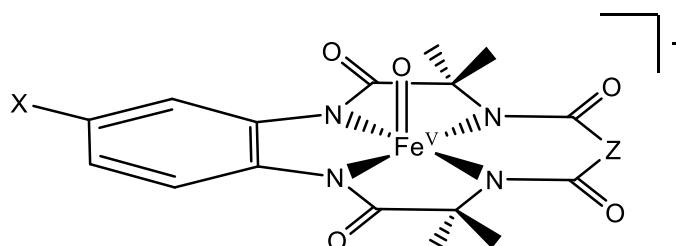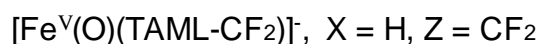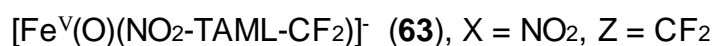**Figure 14.** Potential energy surface of $[Fe^{IV}(OH)(TAML\text{-}CMe_2)]^-$ (**62**).[51] Reproduced with permission of the publisher.

Other improvements can be made to first generation TAML activators by the use of electron-withdrawing groups in both the head (X) and tail (Z) parts of the macrocycle (**Figure 15**). In 2015 Collins *et al.* reported a complex which included a NO_2 group on the aromatic head and a CF_2 group on the malonyl tail, $[Fe^V(O)(NO_2\text{-}TAML\text{-}CF_2)]^-$ (**63**) and its oxidative reactivity towards cyclohexane, ethylbenzene and thioanisole exceeds that of **55** by 2.6, 2.1 and 4.3 times, respectively.[52] This is the most reactive TAML activator; however unlike **60** it is only stable to oxidative decay at -40 °C. The higher HAA and OAT reactivity of **63** is a result of the higher Lewis acidity of the starting complex $[Fe^{III}(H_2O)(NO_2\text{-}TAML\text{-}CF_2)]^-$ as this should be much more reactive towards *m*CPBA in the oxidation process. It is believed that the higher Lewis acidity enhances the coordination of the OH group of the peroxyacid, which then enhances proton transfer to the carbonyl oxygen and this facilitates rapid O-O bond heterolysis.

Previous work by Collins investigated the individual effects of these electron-withdrawing groups on **63**.[53] The CF_2 group on the malonyl tail was found to decrease the rate constant of proton-induced demetalation by 10^{10}-fold and completely eliminate buffer ion-induced demetalation compared to **55**. This also increases the rate constants of HAA and OAT towards various substrates; however it also significantly increases the rate constant of oxidative decay which counteracts its effectiveness. The NO_2 group on the aromatic head was found to increase the rate constants of HAA and OAT towards various substrates and also decrease the rate constant of oxidative decay compared to **55** as this inhibits electron transfer from the phenyl group to the Fe centre. Therefore, a CF_2 group on the malonyl tail (Z) increases the complex's reactivity, whilst a NO_2 group on the aromatic head (X) increases the complex's lifetime. However, utilizing both of these effects results in a TAML activator that is far superior to **55**, as mentioned previously.

Figure 15. Various $[Fe^V(O)(TAML)]^-$ complexes: [47,48,52,53]

$[Fe^V(O)(TAML\text{-}CMe_2)]^-$ (**55**), X = H, Z = CMe_2

$[Fe^V(O)(TAML\text{-}CEt_2)]^-$ (**59**), X = H, Z = CEt_2

$[Fe^V(O)(TAML\text{-}NMe)]^-$ (**60**), X = H, Z = NMe

$[Fe^V(O)(NO_2\text{-}TAML\text{-}CF_2)]^-$ (**63**), X = NO_2, Z = CF_2

$[Fe^V(O)(TAML\text{-}CF_2)]^-$, X = H, Z = CF_2

$[Fe^V(O)(NO_2\text{-}TAML\text{-}CMe_2)]^-$, X = NO_2, Z = CMe_2
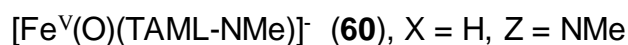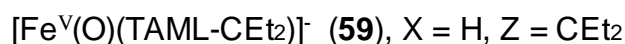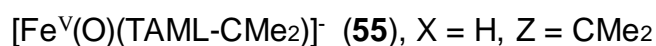
3.1.3.2 **Pentadentate Monoamido Ligands**

Another impressive class of ligands that are capable of tuning the properties of an Fe^V oxo group are pentadentate monoamido ligands.[33]
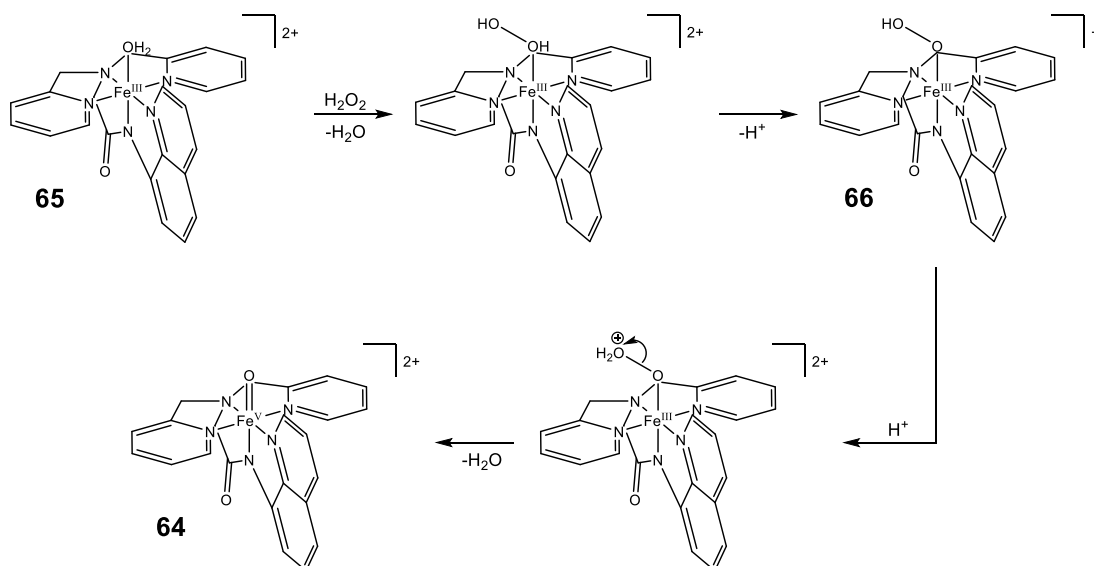
Scheme 19. Formation of $[Fe^V(O)(dpaq)]^{2+}$ (**64**) from $[Fe^{III}(H_2O)(dpaq)]^{2+}$ (**65**).[54]

In 2012 Hitomi *et al.* reported a reactive Fe^V oxo complex, $[Fe^V(O)(dpaq)]^{2+}$ (**64**) that is capable of regioselective C-H bond hydroxylation of alkanes.[54] The starting complex $[Fe^{III}(H_2O)(dpaq)]^{2+}$ (**65**) was oxidized to the reactive species **64** using H_2O_2 in MeCN at 25 °C and this was found to proceed *via* an Fe^{III} peroxo species $[Fe^{III}(OOH)(dpaq)]^+$ (**66**) which is then protonated at the distal oxygen and undergoes O-O bond heterolysis to produce the Fe^V oxo group (**Scheme 19**). It is believed that the protonation of the peroxo group facilitates O-O bond heterolysis in collaboration with the electron-donating amide group, a push/pull concept. This oxidation process is the same for $[Fe^{III}(PaPy_3)]^+$ (**67**) which possesses another pentadentate

monoamido ligand (**Figure 16**); however this occurs less efficiently than for **65** as dpaq is a better electron donor than PaPy$_3$.[54] In contrast to these complexes, [Fe^{II}(N$_4$Py)(MeCN)]$^{2+}$ is known to promote O-O bond homolysis when oxidized to [Fe^{III}(N$_4$Py)(OOH)]$^{2+}$ using H$_2$O$_2$, possibly because it does not have an electron-donating amide ligand in the axial position.[55]

67
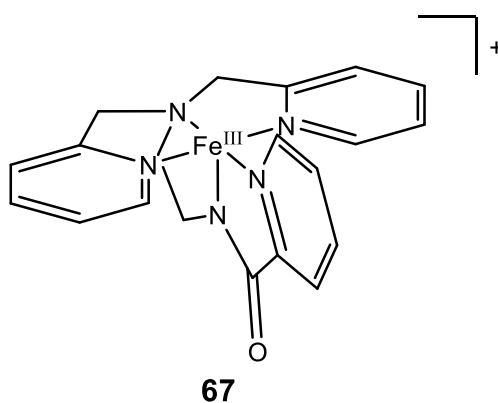
Figure 16. [Fe^{III}(PaPy$_3$)]$^+$ complex (**67**).[56]

Complex **64** demonstrated not just high selectivity for the 3° C-H bond in *cis*-4-methylcyclohexyl-1-pivalate (**68**) but also high stereoselectivity in which it hydroxylates the 3° C-H bond with retention of configuration, producing the *trans* alcohol (**69**) as opposed to the *cis* alcohol (**70**) in 94% yield (**Scheme 20**).[54] This is evident in the natural process in which cytochrome P450 enzymes perform C-H bond hydroxylation with retention of configuration, as mentioned earlier.[22]
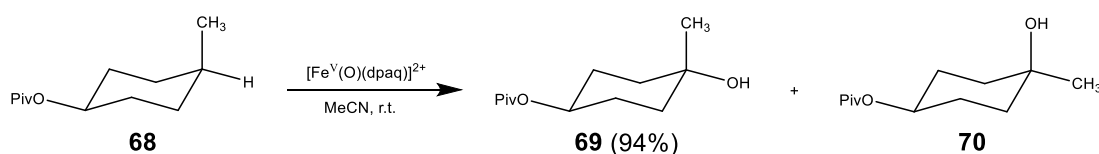

Scheme 20. Stereoselective hydroxylation of *cis*-4-methylcyclohexyl-1-pivalate (**68**).[54]

Further work by Hitomi investigated the HAA and OAT reactivity of various derivatives of $[Fe^V(O)(dpaq^R)]^{2+}$ (**71**) towards adamantane and (2*E*)-3, 7-dimethyl-2, 6 octadien-1-yl 4-methoxybenzoate, respectively (**Figure 17**).[57] Two different trends in selectivity were observed.

For HAA selectivity: NO_2 > Cl > H > OCH_3.

For OAT selectivity: OCH_3 > H > Cl > NO_2.

It was found that the most electron-withdrawing substituents demonstrated the highest selectivity towards 3° C-H bonds over 2° C-H bonds. The opposite trend was observed for alkene epoxidation in which most electron-donating substituents demonstrated the highest selectivity towards the electron poor C=C bond over the electron rich C=C bond.

71
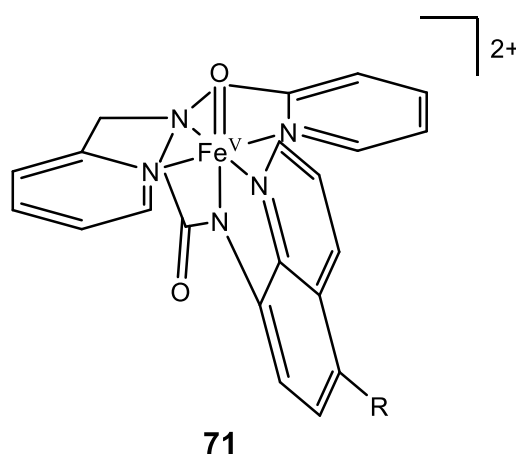
Figure 17. $[Fe^V(O)(dpaq^R)]^{2+}$ complex (**71**). R represents the different substituents at the 5-position of the quinoline moiety in the dpaq ligand: OCH_3, H, Cl and NO_2.[57]

For the HAA selectivity trend it is believed that an electron-withdrawing substituent on the dpaq ligand increases the activation energy ($\Delta G^{\neq}$) for the HAA step and thereby improves the selectivity for the hydroxylation of C-H bonds. The larger $\Delta G^{\neq}$ should be reflected by a smaller driving force (ΔG) for

HAA by the $[Fe^{III}(MeCN)(dpaq^{NO2})]^{2+}$ complex. The driving force (ΔG) for HAA should correlate with the difference in BDEs of the C-H bond of adamantane and the O-H bond of the $Fe^{IV}(OH)$ species:

$$\Delta G = BDE(C\text{-}H) - BDE(O\text{-}H)$$

Therefore, the electron-withdrawing substituent on the dpaq ligand should harness the reactivity of the Fe^V oxo species toward HAA by decreasing the BDE(O-H) of the $Fe^{IV}(OH)$ species (**Figure 18**). The BDE(O-H) of the $Fe^{IV}(OH)$ species is related to the 1 electron reduction potential (E_{red}) of the Fe^V oxo species and the pK_a value for the equilibrium between the Fe^{IV} oxo and $Fe^{IV}(OH)$ species by the expression:

$$BDE(O\text{-}H) = 23.06E_{red} + 1.37pK_a + C$$

C is a constant that accounts for the thermodynamic properties of the hydrogen atom.[58] As the substituent group becomes more electron-withdrawing, the pK_a value should decrease which contributes to a decrease in BDE(O-H) according to the above equation, but the E_{red} value should increase, which increases BDE(O-H). As the obtained results indicate that the electron-withdrawing substituent on the ligand causes a decrease in BDE(O-H), the contribution from the pK_a term to BDE(O-H) must be greater than that from the E_{red} term. That is, the reactivity of $[Fe^{III}(MeCN)(dpaq^R)]^{2+}$ complexes toward alkane hydroxylation should be controlled by the oxo basicity rather than by the E_{red} of the Fe^V oxo species.[57]
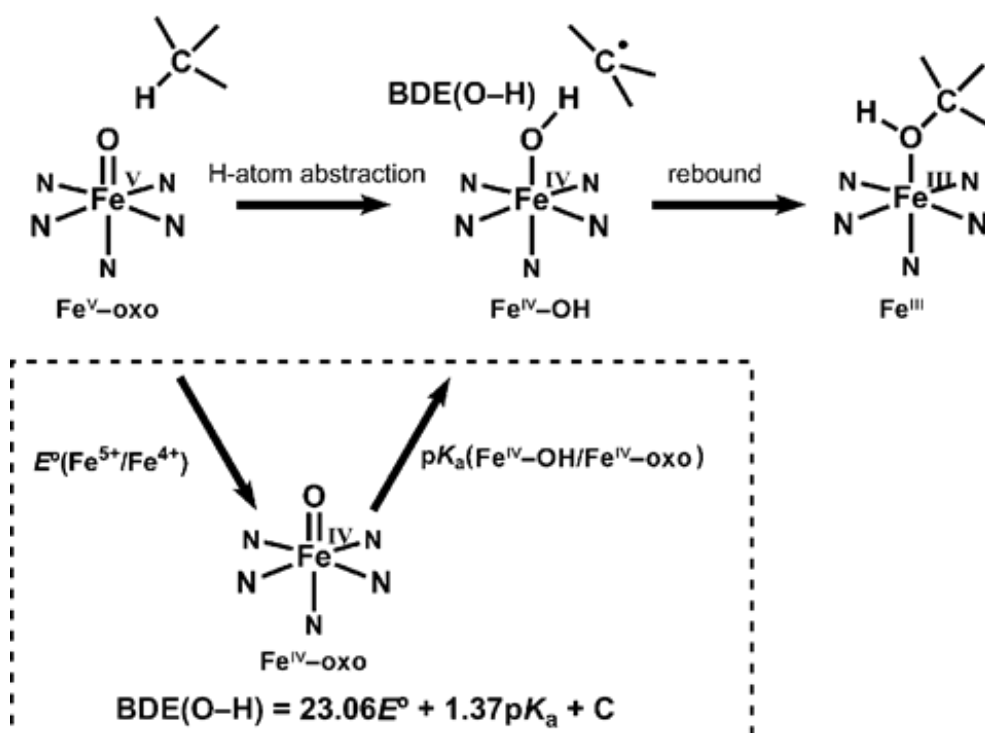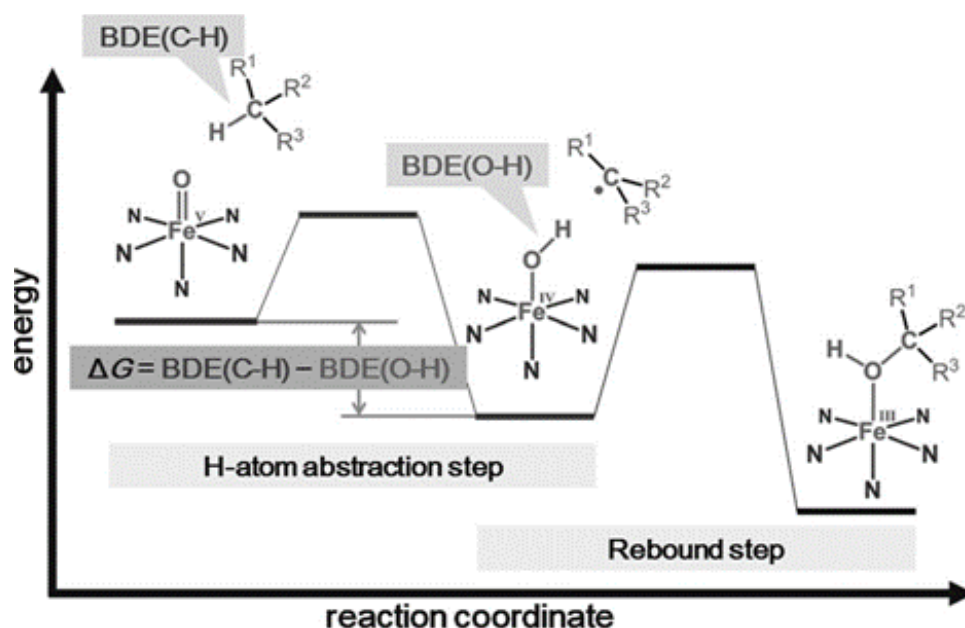
Figure 18. Energy diagram (Top) and rebound mechanism (Bottom) of alkane hydroxylation by [Fe^V(O)(dpaq^R)]$^{2+}$ (**71**). The equation for the O-H bond strength is given in terms of the 1 electron E$_{red}$ of the Fe^V oxo species and the pK_a of the Fe^{IV}(OH) species.[57] Reproduced with permission of the publisher.

3.2 Diiron Systems

3.2.1 Natural Enzyme Background

Methane monooxygenase (MMO) is an enzyme that is capable of oxidizing the C-H bonds in methane, as well as other alkyl and aryl compounds and this is found in methanotrophic bacteria, a class of gram-negative bacteria that exists at the interface of aerobic and anaerobic environments.[59] MMO is a very unique oxidation enzyme as it is the only one that can efficiently catalyse the hydroxylation of methane under ambient conditions, not even cytochrome P450 can accomplish this. This is one of the most difficult chemical processes in nature as methane has the highest alkane C-H BDE of 105 kcal mol^{-1}. Methane is extremely inert towards activation because its non-polar C-H bonds give its tetrahedral structure no overall dipole moment and it has negligible polarizability. This is underpinned by the relatively high energy of the CH_3^+ ion which makes C-H bond heterolysis unfavourable. Also, methane's high ionization potential, negligible electron affinity and high HOMO-LUMO gap all make it unfavourable for redox type reactions.[60]

There are two distinct forms of MMO: soluble methane monooxygenase (sMMO) and particulate methane monooxygenase (pMMO), which are mutually exclusive. Certain methanotrophs such as *Methylococcus capsulatus* (Bath) and *Methylosinus trichosporium* OB3b can produce both sMMO and pMMO, based on copper availability.[61] An environment with a low copper concentration promotes the production of sMMO, whereas a high copper concentration suppresses sMMO production and promotes the production of pMMO.[62] Each form of MMO will be discussed in turn.
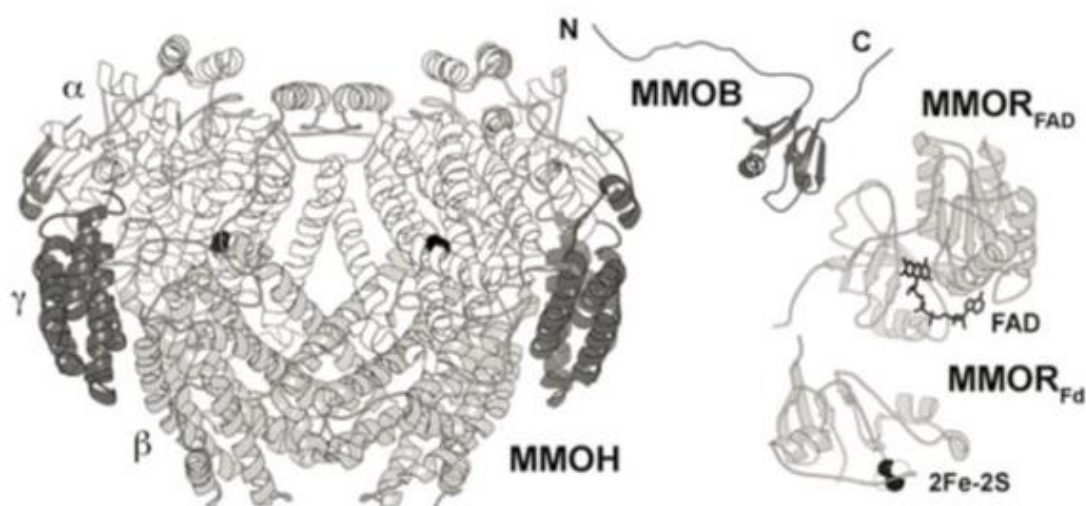
Figure 19. Full sMMO enzyme with all components.[59] Reproduced with permission of the publisher.

The best characterised and the most understood form is sMMO. This enzyme consists of a three-component heterodimer $(\alpha\beta\gamma)_2$, known as MMOH and this is a hydroxylase which contains the diiron active site in the α-subunit (**Figure 19**).[63,64] It also consists of MMOR which is a reductase that contains Fe_2S_2 and FAD, and this supplies electrons to MMOH by consuming NADH. It also consists of MMOB which is a cofactorless protein that regulates activity by binding to the MMOH α-subunit to induce changes in protein structure and this effectively links NADH consumption with substrate oxidation.

sMMO is able to hydroxylate a large scope of hydrocarbon substrates such as linear and branched alkanes and alkenes of up to eight carbons in length. This also includes aromatic, heterocyclic and halogenated compounds.[65,66,67]

72
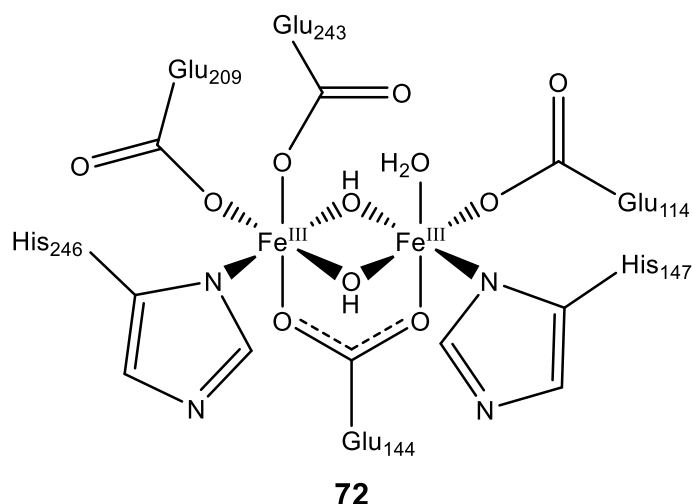
Figure 20. sMMO enzyme active site (resting state).[59]

The sMMO enzyme active site (**72**) consists of two high spin Fe^{III} ions which are spaced approximately 3 Å apart and are bridged by two hydroxides and a glutamate ligand, which antiferromagnetically couples the Fe^{III} ions and therefore results in a diamagnetic ground state. The two Fe^{III} ions are also terminally coordinated to four glutamates, two histidines and a water ligand (**Figure 20**).[68,69,70]

The mechanism of C-H bond hydroxylation by sMMO enzymes is shown in **Scheme 21** and is explained as follows. The first step involves a 2 electron reduction of the resting high spin Fe^{III}_2 species (**72**) to generate a weakly ferromagnetically coupled, high spin Fe^{II}_2 species (**73**).[71,72] This reduction is accompanied by the protonation of both hydroxides which liberates H_2O and results in the terminal Glu_{243} bridging both Fe ions.[69,70] O_2 then inserts itself between the two Fe^{II} ions, displacing H_2O and forming an antiferromagnetically coupled, high spin Fe^{III}_2 species (**74**).[73,74] This peroxo complex is known as "intermediate P". It is believed that proton transfer between the H_2O and the bridging Glu_{243} yields **75**, which then opens up to form an open peroxo complex (**76**) and proton transfer between the OH and the peroxo group closes the Fe^{III}_2 complex again, yielding **77**.[13] A further proton transfer between the protonated Glu_{243} and the peroxo group breaks

the O-O bond in a process that is best described as proton-assisted heterolytic cleavage.[13,75] This generates an antiferromagnetically coupled $Fe^{IV}_2(\mu\text{-oxo})_2$ complex (**78**), known as "intermediate Q".[76,77,78] The substrate approaches, then intermediate Q abstracts a hydrogen atom from it to yield an Fe^{III}_2 product-bound complex (**79**).[73,77] Finally, H_2O displaces the hydroxylated product to regenerate the resting Fe^{III}_2 enzyme (**72**) and this is believed to be the RDS.
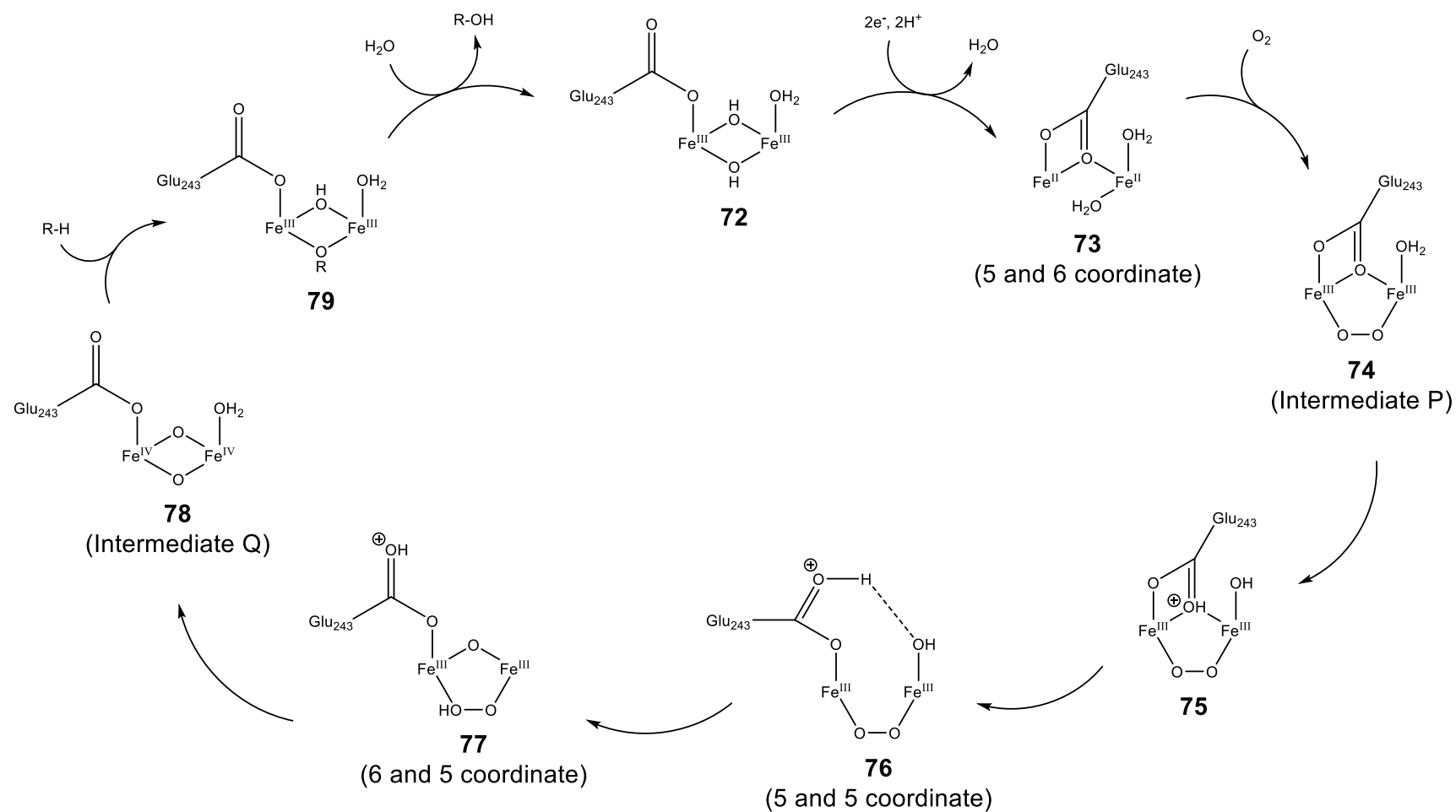
Scheme 21. sMMO catalytic cycle. Glu209, μ-Glu144, Glu114, His246 and His147 ligands have been omitted for clarity. Each Fe has a coordination number of 6 (octahedral), except from those otherwise labelled.[59]

The other form of MMO is pMMO. This form is membrane-bound which makes it significantly harder to characterise and therefore it is much more poorly understood than sMMO.[59,60] This enzyme consists of a three-component homotrimer $(\alpha\beta\gamma)_3$ and these components are each known as pmoA, pmoB and pmoC (**Figure 21**).[79] pMMO also differs from sMMO in that its metal cofactors contain copper instead of iron; therefore an environment with a high Cu concentration promotes pMMO production, as mentioned previously.[62] It is believed that pMMO contains approximately 15 Cu ions and the active site consists of a dicopper center which is coordinated to three histidine ligands and is located within the pmoB subunit.[80,81] pMMO can only hydroxylate straight-chain alkanes of up to five carbons in length and epoxidize alkenes of up to four carbons in length.[82,83] C-H bond hydroxylation proceeds with full retention of configuration and this indicates that a concerted OAT mechanism is involved, rather than a radical rebound mechanism.[84]

This form of MMO will not be discussed any further as this review is only concerned with biomimetic hydroxylation complexes that contain iron.
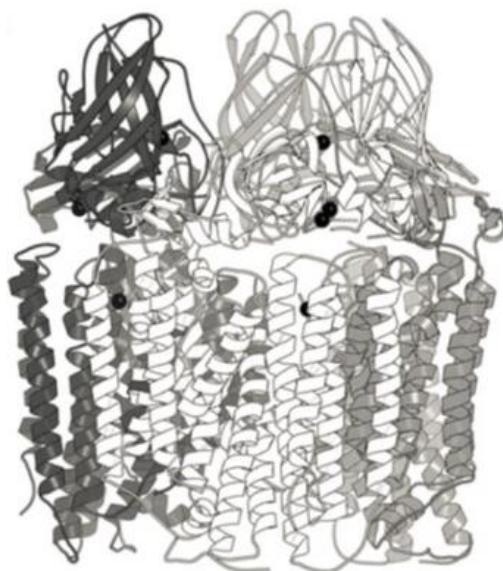
Figure 21. Full pMMO enzyme with all components.[59] Reproduced with permission of the publisher.

3.2.2 Fe_2O_2 Diamond Core Complexes

In contrast to monoiron complexes there are fewer examples of diiron complexes that engage in C-H bond hydroxylation *via* HAA.[33]

In 1995 Que *et al.* reported the first synthesis and characterisation of a diiron complex with a Fe_2O_2 diamond core structure $[Fe^{III}(\mu\text{-}O)_2Fe^{IV}(5\text{-}Me_3\text{-}TPA)_2]^{3+}$ (**80**) (**Figure 22**), similar to that of sMMO intermediate Q.[85] This was generated from the starting complex $[Fe^{III}_2O(5\text{-}Me\text{-}TPA)_2(OH)(H_2O)]^{3+}$ using 1 equivalent of *m*CPBA in MeCN at -40 °C. By using a combination of EPR, Mössbauer and EXAFS spectroscopic analysis **80** was believed to consist of a valence-delocalised low spin ($S = \frac{1}{2}$) Fe^{III} – low spin ($S = 1$) Fe^{IV} pair coupled by double exchange.

Interestingly, the 6-Me derivative $[Fe^{III}(\mu\text{-}O)_2Fe^{IV}(6\text{-}Me_3\text{-}TPA)_2]^{3+}$ was found to consist of an antiferromagnetically coupled, valence-localised high spin ($S = \frac{5}{2}$) Fe^{III} – high spin ($S = 2$) Fe^{IV} pair.[86,87] This difference in Fe spin state in the two complexes is attributed to the 6-Me substituent as this induces steric strain that inhibits the formation of short metal-ligand bonds which are required for a low spin state.

80
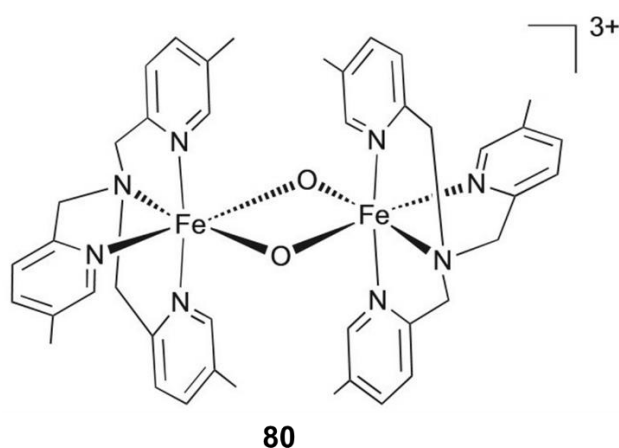
Figure 22. $[Fe^{III}(\mu\text{-}O)_2Fe^{IV}(5\text{-}Me_3\text{-}TPA)_2]^{3+}$ complex (**80**).[85]

Further work by Que investigated the HAA reactivity of the unsubstituted derivative $[Fe^{III}(\mu\text{-}O)_2Fe^{IV}(TPA)_2]^{3+}$ (**81**) towards cumene, ethylbenzene and cycloheptane under various conditions.[88] This demonstrated quite a poor HAA capability which was attributed to it only having one Fe^{IV} centre, unlike sMMO intermediate Q which has two Fe^{IV} centres. Hydroxylation and desaturation were found to be competing processes similar to those by sMMO and Δ9 desaturase, respectively (**Table 3**).

Substrate	BDE (kcal mol^{-1})	Products	Yield
Cumene	85	PhC(OH)(CH$_3$)$_2$	0.17
		PhC(CH$_3$)=CH$_2$	0.27
Cumene (under O$_2$)	85	PhC(OH)(CH$_3$)$_2$	0.82
		PhC(O)CH$_3$	0.15
Ethylbenzene	87	PhCH(OH)CH$_3$	0.14
		PhCH=CH$_2$	0.14
		PhC(O)CH$_3$	Trace
Cycloheptane	94	None	0

Table 3. Hydrocarbon oxidations by $[Fe^{III}(\mu\text{-}O)_2Fe^{IV}(TPA)_2]^{3+}$ (**81**).[88]

A significant KIE of 20 was observed when ethylbenzene was compared with ethylbenzene-d_{10} at -40 °C which supports the conclusion that the cleavage of the substrate's α-C-H bond is the RDS. However, cleavage of the substrate's β-C-H bond only has a KIE of 1.3 which indicates that desaturation involves an asynchronous scission of the two C-H bonds.[89] When cumene oxidation was performed under O$_2$ it was found that O$_2$ traps the alkyl radical to form the cumylperoxy radical, during which no ^{18}O is incorporated into the products from H$_2$^{18}O (**Scheme 22**). This supports the conclusion that hydroxylation proceeds *via* an oxygen rebound step in which the alkyl radical quickly reacts with another equivalent of **81** to yield the

alcohol product. It is unclear what dictates whether **81** engages in hydroxylation or desaturation. It possibly depends on the difference in the energy barriers of C-O bond formation and abstraction of the β-hydrogen atom, respectively.
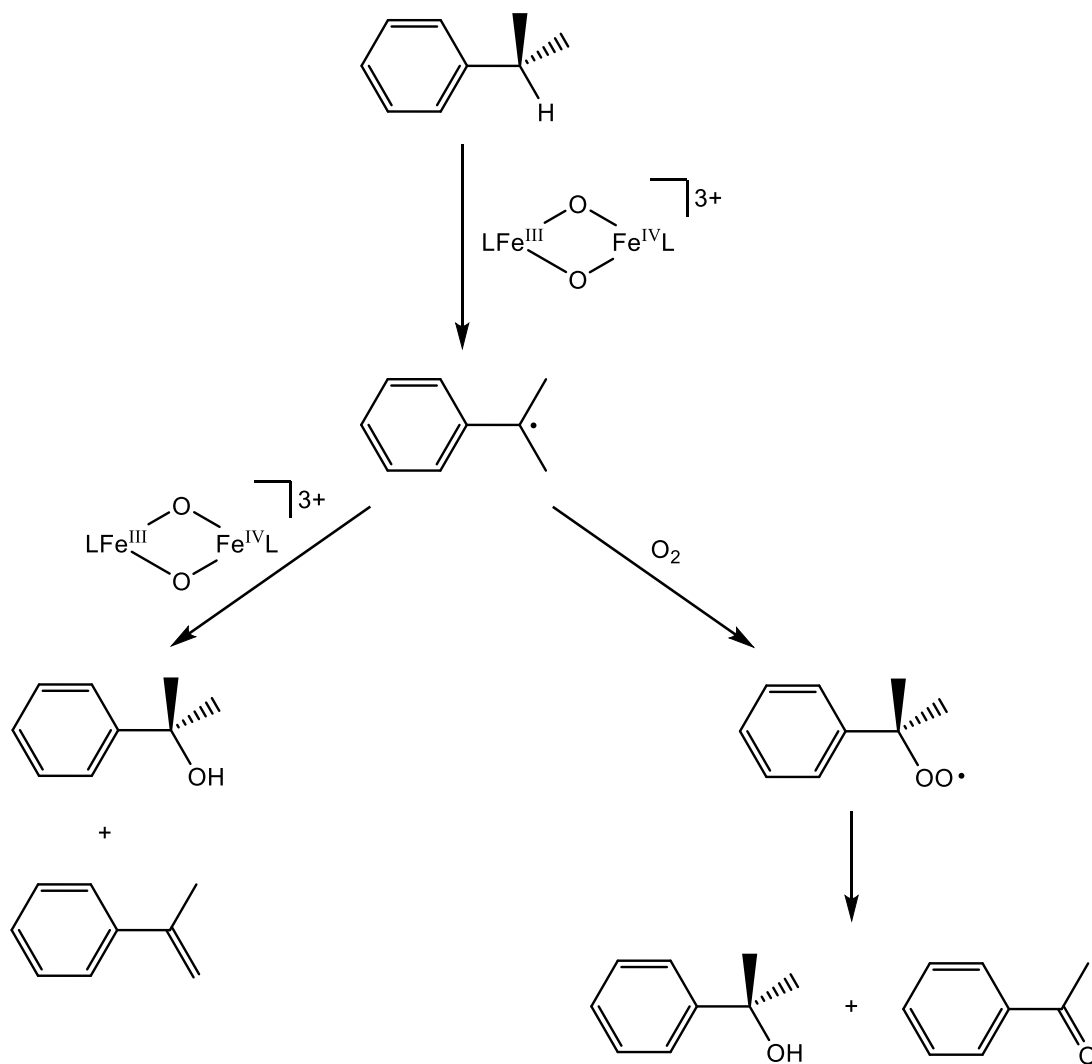
Scheme 22. Proposed reaction mechanism for the oxidation of cumene by $[Fe^{III}(\mu\text{-O})_2Fe^{IV}(TPA)_2]^{3+}$ (**81**).[88]

In 2007 Xue *et al.* reported the first synthesis and characterisation of a $Fe^{IV}_2O_2$ complex $[Fe^{IV}_2(\mu\text{-O})_2(3,5\text{-Me}_6\text{-4-OMe}_3\text{-TPA})_2]^{4+}$ (**82**) (**Figure 23**).[90]

This consists of two antiferromagnetically coupled Fe^{IV} centres with an overall $S = 0$ ground state, which is similar to sMMO intermediate Q.[76,77,78] This was generated from the starting complex [Fe^{III}(μ-O)$_2Fe^{IV}$(3,5-Me$_6$-4-OMe$_3$-TPA)$_2$]$^{3+}$ (**83**) using bulk electrolysis at 900 mV (relative to Fc$^{+/0}$), in MeCN at -40 °C. However, this could not be achieved for **80** as its pyridine rings were not electron-donating enough to stabilize the corresponding $Fe^{IV}_2O_2$ complex, which instantly self-decays.

82
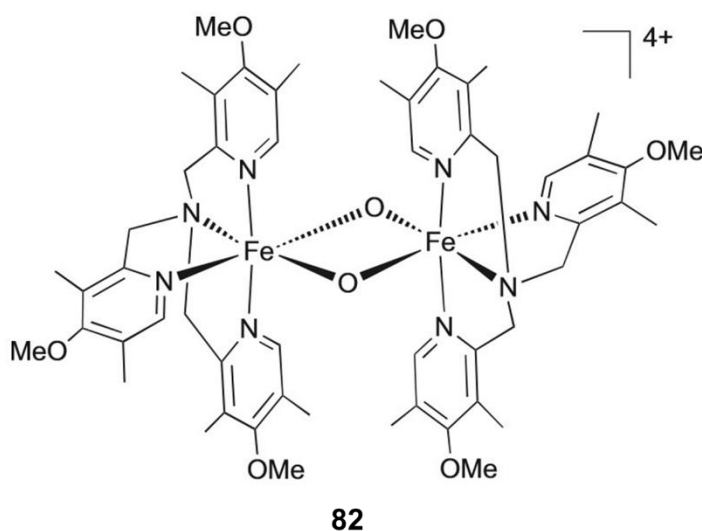
Figure 23. [Fe^{IV}_2(μ-O)$_2$(3,5-Me$_6$-4-OMe$_3$-TPA)$_2$]$^{4+}$ complex (**82**).[90]

Complex **82** proved to be a much more reactive complex when tested on DHA. This performed as a 1 electron oxidant producing anthracene and anthraquinone in respective yields of 14% and 13%, with a pseudo-first order rate constant of 5.1 x 10^{-4} s^{-1}. Interestingly, the monoiron complex [Fe^{IV}(O)(3,5-Me$_6$-4-OMe$_3$-TPA)(NCMe)]$^{2+}$ (**84**) (**Figure 24**) reacts with DHA 100 times faster (4.2 x 10^{-2} s^{-1}) despite the fact that its E_{red} is approximately 200 mV lower.[90] This is rationalised by previous work by Bordwell and Mayer which correlates the HAA reactivity of a metal oxo complex with the BDE of its newly formed O-H bond.[91,92] It was found that the O-H BDE value is a function of both the E_{red} of M=O and the pK_a of M-OH. Therefore, the lower

E_{red} of **84** is compensated for by the higher pK_a of its Fe^{III}-OH reduced form, as this is 3-4 units higher than Fe^{III}-OH-Fe^{IV}. It is believed that the pK_a of Fe^{III}-OH-Fe^{IV} is significantly lower than that of Fe^{III}-OH because of the additional highly Lewis acidic Fe^{IV} centre coordinated to the OH group.

84
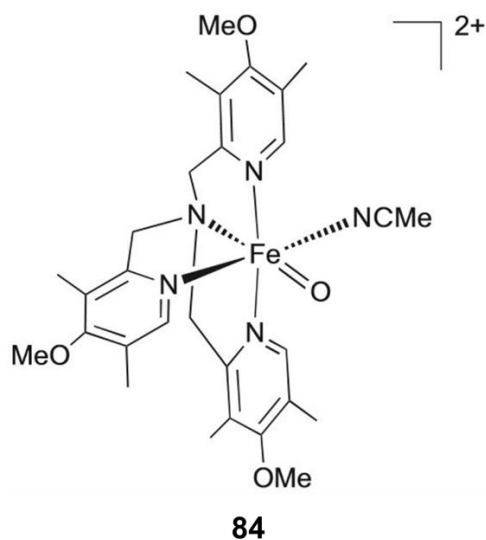
Figure 24. $[Fe^{IV}(O)(3,5-Me_6-4-OMe_3-TPA)(NCMe)]^{2+}$ complex (**84**).[90]

3.2.3 Fe₂O₃ **Open Core Complexes**

This theory and understanding of how terminal oxo monoiron complexes react with hydrocarbon substrates relative to bridging oxo diiron complexes was carried forward and used to develop Fe₂O₃ open core complexes. These are diiron complexes with only one bridging oxo group and also one or two terminal oxo groups, and therefore these display a much more open structure.
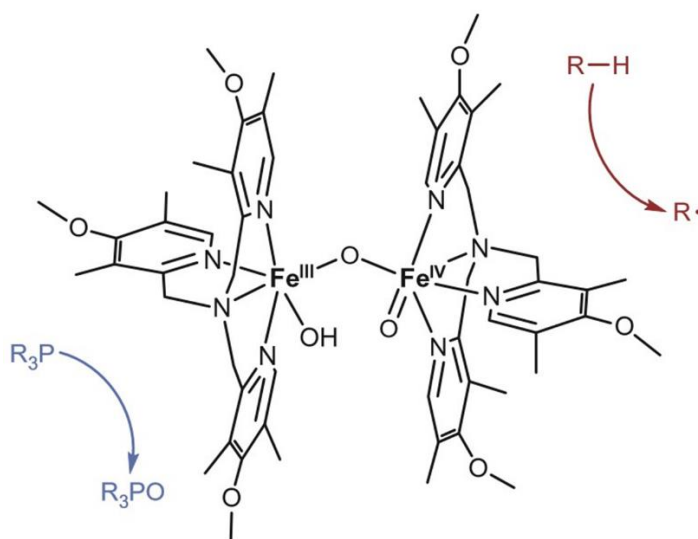
85

Scheme 23. Open core structure of $[HO\text{-}(L)Fe^{III}\text{-}O\text{-}Fe^{IV}(L)=O]^{2+}$ (**85**) displaying both HAA (red) and OAT (blue) reactivity. L is 3,5-Me₆-4-OMe₃-TPA, in which all the CH₂ groups are deuterated to avoid ligand oxidation.[93] Reproduced with permission of the publisher.

In 2010 Xue *et al.* reported a highly reactive Fe₂O₃ open core complex [HO-(L)Fe^{III}-O-Fe^{IV}(L)=O]²⁺ (**85**) which demonstrated a million-fold increase in HAA reactivity towards DHA (28 M⁻¹ s⁻¹) compared to its Fe₂O₂ diamond core

precursor complex $[Fe^{III}(\mu\text{-}O)_2Fe^{IV}(3,5\text{-}Me_6\text{-}4\text{-}OMe_3\text{-}TPA)_2]^{3+}$ (**83**) (**Scheme 23**).[93] This was found to consist of an antiferromagnetically coupled, valence-localised high spin ($S = {}^{5}/_{2}$) Fe^{III} – high spin ($S = 2$) Fe^{IV} pair. Complex **85** was tested in both HAA and OAT reactions and compared against a range of analogous diamond core and open core diiron complexes containing the same ligand, including the corresponding monoiron complex, under the same conditions (**Figure 25**). All the other Fe complexes had low spin Fe centres.
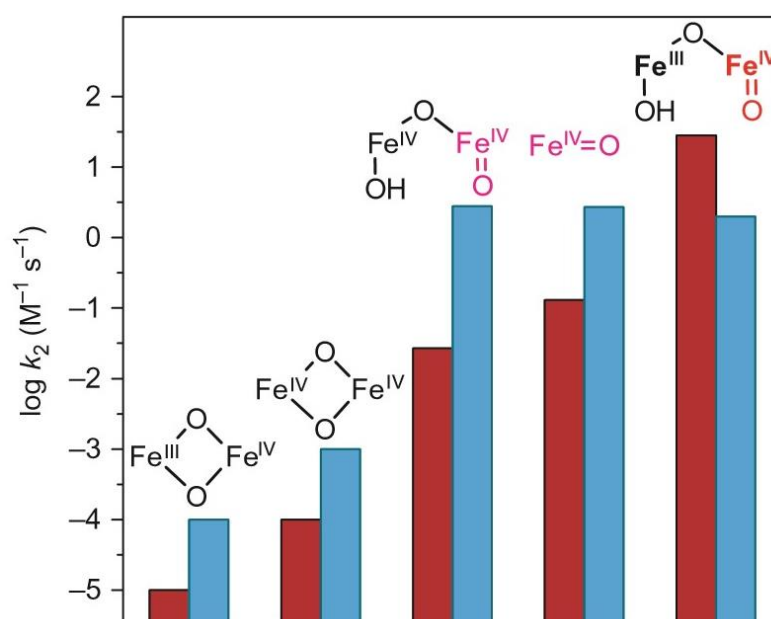
Figure 25. HAA (red) and OAT (blue) reaction rate constants of analogous Fe complexes, each containing the same ligand (3,5-Me$_6$-4-OMe$_3$-TPA) in a 3:1 CH$_2$Cl$_2$/MeCN solution at -80 °C.[93] Reproduced with permission of the publisher.

In the HAA reactions anthracene was obtained as the sole product from DHA. The large difference in reactivity between the Fe$_2$O$_3$ open core complexes and the Fe$_2$O$_2$ diamond core complexes is attributed to the higher pK_a of the Fe^{III}-OH reduced form of the Fe$_2$O$_3$ open core complexes, as explained earlier.[91,92] This shows how the opening of a Fe$_2$O$_2$ diamond core using OH$^-$

and therefore the formation of a terminal Fe^{IV} oxo group unleashes its oxidizing potential. The large difference in reactivity between the two Fe_2O_3 open core complexes and also the monoiron complex is attributed to the $S = 2$ high spin state of the Fe^{IV} oxo centre in **85** because it can engage in HAA *via* an additional σ-FMO pathway and this permits DHA to approach the oxo group from an additional vertical trajectory, as explained earlier (**Figure 5**).[36] Also, despite the fact that the more oxidized Fe_2O_2 diamond core complex **82** has the highest E_{red} of the series **85** is still 10^5-fold more reactive. Therefore, it is the structure and the spin state that really determine the HAA reactivity of diiron complexes.[93]

In the OAT reactions all the complexes were tested on diphenyl(pentafluorophenyl)phosphine under the same conditions in which diphenyl(pentafluorophenyl)phosphine oxide was obtained. Interestingly, the Fe_2O_2 diamond core complexes reacted at least 10^3-fold slower than the other complexes with terminal Fe^{IV} oxo groups. It is believed that Fe-O bond cleavage would be required in order to open up a tightly bound Fe_2O_2 diamond core before OAT could take place. Therefore, a terminal Fe^{IV} oxo group can transfer an oxygen atom to a phosphine substrate much more efficiently, however the Fe spin state is not important.[93]

86
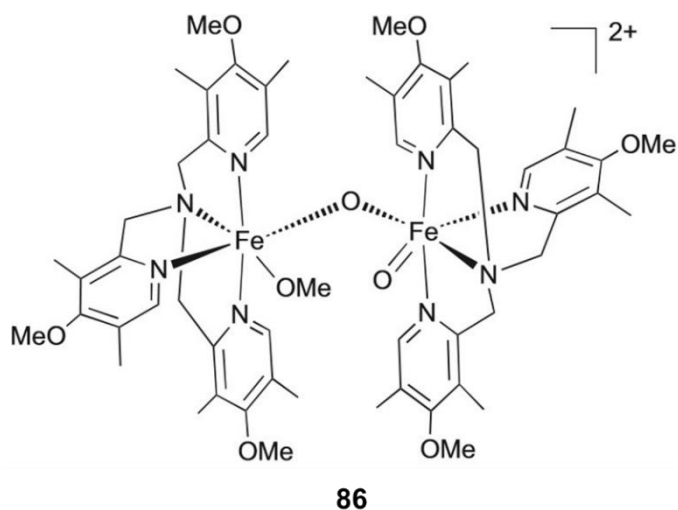
Figure 26. $[CH_3O\text{-}(L)Fe^{III}\text{-}O\text{-}Fe^{IV}(L)\text{=}O]^{2+}$ complex (**86**).[94]

Further work by Xue significantly improved **85** by replacing the OH group on the Fe^{III} centre with a OCH_3 group to produce $[CH_3O-(L)Fe^{III}-O-Fe^{IV}(L)=O]^{2+}$ (**86**) which is 13-fold more reactive towards DHA (360 M^{-1} s^{-1}), under the same conditions (**Figure 26**).[94] This was also found to consist of an antiferromagnetically coupled, valence-localised high spin ($S = {}^5/_2$) Fe^{III} – high spin ($S = 2$) Fe^{IV} pair. This increase in HAA reactivity is attributed to the absence of a hydrogen-bonding interaction which would normally exist between the hydroxyl and oxo groups in **85** and would therefore inhibit HAA.

Interestingly, intramolecular oxidation of the OCH_3 group (C-H BDE = 96 kcal mol^{-1}) was found to compete with intermolecular Ph_3CH oxidation (C-H BDE = 81 kcal mol^{-1}) despite the significantly weaker C-H bond of the Ph_3CH substrate. Formaldehyde was obtained in approximately 28% yield whilst no Ph_3COH was detected when either 0 mM or 2 mM Ph_3CH was added. However, when 10 mM Ph_3CH was added the reaction was faster, the formaldehyde yield decreased to 16% and 6% Ph_3COH was detected (**Scheme 24**).
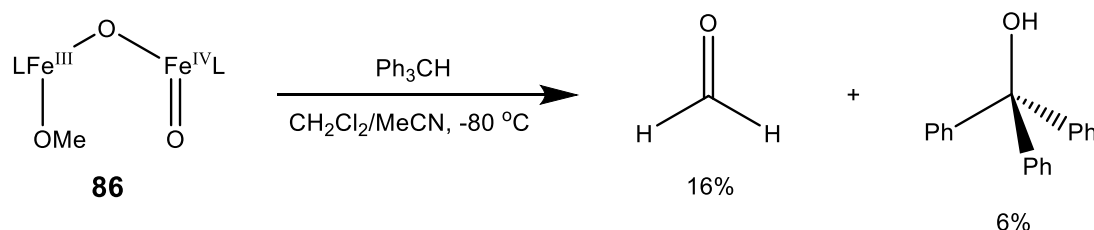
Scheme 24. Competing intramolecular and intermolecular oxidation reactions by $[CH_3O-(L)Fe^{III}-O-Fe^{IV}(L)=O]^{2+}$ (**86**).[94]

This enhancement of the HAA reactivity of Fe_2O_2 diamond core complexes was also applied to **83** in which alcohols of various sizes were tested as the sole substrates. When ROH and a base (2,6-lutidine) were added to this the rather sluggish diamond core **83** undergoes ring-opening *via* attack from the alcohol to produce the highly reactive open core complex [RO-(L)Fe^{III}-O-

$Fe^{IV}(L)=O]^{2+}$ (**87**) which instantly and intramolecularly oxidizes the OR group to the corresponding aldehyde (**Scheme 25**). It was found that the steric bulk of the alcohol substrate also influenced the enhancement in HAA reactivity as well as its C-H BDE. It is believed that the smaller alcohols can bind to the Fe^{III} centre more easily and therefore shift the equilibrium further to the right.
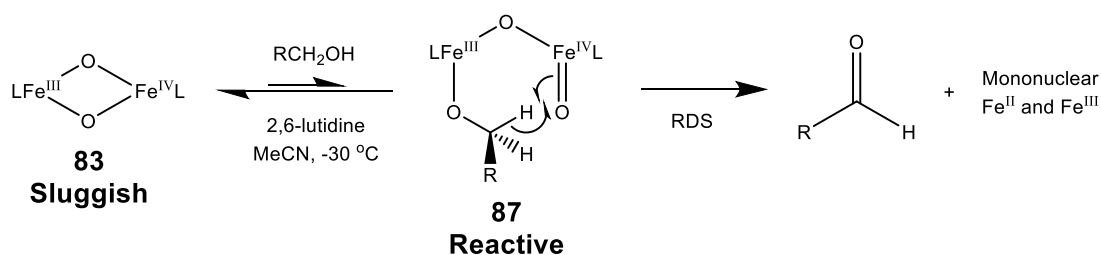
Scheme 25. Ring-opening activation of $[Fe^{III}(\mu-O)_2Fe^{IV}(3,5-Me_6-4-OMe_3-TPA)_2]^{3+}$ (**83**) and subsequent alcohol oxidation.[94]

Therefore, this substrate-induced activation of a rather sluggish Fe_2O_2 diamond core complex and the ability of the subsequently highly reactive Fe_2O_3 open core complex to selectively attack stronger C-H bonds in the presence of weaker ones really suggests that sMMO could employ a similar mechanism. It is possible that ring-opening would only occur when a small substrate such as methane gets close enough to the Fe_2O_2 diamond core of sMMO intermediate Q (**78**) as this would protect the weaker C-H bonds in the surrounding amino acid residues from oxidation. However, it is unclear how exactly this mechanism could be applied to an alkane substrate.[94]
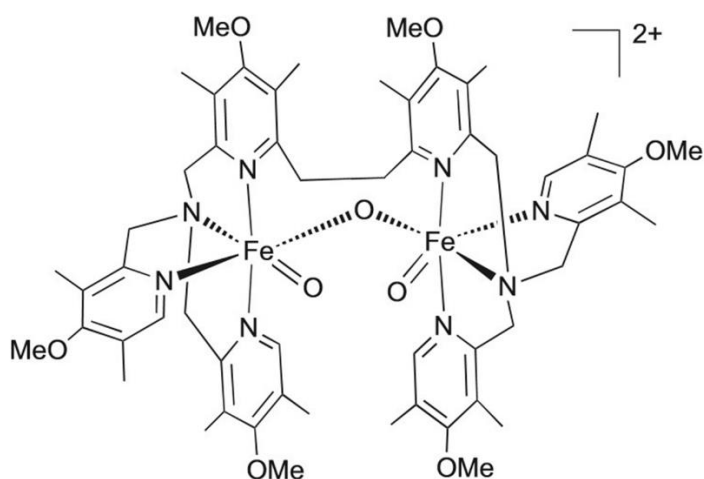
88

Figure 27. $[Fe^{IV}_2(\mu\text{-O})(O)_2(6\text{-hpa})]^{2+}$ complex (**88**).[95]

In 2012 Kodera *et al.* reported the first synthesis and characterisation of a high spin $Fe^{IV}_2(\mu\text{-O})$ complex $[Fe^{IV}_2(\mu\text{-O})(O)_2(6\text{-hpa})]^{2+}$ (**88**) (**Figure 27**).[95] The starting complex $[Fe^{III}_2(\mu\text{-O})(H_2O)_2(6\text{-hpa})]^{4+}$ (**89**) was oxidized to the reactive species **88** using 1.2 equivalents of H_2O_2 and 2 equivalents of NEt_3 in MeCN at -40 °C and this was found to proceed *via* an Fe^{III}_2 peroxo species $[Fe^{III}_2(\mu\text{-O})(\mu\text{-O}_2)_2(6\text{-hpa})]^{2+}$ (**90**) which undergoes reversible O-O bond homolysis to produce the two terminal Fe^{IV} oxo groups (**Scheme 26**). This is the first spectroscopic observation of O_2 activation of a Fe^{III}_2 peroxo complex to a high spin $Fe^{IV}_2(\mu\text{-O})$ complex *via* reversible O-O bond scission and this therefore serves as a functional model for the conversion of intermediate P (**74**) to Q (**78**) in the sMMO catalytic cycle. Therefore, it is possible that intermediate Q (**78**) actually exists as a Fe_2O_3 open core complex with two terminal oxo groups, instead of a Fe_2O_2 diamond core complex.
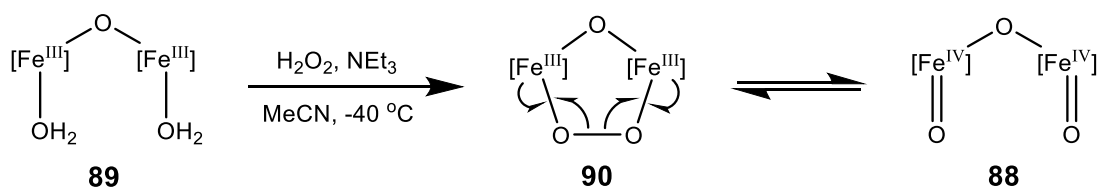
Scheme 26. Formation of $[Fe^{IV}_2(\mu\text{-}O)(O)_2(6\text{-hpa})]^{2+}$ **(88)** from $[Fe^{III}_2(\mu\text{-}O)(H_2O)_2(6\text{-hpa})]^{4+}$ **(89)**.[95]

Complex **88** demonstrated moderate epoxidation (OAT) reactivity (1.3 x 10^{-3} s^{-1}) towards *trans*-β-methylstyrene **(91)**, in which *trans*-β-methylstyrene oxide **(92)** was obtained as the sole product (**Scheme 27**) and this indicates that no HAA takes place.
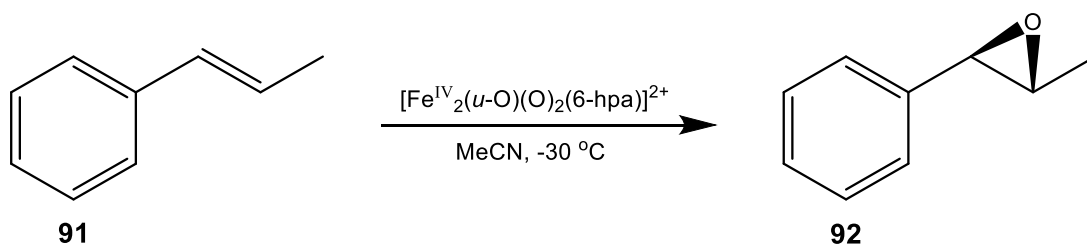
Scheme 27. Epoxidation of *trans*-β-methylstyrene **(91)** by $[Fe^{IV}_2(\mu\text{-}O)(O)_2(6\text{-hpa})]^{2+}$ **(88)**.[95]

Complex **88** is believed to consist of an antiferromagnetically coupled, valence-localised high spin ($S = 2$) Fe^{IV} – high spin ($S = 2$) Fe^{IV} pair as its Mössbauer spectra was nearly identical to that of a similar complex $[O=(L)Fe^{IV}\text{-}O\text{-}Fe^{IV}(L)=O]^{2+}$ **(93)** investigated by Xue *et al.* (**Figure 28**).[96] However, these two complexes differ greatly in thermal stability as **93** is only stable at -80 °C despite the fact that 3,5-Me$_6$-4-OMe$_3$-TPA is more electron-donating, whereas **88** is stable at -40 °C. This difference is attributed to the ethyl tether in 6-hpa as this dinucleating ligand possibly holds the complex together much better.
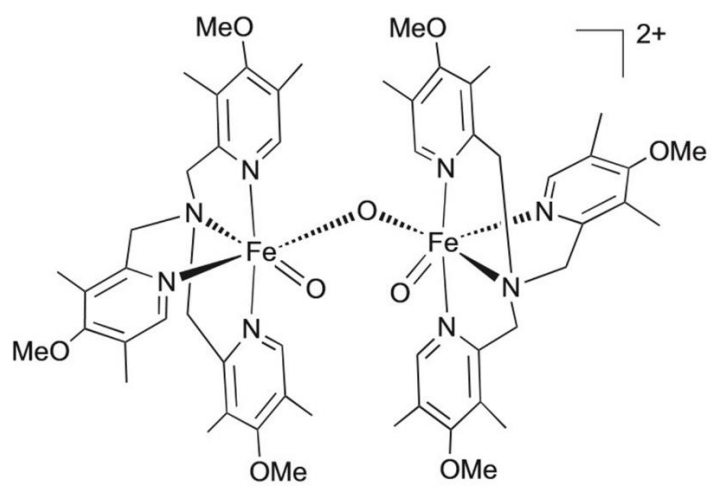
93

Figure 28. $[O=(L)Fe^{IV}-O-Fe^{IV}(L)=O]^{2+}$ complex (**93**).[96]

3.2.4 Carboxylate-Bridged Complexes

Carboxylate-bridged complexes are another interesting class of diiron hydroxylation catalysts. These are worth investigating because at least one bridging carboxylate ligand (glutamic acid) is found in each sMMO intermediate and therefore they significantly contribute to the structural architecture of sMMO.[59]
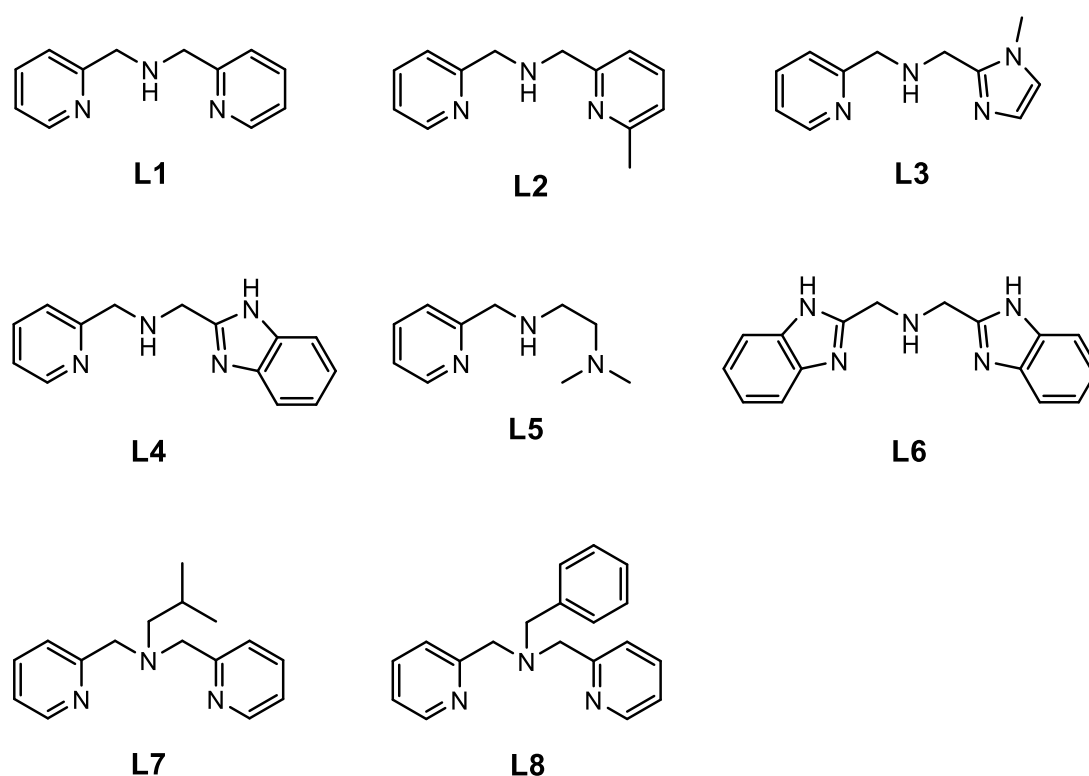
Figure 29. Tridentate 3N ligands used in diiron carboxylate-bridged complexes.[97]

In 2014 Sankaralingam and Palaniandavar reported a series of dibenzoate-bridged Fe^{III}_2 complexes with various tridentate 3N ligands (**Figure 29, L1 - 6**).[97] Each of these was oxidized to their corresponding reactive species

using *m*CPBA in a 4:1 CH₂Cl₂/MeCN solution at 25 °C and subsequently tested on the oxidation of cyclohexane.
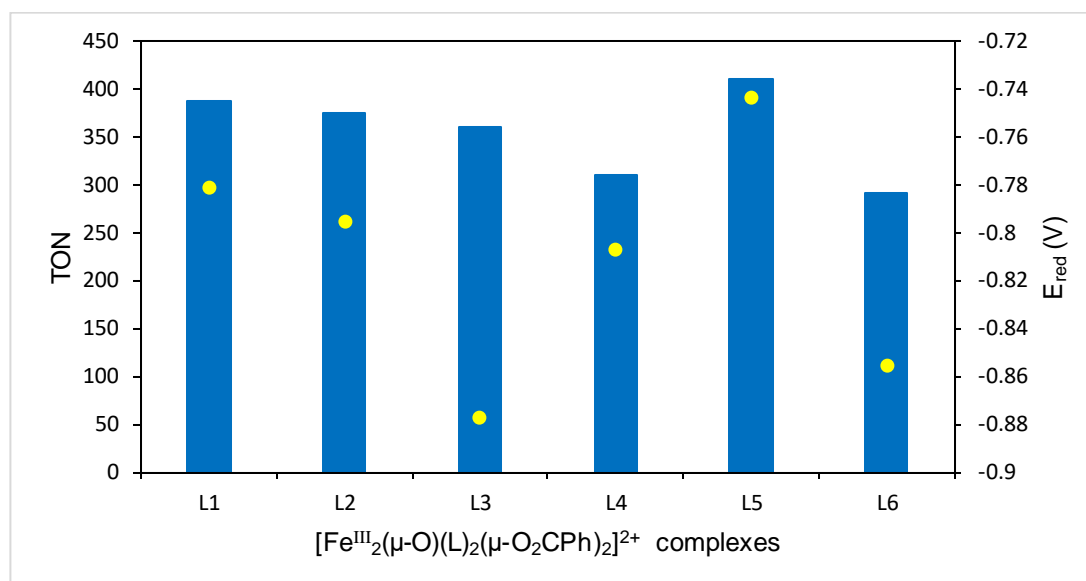
Figure 30. Comparison between the oxidation reaction TON (blue columns) and the E_{red} (yellow dots) of the $[Fe^{III}_2(\mu\text{-O})(L)_2(\mu\text{-O}_2CPh)_2]^{2+}$ starting complexes.[97]

A trend in cyclohexane oxidation (expressed in turnover numbers) was observed and this was found to correlate with the decreasing E_{red} of the $[Fe^{III}_2(\mu\text{-O})(L)_2(\mu\text{-O}_2CPh)_2]^{2+}$ starting complexes, in which the most electron-donating ligands (π-basic) give the lowest TONs (**Figure 30**). The decreased Lewis acidity of the Fe centre does not facilitate the exchange of a benzoate ligand with *m*CPBA and, therefore, this inhibits the formation of the reactive species. $[Fe^{III}_2(\mu\text{-O})(L5)_2(\mu\text{-O}_2CPh)_2]^{2+}$ (**94**) has the highest total TON (411) as it has the highest E_{red} (-0.743 V) (**Figure 31**). These complexes also hydroxylate adamantane with a high selectivity (3°/2° = 15.7 ~ 28.1) which indicates the involvement of metal-based oxidants rather than non-selective freely diffusing radical species.
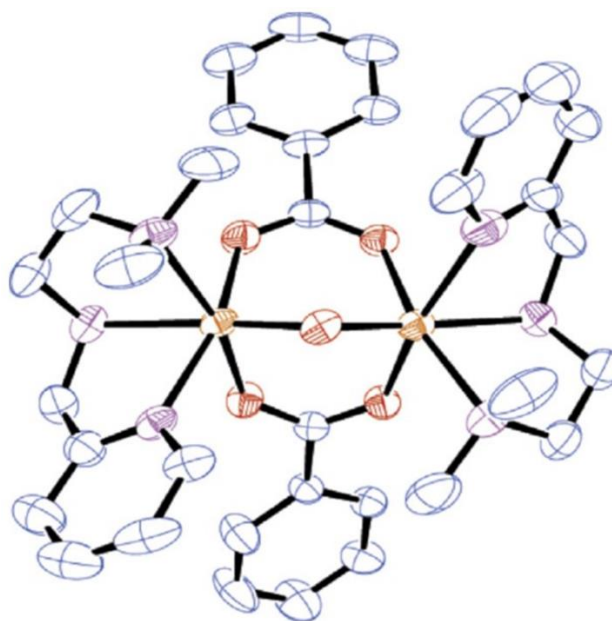
94

Figure 31. X-ray crystal structure of $[Fe^{III}_2(\mu\text{-}O)(L5)_2(\mu\text{-}O_2CPh)_2]^{2+}$ (**94**). Hydrogen atoms have been omitted for clarity.[97] Reproduced with permission of the publisher.

It is believed that one of the benzoate bridges on the starting complex (**95**) exchanges with *m*CPBA to produce a peroxo acid intermediate (**96**) which then either undergoes O-O bond heterolysis to generate an Fe^V oxo reactive species (**97**) or O-O bond homolysis to generate an Fe^{IV} oxo reactive species (**98**). Both of these can then hydroxylate cyclohexane and the resulting common $Fe^{III}_2(\mu\text{-}O)$ complex (**99**) is reoxidized to **96** (**Scheme 28**). O-O bond homolysis was found to be the major reaction pathway as chlorobenzene was produced in 60% yield.[97] The reaction's mechanistic route may depend on the Fe oxidation state as Que *et al.* previously reported that $[Fe^{II}(N_4Py)(CH_3CN)]^{2+}$ favours O-O bond heterolysis, whilst $[Fe^{III}(N_4Py)(CH_3CN)]^{3+}$ favours O-O bond homolysis.[98]
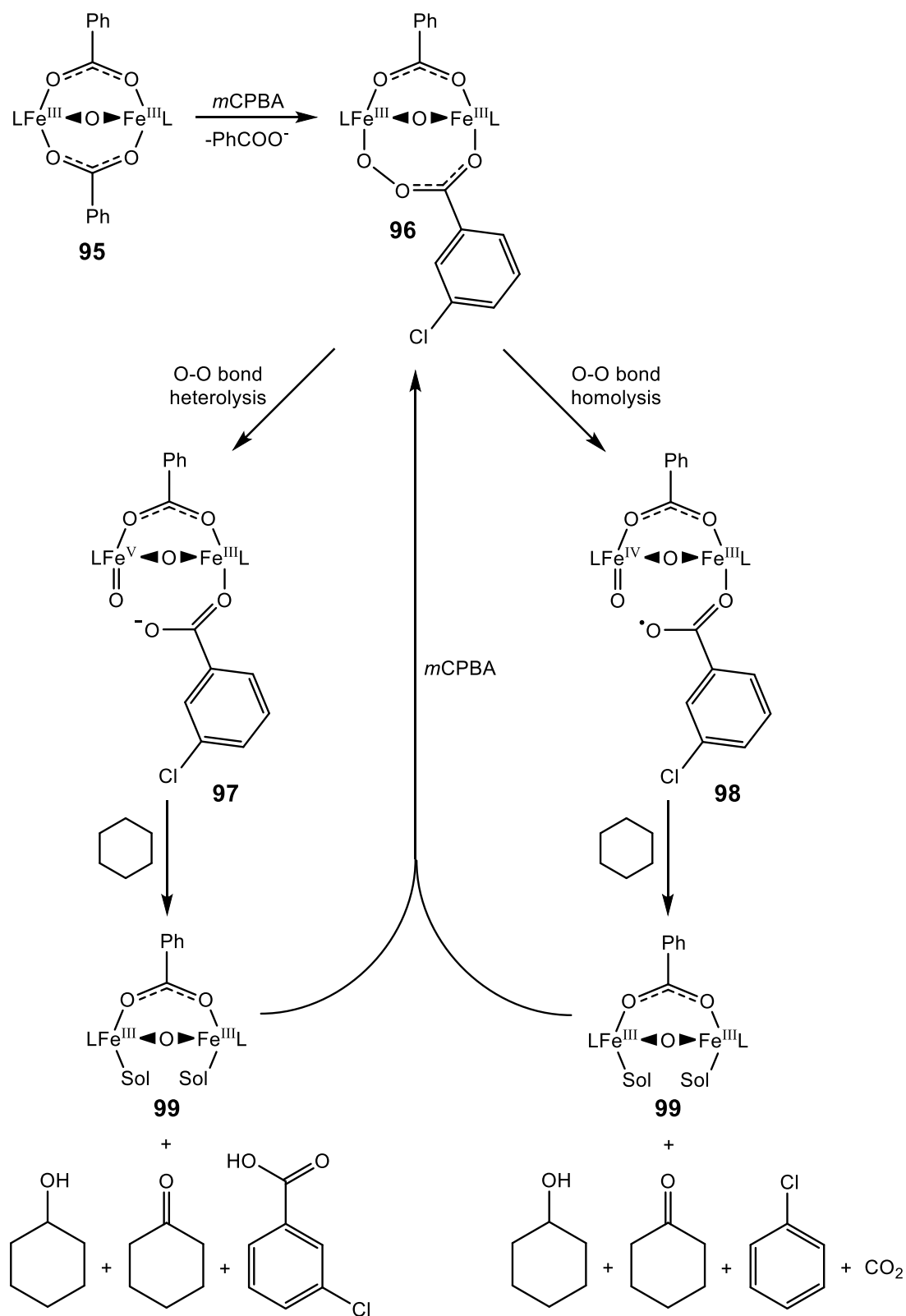
Scheme 28. Proposed cyclohexane oxidation mechanism. L is an unspecified tridentate 3N ligand.[97]

Previous work by Palaniandavar *et al.* revealed that diacetate-bridged Fe^{III}_2 complexes with various tridentate 3N ligands (**Figure 29, L8 - 9**) are less reactive than their dibenzoate-bridged counterpart complexes.[99] Similar to that mentioned previously, this is attributed to the greater electron-donating ability (stronger coordination) of the acetate ligand which inhibits its exchange with *m*CPBA and therefore the formation of the reactive species.

Interestingly, it was found that after approximately 50 turnovers, complex **99** degrades to a mononuclear complex $[Fe(L)(RCO_2)(Sol)_2]^{2+}$ (**100**) (**Scheme 29**). One of the solvent ligands exchanges with *m*CPBA to produce a mononuclear peroxo acid intermediate (**101**) which then either undergoes O-O bond heterolysis to generate an Fe^V oxo reactive species or O-O bond homolysis to generate an Fe^{IV} oxo reactive species (**102**). Both of these can then hydroxylate cyclohexane. This process is similar to that mentioned previously, however O-O bond heterolysis was found to be the major pathway as *m*-chlorobenzoic acid is produced in greater yield.[99]
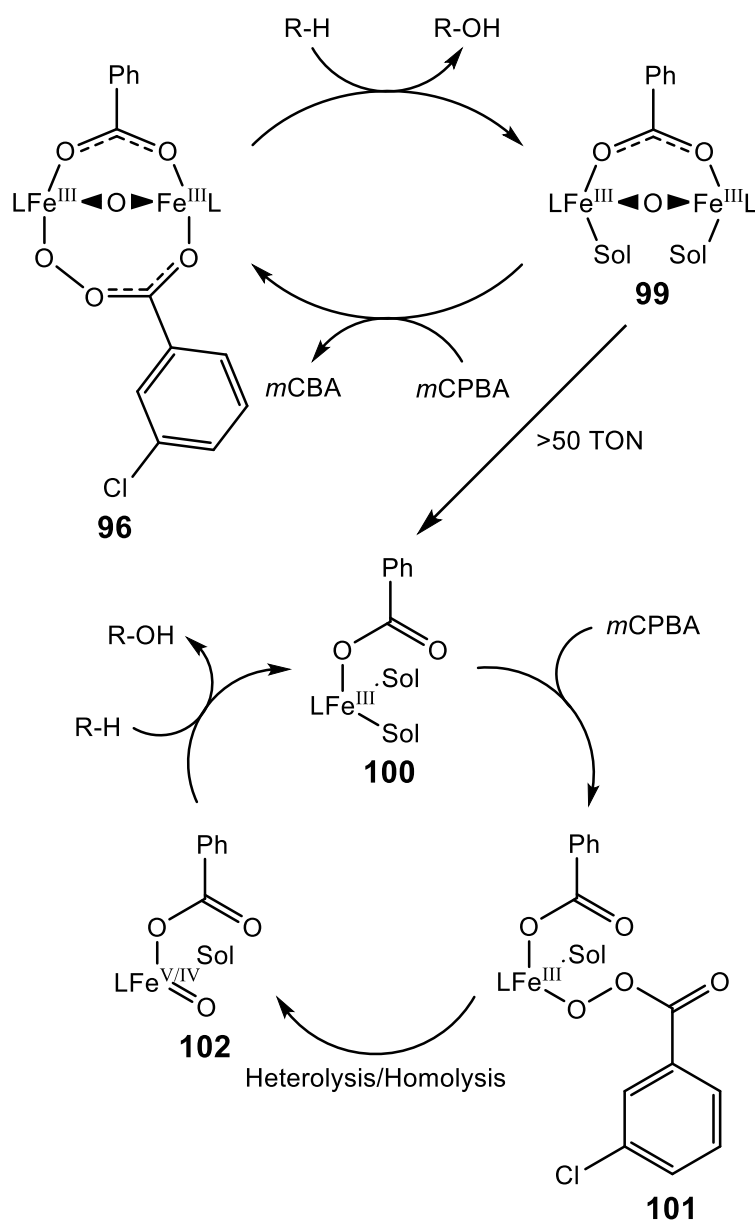
Scheme 29. Proposed mononuclear Fe complex catalytic cycle in alkane hydroxylation. L is an unspecified tridentate 3N ligand.[99]

3.2.5 **Nitrido-Bridged Complexes**

Finally, nitrido-bridged complexes are a rather unusual class of diiron hydroxylation catalysts which differ from all of the complexes previously described in this section because their Fe centres are primarily bridged by a nitrogen atom instead of an oxygen atom.[33] The first nitrido-bridged diiron complex, $[(TPP)Fe^{IV}(\mu\text{-}N)Fe^{III}(TPP)]$ was prepared by Summerville and Cohen in 1976.[100]

103
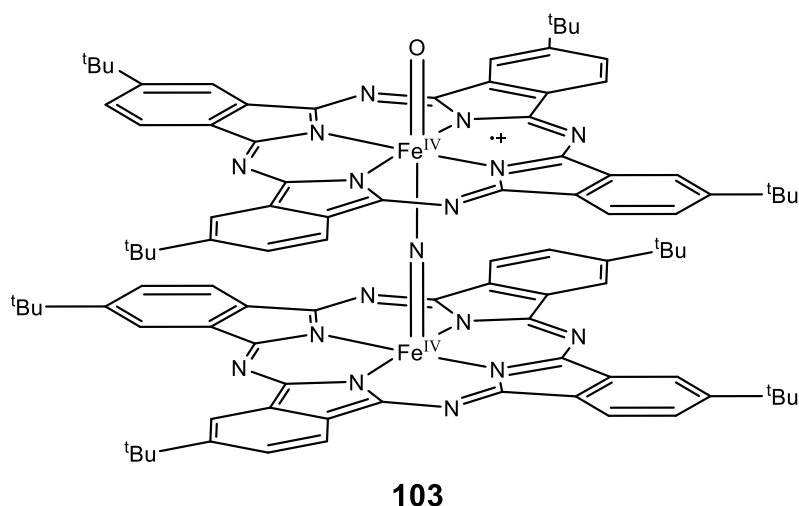
Figure 32. $[(Pc^tBu_4)Fe^{IV}(\mu\text{-}N)Fe^{IV}(Pc^tBu_4^{\cdot+})(O)]$ complex (**103**).[101]

In 2008 Sorokin *et al.* reported a highly reactive nitrido-bridged complex $[(Pc^tBu_4)Fe^{IV}(\mu\text{-}N)Fe^{IV}(Pc^tBu_4^{\cdot+})(O)]$ (**103**) (**Figure 32**) which demonstrated the ability to oxidize methane under ambient conditions, heterogeneously.[101] The neutral starting complex $[(Pc^tBu_4)Fe^{IV}(\mu\text{-}N)Fe^{III}(Pc^tBu_4)]$ (**104**) (supported on silica) was oxidized to **103** using excess H_2O_2 in H_2O at 50 °C and this was found to proceed *via* an Fe_2 peroxo species $[(Pc^tBu_4)Fe^{IV}(\mu\text{-}N)Fe^{III}(Pc^tBu_4)(OOH)]^-$ (**105**) which then undergoes O-O bond heterolysis to

76

produce an Fe^V oxo complex (**106**) and electron transfer yields the Fe^{IV} cation-radical porphyrin (**Scheme 30**).[101,102]
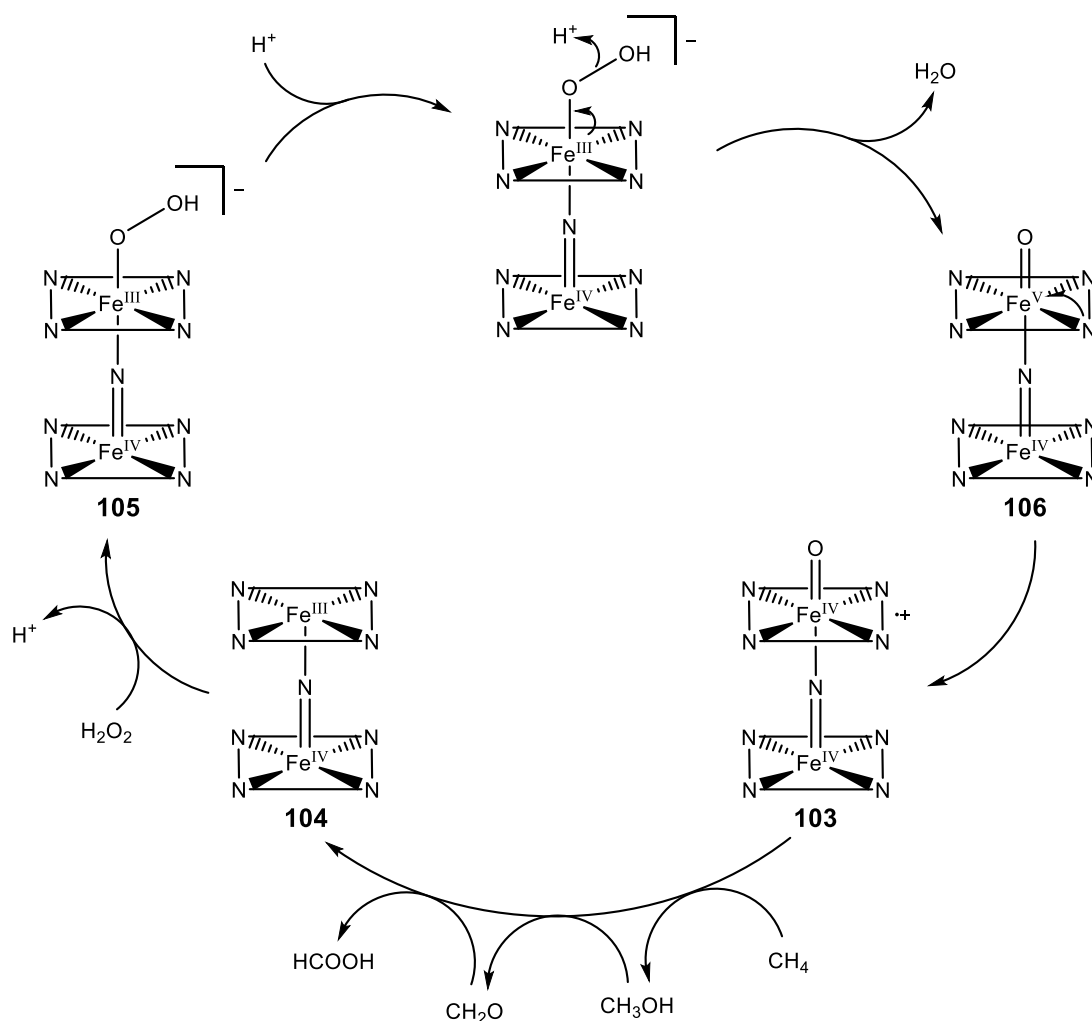
Scheme 30. Proposed reaction mechanism for the oxidation of methane by $[(Pc^tBu_4)Fe^{IV}(\mu\text{-}N)Fe^{IV}(Pc^tBu_4^{-+})(O)]$ (**103**).[101,102]

Formic acid and formaldehyde were obtained as the major oxidation products (21 and 10.7 turnovers, respectively) due to the over-oxidation of methanol. Interestingly, the formic acid TON increased more than 3-fold when 0.1 M H_2SO_4 was added as protonation of the distal oxygen in **105** facilitates O-O bond heterolysis (**Scheme 30**).[101,102] Complex **103** was found to be so

reactive that it had to be tested in H_2O as to prevent oxidation of the MeCN solvent.[101]

Overall, **103** really shows potential as being a promising large scale alkane oxidation catalyst due to its remarkable thermal stability, its compatibility with a clean oxidant (H_2O_2) in a clean solvent (H_2O) and that it can be simply filtered off after the reaction is finished.[101] Also, phthalocyanines, such as that in **103** can be accessible in bulk quantities and are therefore much cheaper than other porphyrin and non-heme ligands.[103]

107
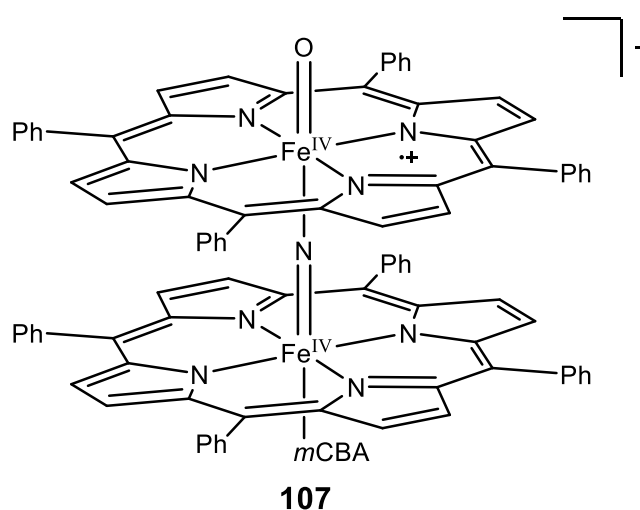
Figure 33. [(TPP)(*m*CBA)Fe^{IV}(μ-N)Fe^{IV}(TPP$^{·+}$)(O)]$^-$ complex (**107**).[104]

Sorokin later reported another highly reactive nitrido-bridged complex [(TPP)(*m*CBA)Fe^{IV}(μ-N)Fe^{IV}(TPP$^{·+}$)(O)]$^-$ (**107**) (**Figure 33**) which also demonstrated the ability to oxidize methane under ambient conditions, heterogeneously.[104] This complex was found to consist of an antiferromagnetically coupled, valence-delocalised high spin (S = 2) Fe^{IV} – high spin (S = 2) Fe^{IV} pair with a total spin of ½ (including the porphyrin radical).[105]

108 → **109**

Reagents: [(TPP)(*m*CBA)Fe^{IV}(*u*-N)Fe^{IV}(TPP$^{·+}$)(O)]$^-$, 1:1 MeCN/CH$_2$Cl$_2$, -60 °C
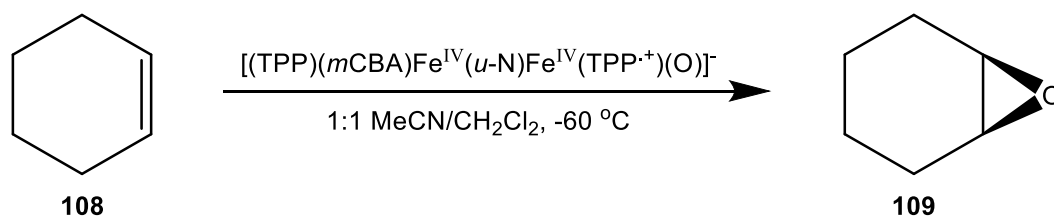
Scheme 31. Epoxidation of cyclohexene (**108**) by [(TPP)(*m*CBA)Fe^{IV}(μ-N)Fe^{IV}(TPP$^{·+}$)(O)]$^-$ (**107**).[104]

Remarkably, formic acid was obtained as the major oxidation product (13.7 turnovers) with a trace amount of formaldehyde. Complex **107** also demonstrated good epoxidation (OAT) reactivity (0.37 M^{-1} s^{-1}) towards cyclohexene (**108**), in which cyclohexene oxide (**109**) was obtained as the sole product (**Scheme 31**) and this indicates that no HAA takes place. Interestingly, the mononuclear analogue [(TPP)Fe^{IV}(O)]$^+$ was found to oxidize adamantane 130 times more slowly and was unable to oxidize cyclohexane under the same conditions, therefore the dimetallic structure of **107** must have an important influence on its reactivity.[104]

Further work by Ansari *et al.* revealed that the greater reactivity of **107** can be attributed to its greater degree of delocalisation as this facilitates the flow of electron density from the (*m*CBA)Fe^{IV} group, through the nitrido bridge to the Fe^{IV} oxo group where it then weakens the Fe^{IV}=O bond. The electron donation also stabilizes the newly formed Fe^{III}O-H bond after HAA has taken place.[105] This is very similar to the axial ligand effect (*trans* effect) which is observed in monoiron complexes.[37,38,39] Therefore, analogous oxo-bridged diiron complexes should be less reactive because their single (σ) bonded oxygen bridge is unable to resonate electron density from one Fe to another (localised) like a double (π) bonded nitrogen bridge. A DFT study by Silaghi-Dumitrescu *et al.* concluded that the nitrido bridge acts as a remarkable charge reservoir whilst the oxo bridge remains redox-inert.[106]

4 Conclusions

Biomimetic C-H bond oxidation catalysts have evolved remarkably over the last 20 years by overcoming many practical issues such as poor reactivity, selectivity and thermal stability and have therefore shown that iron can seriously compete with the more traditional transition metals used in C-H bond activation chemistry. We will now draw various conclusions on the various types of iron complexes that have been discussed in this review.

Overall, diiron complexes perform HAA much better than monoiron complexes and heme Fe complexes are superior to non-heme Fe complexes, however it is unclear what exactly influences their dominance.[33]

For monoiron complexes and diiron complexes HAA reactivity is primarily governed by their spin states. In both cases high spin ($S = 2$) Fe^{IV} oxo complexes are much more reactive than low spin ($S = 1$) Fe^{IV} oxo complexes because they can engage in HAA *via* an additional σ-FMO pathway and this permits the substrate to approach the oxo group from an additional vertical trajectory (**Figure 5**). Whereas low spin ($S = 1$) Fe^{IV} oxo complexes can only engage in HAA *via* a π-FMO pathway and this restricts the substrate to approach the oxo group from a horizontal trajectory.[36]

For monoiron complexes and nitrido-bridged complexes HAA reactivity is also governed by the axial ligand effect. In both cases the complex with the most electron-donating ligand in the axial position is the most reactive (**Figure 7**) because the more electron-donating ligands compete with the oxo group for the Fe d_π orbitals which weakens the Fe^{IV}=O bond, making the oxo group more basic (higher pK_a) and forming a stronger O-H bond.[38]

Although the HAA reactivity of both monoiron and diiron complexes generally correlates with their E_{red} values, they must still be supported in their high oxidation states by electron-donating ligands in order to ensure sufficient thermal stability. This was highlighted by the fifth generation TAML complex

60 which is stable at 25 °C, whereas the first generation TAML complex **55** is only stable at -40 °C.[46,48]

Fe^V pentadentate monoamido complexes demonstrate excellent stereoselectivity in which they hydroxylate 3° C-H bonds with retention of configuration (**Scheme 20**) and this process is performed naturally by cytochrome P450 enzymes.[54,22]

In PCET and MCET, conventional monoiron complexes suddenly play by a very different set of rules when a proton or a redox-inactive metal binds to the oxo group. Instead of the traditional HAA mechanism, a stepwise electron and proton transfer takes place and the rate constant (k_2) of hydroxylation is therefore determined by the driving force of electron transfer ($-\Delta G_{et}$) from the substrate to the Fe complex instead of the substrate's C-H BDE.[42,43,44]

Fe_2O_3 open core complexes are superior to Fe_2O_2 diamond core complexes in HAA reactivity, regardless of their spin state because they are able to form a stronger FeO-H bond (higher pK_a) by the use of a terminal oxo group as opposed to a bridging oxo group.[91,92] Rather sluggish Fe_2O_2 diamond core complexes can actually be transformed into highly reactive Fe_2O_3 open core complexes upon attack from a basic substrate (substrate-induced activation) and then the substrate C-H bonds can be selectively oxidized in the presence of weaker ones (**Scheme 25**).[94] Therefore, sMMO could employ a similar mechanism in which ring-opening would only occur when a small substrate such as methane gets close enough to the Fe_2O_2 diamond core of sMMO intermediate Q as this would protect the weaker C-H bonds in the surrounding amino acid residues from oxidation. In fact sMMO intermediate Q could actually exist as a Fe_2O_3 open core complex with two terminal oxo groups instead of a Fe_2O_2 diamond core complex because reversible O-O bond homolysis has been found to serve as a functional model for the conversion of intermediate P to Q in the sMMO catalytic cycle (**Scheme 26**).[95]

Unfortunately, carboxylate-bridged complexes do not behave as expected because after approximately 50 turnovers they degrade to mononuclear Fe complexes which can then subsequently engage in substrate hydroxylation (**Scheme 29**).[99] Despite this disappointment, they were still worth investigating because at least one bridging carboxylate ligand (glutamic acid) is found in each sMMO intermediate and therefore they significantly contribute to the structural architecture of sMMO.[59]

Finally, nitrido-bridged complexes proved to be the most practically promising C-H bond hydroxylation catalysts due to their remarkable thermal stability, their compatibility with a clean oxidant (H_2O_2) in a clean solvent (H_2O) and that they can be employed heterogeneously.[101,102,104] They are far more reactive than analogous oxo-bridged diiron complexes due to their greater degree of delocalisation because a single (σ) bonded oxygen bridge is unable to resonate electron density from one Fe to another (localised) like a double (π) bonded nitrogen bridge.[105] Therefore, the nitrido bridge acts as a remarkable charge reservoir whilst the oxo bridge remains redox-inert.[106]

5 References

1 J. J. Li, *C-H Bond Activation in Organic Synthesis*, CRC Press, Boca Raton, **2015**, Chapter 1, 1-20.

2 A. Sivaramakrishna, P. Suman, E. V. Goud, S. Janardan, C. Sravani, T. Sandeep, K. Vijayakrishna, H. S. Clayton, *J. Coord. Chem.*, **2013**, 66, 2091-2109.

3 S. J. Blanksby, G. B. Ellison, *Acc. Chem. Res.*, **2003**, 36, 255-263.

4 A. S. Borovik, *Chem. Soc. Rev.*, **2011**, 40, 1870-1874.

5 M. P. Doyle, R. Duffy, M. Ratnikov, L. Zhou, *Chem. Rev.*, **2010**, 110, 704-724.

6 M. M. Diaz-Requejo, A. Caballero, M. Fructos, P. Pérez, *Alkane C-H Activation by Single-Site Metal Catalysis*, Springer, Dordrecht, **2012**, Chapter 6, 229-264.

7 D. Balcells, E. Clot, O. Eisenstein, *Chem. Rev.*, **2010**, 110, 749-823.

8 E. Clot, C. Mégret, O. Eisenstein, R. N. Perutz, *J. Am. Chem. Soc.*, **2009**, 131, 7817-7827.

9 www.infomine.com (October 2016)

10 J. W. Morgan, E. Anders, *Proc. Natl. Acad. Sci. USA*, **1980**, 77, 6973-6977.

11 Y. S. Han, A. S. Kumar, T. Han, *Toxicol. Environ. Health. Sci.*, **2009**, 1, 24-31.

12 B. Meunier, S. P. de Visser, S. Shaik, *Chem. Rev.*, **2004**, 104, 3947-3980.

13 C. E. Tinberg, S. J. Lippard, *Acc. Chem. Res.*, **2011**, 44, 280-288.

14 T. Sakakura, T. Sodeyama, K. Sasaki, K. Wada, M. Tanaka, *J. Am. Chem. Soc.*, **1990**, 112, 7221-7229.

15 J. Y. K. Tsang, M. S. A. Buschhaus, P. Legzdins, *J. Am. Chem. Soc.*, **2007**, 129, 5372-5373.

16 H. Chen, J. F. Hartwig. *Angew. Chem. Int. Ed.*, **1999**, 38, 3391-3393.

17 H. Chen, S. Schlecht, T. C. Semple, J. F. Hartwig, *Science*, **2000**, 287, 1995-1997.

18 W. Xu, G. P. Rosini, M. Gupta, C. M. Jensen, W. C. Kaska, K. Krogh-Jespersena, A. S. Goldman, *Chem. Commun.*, **1997**, 23, 2273-2274.

19 K. Krogh-Jespersen, M. Czerw, M. Kanzelberger, A. S. Goldman, *J. Chem. Inf. Comput. Sci.*, **2001**, 41, 56-63.

20 R. A. Periana, D. J. Taube, S. Gamble, H. Taube, T. Satoh, H. Fujii, *Science*, **1998**, 280, 560-564.

21 O. A. Mironov, S. M. Bischof, M. M. Konnick, B. G. Hashiguchi, V. R. Ziatdinov, W. A. Goddard, III, M. Ahlquist, R. A. Periana, *J. Am. Chem. Soc.*, **2013**, 135, 14644-14658.

22 T. D. H. Bugg, *Introduction to Enzyme and Coenzyme Chemistry*, Third Edition, Wiley, Chichester, 2012.

23 D. C. Lamb, M. R. Waterman, *Phil. Trans. R. Soc. B.*, **2013**, 368, 1612.

24 D. R. Nelson, L. Koymans, T. Kamataki, J. J. Stegeman, R. Feyereisen, D. J. Waxman, M. R. Waterman, O. Gotoh, M. J. Coon, R. W. Estabrook, I. C. Gunsalus, D. W. Nebert, *Pharmacogenetics*, **1996**, 6, 1-42.

25 T. Omura, R. Sato, *J. Biol. Chem.*, **1962**, 237, 1375-1376.

26 J. Rittle, M. T. Green, *Science*, **2010**, 330, 933-937.

27 F. P. Guengerich, *J. Biol. Chem.*, **2013**, 288, 17063-17064.

28 C. M. Krest, E. L. Onderko, T. H. Yoska, J. C. Calixto, R. F. Karp, J. Livada, J. Rittle, M. T. Green, *J. Biol. Chem.*, **2013**, 288, 17074-17081.

29 M. Sono, M. P. Roach, E. D. Coulter, J. H. Dawson, *Chem. Rev.*, **1996**, 96, 2841-2887.

30 W. Nam, Y. M. Lee, S. Fukuzumi, *Acc. Chem. Res.*, **2014**, 47, 1146-1154.

31 S. R. Bell, J. T. Groves, *J. Am. Chem. Soc.*, **2009**, 131, 9640-9641.

32 M. S. Seo, N. H. Kim, K. B. Cho, J. E. So, S. K. Park, M. Clémancey, R. Garcia-Serres, J. M. Latour, S. Shaik, W. Nam, *Chem. Sci.*, **2011**, 2, 1039-1045.

33 K. P. Bryliakov, E. P. Talsi, *Coord. Chem. Rev.*, **2014**, 276, 73-96.

34 J. England, Y. Guo, K. M. V. Heuvelen, M. A. Cranswick, G. T. Rohde, E. L. Bominaar, E Münck, L. Que, Jr, *J. Am. Chem. Soc.*, **2011**, 133, 11880-11883.

35 J. England, Y. Guo, E. R. Farquhar, V. G. Young, Jr, E. Münck, L. Que, Jr, *J. Am. Chem. Soc.*, **2010**, 132, 8635-8644.

36 A. Decker, J.-U. Rohde, E. J. Klinker, S. D. Wong, L. Que, Jr, E. I. Solomon, *J. Am. Chem. Soc.*, **2007**, 129, 15983-15996.

37 C. V. Sastri, J. Lee, K. Oh, Y. J. Lee, J. Lee, T. A. Jackson, K. Ray, H. Hirao, W. Shin, J. A. Halfen, J. Kim, L. Que, Jr, S. Shaik, W. Nam, *Proc. Natl. Acad. Sci. USA*, **2007**, 104, 19181-19186.

38 M. R. Bukowski, K. D. Koehntop, A. Stubna, E. L. Bominaar, J. A. Halfen, E. Münck, W. Nam, L. Que, Jr, *Science*, **2005**, 310, 1000-1002.

39 Y. Kang, H. Chen, Y. J. Jeong, W. Lai, E. H. Bae, S. Shaik, W. Nam, *Chem. Eur. J.*, **2009**, 15, 10039-10046.

40 H. Hirao, L. Que, Jr, W. Nam, S. Shaik, *Chem. Eur. J.*, **2008**, 14, 1740-1756.

41 T. Chantarojsiri, Y. Sun, J. R. Long, C. J. Chang, *Inorg. Chem.*, **2015**, 54, 5879-5887.

42 J. Park, Y. Morimoto, Y. M. Lee, W. Nam, S. Fukuzumi, *Inorg. Chem.*, **2014**, 53, 3618-3628.

43 J. Park, Y. M. Lee, W. Nam, S. Fukuzumi, *J. Am. Chem. Soc.*, **2013**, 135, 5052-5061.

44 Y. Morimoto, J. Park, T. Suenobu, Y. M. Lee, W. Nam, S. Fukuzumi, *Inorg. Chem.*, **2012**, 51, 10025-10036.

45 S. Fukuzumi, Y. Morimoto, H. Kotani, P. Naumov, Y. M. Lee, W. Nam, *Nat. Chem.*, **2010**, 2, 756-759.

46 F. Tiago de Oliveira, A. Chanda, D. Banerjee, X. Shan, S. Mondal, L. Que, Jr, E. L. Bominaar, E. Münck, T. J. Collins, *Science*, **2007**, 315, 835-838.

47 S. Kundu, J. V. K. Thompson, A. D. Ryabov, T. J. Collins, *J. Am. Chem. Soc.*, **2011**, 133, 18546-18549.

48 M. Ghosh, K. K. Singh, C. Panda, A. Weitz, M. P. Hendrich, T. J. Collins, B. B. Dhar, S. S. Gupta, *J. Am. Chem. Soc.*, **2014**, 136, 9524-9527.

49 C. Panda, M. Ghosh, T. Panda, R. Banerjee, S. S. Gupta, *Chem. Commun.*, **2011**, 47, 8016-8018.

50 J. Kaizer, E. J. Klinker, N. Y. Oh, J.-U. Rohde, W. J. Song, A. Stubna, J. Kim, E. Münck, W. Nam, L. Que, Jr, *J. Am. Chem. Soc.*, **2004**, 126, 472-473.

51 E. Kwon, K.-B. Cho, S. Hong, W. Nam, *Chem. Commun.*, **2014**, 50, 5572-5575.

52 Q. Ren, Y. Guo, M. R. Mills, A. D. Ryabov, T. J. Collins, *Eur. J. Inorg. Chem.*, **2015**, 8, 1445-1452.

53 D.-L. Popescu, A. Chanda, M. J. Stadler, S. Mondal, J. Tehranchi, A. D. Ryabov, T. J. Collins, *J. Am. Chem. Soc.*, **2008**, 130, 12260-12261.

54 Y. Hitomi, K. Arakawa, T. Funabiki, M. Kodera, *Angew. Chem. Int. Ed.*, **2012**, 51, 3448-3452.

55 G. Roelfes, M. Lubben, R. Hage, L. Que, Jr, B. L. Feringa, *Chem. Eur. J.*, **2000**, 6, 2152-2159.

56 J. M. Rowland, M. Olmstead, P. K. Mascharak, *Inorg. Chem.*, **2001**, 40, 2810-2817.

57 Y. Hitomi, K. Arakawa, M. Kodera, *Chem. Eur. J.*, **2013**, 19, 14697-14701.

58 M. T. Green, *Curr. Opin. Chem. Biol.*, **2009**, 13, 84-88.

59 P. M. H. Kroneck, M. E. S. Torres, *Sustaining Life on Planet Earth: Metalloenzymes Mastering Dioxygen and Other Chewy Gases*, Springer, Cham, **2015**, Chapter 6, 205-256.

60 A. E. Cho, W. A. Goddard III, *Metalloproteins: Theory, Calculations and Experiments*, CRC Press, Boca Raton, **2015**, Chapter 4, 117-163.

61 H. Ali, J. C. Murrell, *Microbiology*, **2009**, 155, 761-771.

62 R. Balasubramanian, A. C. Rosenzweig, *Curr. Opin. Chem. Biol.*, **2008**, 12, 245-249.

63 M. Merkx, D. A. Kopp, M. H. Sazinsky, J. L. Blazyk, J. Müller, S. J. Lippard, *Angew. Chem. Int. Ed.*, **2001**, 40, 2782-2807.

64 B. J. Wallar, J. D. Lipscomb, *Chem. Rev.*, **1996**, 96, 2625-2658.

65 K. K. Andersson, W. A. Froland, S. K. Lee, J. D. Lipscomb, *New J. Chem.*, **1991**, 15, 411-415.

66 B. G. Fox, J. G. Borneman, L. P. Wackett, J. D. Lipscomb, *Biochemistry*, **1990**, 29, 6419-6427.

67 M. J. Rataj, J. E. Kauth, M. I. Donnelly, *J. Biol. Chem.*, **1991**, 266, 18684-18690.

68 A. C. Rosenzweig, C. A. Frederick, S. J. Lippard, P. Nordlund, *Nature*, **1993**, 366, 537-543.

69 A. C. Rosenzweig, P. Nordlund, P. M. Takahara, C. A. Frederick, S. J. Lippard, *Chem. Biol.*, **1995**, 2, 632.

70 D. A. Whittington, S. J. Lippard, *J. Am. Chem. Soc.*, **2001**, 123, 827-838.

71 B. G. Fox, M. P. Hendrich, K. K. Surerus, K. K. Andersson, W. A. Froland, J. D. Lipscomb, E. Münck, *J. Am. Chem. Soc.*, **1993**, 115, 3688-3701.

72 B. M. Hoffman, B. E. Sturgeon, P. E. Doan, V. J. DeRose, K. E. Liu, S. J. Lippard, *J. Am. Chem. Soc.*, **1994**, 116, 6023-6024.

73 K. E. Liu, A. M. Valentine, D. L. Wang, B. H. Huynh, D. E. Edmondson, A. Salifoglou, S. J. Lippard, *J. Am. Chem. Soc.*, **1995**, 117, 10174-10185.

74 A. M. Valentine, S. S. Stahl, S. J. Lippard, *J. Am. Chem. Soc.*, **1999**, 121, 3876-3887.

75 C. E. Tinberg, S. J. Lippard, *Biochemistry*, **2009**, 48, 12145-12158.

76 K. E. Paulsen, Y. Liu, B. G. Fox, J. D. Lipscomb, E. Münck, M. T. Stankovich, *Biochemistry*, **1994**, 33, 713-722.

77 S. K. Lee, J. C. Nesheim, J. D. Lipscomb, *J. Biol. Chem.*, **1993**, 268, 21569-21577.

78 K. E. Liu, D. Wang, B. H. Huynh, D. E. Edmondson, A. Salifoglou, S. J. Lippard, *J. Am. Chem. Soc.*, **1994**, 116, 7465-7466.

79 R. L. Lieberman, A. C. Rosenzweig, *Nature*, **2005**, 434, 177-182.

80 A. C. Rosenzweig, M. H. Sazinsky, *Curr. Opin. Struc. Biol.*, **2006**, 16, 729-735.

81 R. Balasubramanian, S. M. Smith, S. Rawat, L. A. Yatsunyk, T. L. Stemmler, A. C. Rosenzweig, *Nature*, **2010**, 465, 115-119.

82 H. Jiang, Y. Chen, P. X. Jiang, C. Zhang, T. J. Smith, J. C. Murrell, X. H. Xing, *Biochem. Eng. J.*, **2010**, 49, 277-288.

83 S. I. Chan, K. H. C. Chen, S. S. F. Yu, C. L. Chen, S. S. J. Kuo, *Biochemistry*, **2004**, 43, 4421-4430.

84 B. Wilkinson, M. Zhu, N. D. Priestley, *J. Am. Chem. Soc.*, **1996**, 118, 921-922.

85 Y. Dong, H. Fujii, M. P. Hendrich, R. A. Leising, G. Pan, C. R. Randall, E. C. Wilkinson, Y. Zang, L. Que, Jr, B. G. Fox, K. Kauffmann, E. Münck, *J. Am. Chem. Soc.*, **1995**, 117, 2778-2792.

86 Y. Dong, L. Que, Jr, *J. Am. Chem. Soc.*, **1995**, 117, 11377-11378.

87 E. Y. Tshuva, S. J. Lippard, *Chem. Rev.*, **2004**, 104, 987-1012.

88 C. Kim, Y. Dong, L. Que, Jr, *J. Am. Chem. Soc.*, **1997**, 119, 3635-3636.

89 P. H. Buist, B. Behrouzian, *J. Am. Chem. Soc.*, **1996**, 118, 6295-6296.

90 G. Xue, D. Wang, R. De Hont, A. T. Fiedler, X. Shan, E. Münck, L. Que, Jr, *Proc. Natl. Acad. Sci. USA*, **2007**, 104, 20713-20718.

91 F. G. Bordwell, J-P. Cheng, G-Z. Ji, A. V. Satish, X. Zhang, *J. Am. Chem. Soc.*, **1991**, 113, 9790-9795.

92 K. A. Gardner, J. M. Mayer, *Science*, **1995**, 269, 1849-1851.

93 G. Xue, R. De Hont, E. Münck, L. Que, Jr, *Nat. Chem.*, **2010**, 2, 400-405.

94 G. Xue, A. Pokutsa, L. Que, Jr, *J. Am. Chem. Soc.*, **2011**, 133, 16657-16667.

95 M. Kodera, Y. Kawahara, Y. Hitomi, T. Nomura, T. Ogura, Y. Kobayashi, *J. Am. Chem. Soc.*, **2012**, 134, 13236-13239.

96 S. A. Stoian, G. Xue, E. L. Bominaar, L. Que, Jr, E. Münck, *J. Am. Chem. Soc.*, **2014**, 136, 1545-1558.

97 M. Sankaralingam, M. Palaniandavar, *Polyhedron*, **2014**, 67, 171-180.

98 K. Ray, S. M. Lee, L. Que, Jr, *Inorg. Chim. Acta.*, **2008**, 361, 1066-1069.

99 K. Visvaganesan, E. Sureshb, M. Palaniandavar, *Dalton Trans.*, **2009**, 3814-3823.

100 D. A. Summerville, I. A. Cohen, *J. Am. Chem. Soc.*, **1976**, 98, 1747-1752.

101 A. B. Sorokin, E. V. Kudrik, D. Bouchu, *Chem. Commun.*, **2008**, 2562-2564.

102 P. Afanasiev, E. V. Kudrik, J. M. Millet, D. Bouchub, A. B. Sorokin, *Dalton Trans.*, **2011**, 40, 701-710.

103 D. Wöhrle, *Macromol. Rapid Commun.*, **2001**, 22, 68-97.

104 E. V. Kudrik, P. Afanasiev, L. X. Alvarez, P. Dubourdeaux, M. Cle´mancey, J. Latour, G. Blondin, D. Bouchu, F. Albrieux, S. E. Nefedov, A. B. Sorokin, *Nat. Chem.*, **2012**, 4, 1024-1029.

105 M. Ansari, N. Vyas, A. Ansari, G. Rajaraman, *Dalton Trans.*, **2015**, 44, 15232-15243.

106 R. Silaghi-Dumitrescu, S. V. Makarov, M. Uta, I. A. Dereven'kov, P. A. Stuzhin, *New J. Chem.*, **2011**, 35, 1140-1145.